SUPERCONDUCTIVITY PROBLEMS WITH MULTIPLE GINZBURG-LANDAU ORDER PARAMETERS

by

Jani Geyer

Thesis presented in partial fulfilment of the requirements for the degree of Master of Science at the University of Stellenbosch.

Supervisor : Professor Michael Kastner

Co-supervisor : Professor Jörg Schmalian

DECLARATION

By submitting this thesis electronically, I declare that the entirety of the work contained therein is my own, original work, that I am the sole author thereof (save to the extent explicitly otherwise stated), that reproduction and publication thereof by Stellenbosch University will not infringe any third party rights and that I have not previously in its entirety or in part submitted it for obtaining any qualification.

Date: Desember 2011

ABSTRACT

Two problems in the field of materials-based condensed matter physics, specifically in the field of superconductivity, are studied theoretically. In both problems, where each is of current experimental interest, an extension of Ginzburg-Landau theory is used to describe a physical system, with focus on the energy associated to the interface(s) occurring in the respective systems.

The first physical system under consideration is that of a two-band superconductor. Using Ginzburg-Landau theory for two-band superconductors, the interface energy σ_s between normal and superconducting states coexisting at the thermodynamic critical magnetic field is determined. From the theoretical and numerical analysis of the interface energy, it is found that close to the transition temperature, where the Ginzburg-Landau theory is applicable, the two-band problem maps onto an effective single band problem. This finding puts into question the possibility of intermediate, so called *type-1.5* superconductivity, in the regime where the Ginzburg-Landau theory applies.

The second physical system is that of a system with competing superconductivity and anti-ferromagnetism. From Ginzburg-Landau theory for such competing systems in a thermodynamic critical magnetic field, it is shown that two possible interfaces can occur: an interface between a pure anti-ferromagnetic state and a pure superconducting state; and an interface between a state with coexisting superconductivity and anti-ferromagnetism and a pure anti-ferromagnetic state. The energy associated to both these interfaces is analysed theoretically and numerically from which the boundary between type-I and type-II superconductivity is obtained for certain specific cases.

OPSOMMING

Twee probleme in die veld van materiaal-gebaseerde gekondenseerde materie fisika, spesifiek in die veld van supergeleiding, word teoreties bestudeer. In beide probleme, albei tans van eksperimentele belang, word 'n fisiese sisteem beskryf deur 'n uitbreiding van enkel-band Ginzburg-Landau teorie, met fokus op die energie geassosieer met die koppelvlak(ke) wat in die onderskeie sisteme aangetref word.

Die eerste fisiese sisteem wat beskou word is die van 'n twee-band supergeleier. Deur van Ginzburg-Landau teorie vir twee-band supergeleiers gebruik te maak, word die koppelvlak energie σ_s tussen die gelyktydig bestaande normaal- en supergeleidende toestand in die termodinamiese kritieke magneetveld bepaal. Deur beide teoretiese en numeriese analieses word bepaal dat na aan die oorgangstemperatuur, waar Ginzburg-Landau teorie geldig is, die twee-band probleem op 'n effektiewe een-band probleem afbeeld. Hierdie bevinding bevraagteken dus die moontlikheid van onkonvensionele, of sogenaamde *tipe-1.5* supergeleiding, vir gevalle waar Ginzburg-Landau teorie geldig is.

Die tweede fisiese siteem wat beskou word is 'n sisteem met kompeterende supergeleiding en anti-ferromagnetisme. Met behulp van Ginzburg-Landau teorie vir sulke sisteme in 'n termodinamiese kritiese magneetveld word gewys dat daar twee moontlike koppelvlakke kan ontstaan: 'n koppelvlak tussen 'n uitsluitlik anti-ferromagnetiese toestand en 'n uitsluitlik supergeleidende toestand; sowel as 'n koppelvlak tussen 'n uitsluitlik anti-ferromagnetiese toestand en 'n toestand van beide supergeleiding en anti-ferromagnetisme. Die energie geassosieer met beide hierdie koppelvlakke word teoreties en numeries geanaliseer wat lei tot 'n beskrywing van die grenslyn tussen tipe-I en tipe-II supergeleiding in sekere spesifieke gevalle.

CONTENTS

LIST OF FIGURES

LIST OF TABLES

CHAPTER 1
Introduction

Superconductivity is an extraordinary phenomenon. It is a quantum mechanical state characterized by the Meissner effect! The Meissner effect, named after Walther Meissner who discovered it in 1933 together with Robert Ochsenfeld, refers to the expulsion of the magnetic field in certain materials below a specific critical temperature. These materials are known as superconductors, each of which has its own critical temperature, denoted by T_c. The expulsion of the magnetic field lines is illustrated in Fig. 1.1.

Superconductors also have the property that while in the superconducting state the resistivity of the material is zero. In other words the material becomes a perfect conductor of electric current below it critical temperature - hence the name superconductor.

It is not just the temperature that determines whether a superconductor is in its superconducting state. Applying too strong an external magnetic field also causes the superconductor to be in its normal state, where the normal state is the state without superconductivity. Depending on the behaviour in external magnetic fields, superconductors are classified as either type-I or type-II.

In type-I superconductors, the bulk of the superconductor can either be in the superconducting state or in the normal state. No other state is possible. In type-II superconductors a third state is possible. This state is characterized by a vortex lattice[1]. This vortex lattice stems from the fact that it is energetically favourable for the system to have interfaces. An interface refers

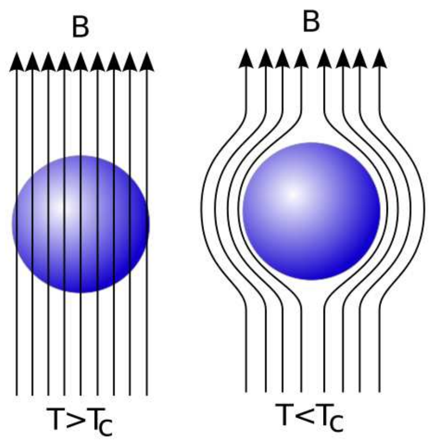

Figure 1.1: A diagram of the Meissner effect which shows the exclusion of the magnetic field lines from the superconductor when below its critical temperature.

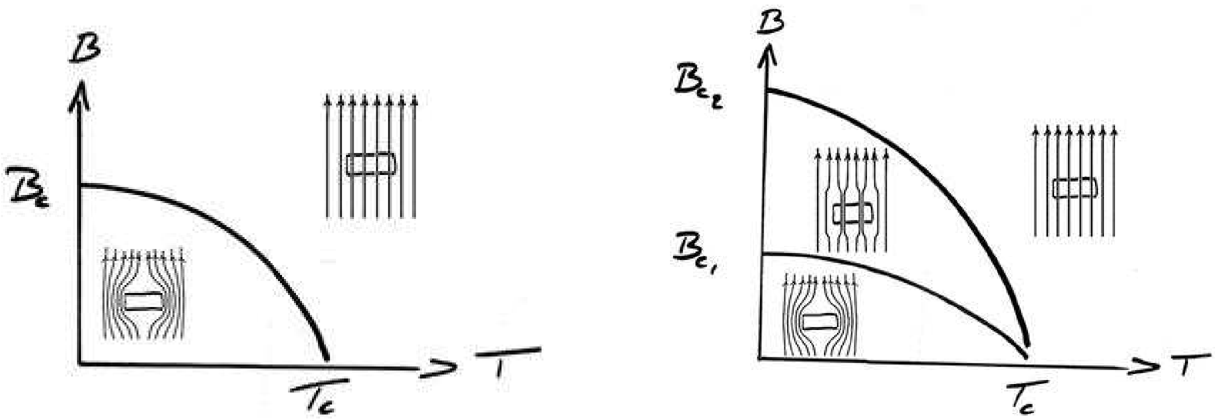

(a) The phase diagram of a type-I superconductor, showing 2 phases: a pure superconducting state and a normal state.

(b) The phase diagram of a type-II superconductor, showing 3 phases: a pure superconducting state, a vortex lattice and a normal state.

Figure 1.2: The phase diagrams of type-I and type-II superconductors as a function of temperature and external magnetic field. To note: in this figure, taken from [2], the external magnetic field is denoted by B. In this thesis it will be denoted by H.

to the surface between a purely superconducting region and a normal state region at a specific thermodynamic critical field.

Thus, for a type-I superconductor the interface energy per unit area, σ_s, is positive. This means it will require energy for the system to form interfaces, which is why such a state is not possible for type-I superconductors[3]. For a type-II superconductor σ_s is negative. This means the system gains energy by creating interfaces. Using this as a starting point, A. A. Abrikosov determined that the bulk state of a type-II superconductor is characterized by vortex formation. For his contribution to the understanding of these vortex latices, A. A. Abrikosov was awarded the Nobel prize in physics in 2003, together with V. L. Ginzburg and A. J. Leggett for their 'pioneering contributions to the theory of superconductors and superfluids'.

In both types of superconductors the possible macrostates can be obtained by adjusting either the temperature or the external magnetic field. This can be summarized in two phase diagrams, one for type-I superconductors and one for type-II superconductors. See Fig. 1.2.

In order to theoretically determine in which of the two superconducting phases the system is in, one must therefore obtain an analytic expression for σ_s. From such an expression the sign of σ_s will be clear, which means the state of the superconductor will have been determined.

In traditional one-band superconductors this has been studied by V. L. Ginzburg and L. D. Landau[3]. Using Ginzburg-Landau (GL) theory it is possible to obtain a functional which, when minimized, yields σ_s for a one-band superconductor. This functional only depends on a

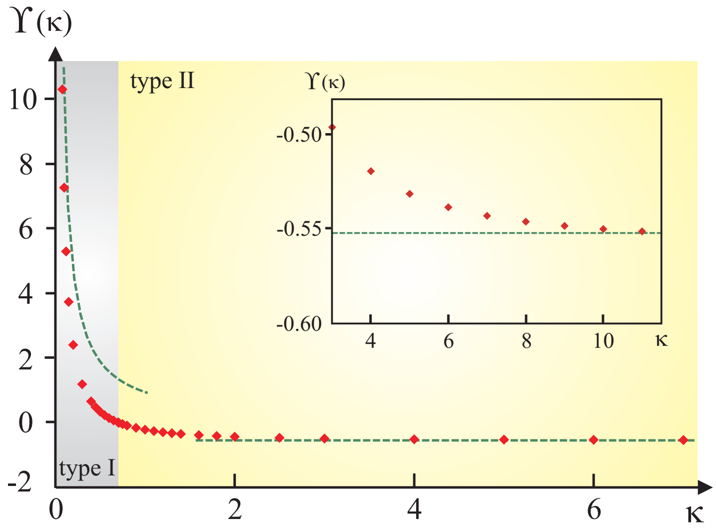

Figure 1.3: The function, $\Upsilon(\kappa)$, of the one-band problem calculated numerically (full points). The theoretically derived limits are given by the dashed lines. The inset shows an enlargement.

single parameter, namely the dimensionless GL parameter κ, and can be solved using numerical techniques. The solution gives the following expression

$$\sigma_s = \lambda \frac{H_c^2}{4\pi} \Upsilon(\kappa), \tag{1.1}$$

where λ and H_c are constants of the system, and $\Upsilon(\kappa)$ is the value of the minimized functional which can be obtained numerically. This equation, as well as the GL theory from which it can be derived, will be discussed in chapter 2. The numerical solution for Υ is shown in Fig. 1.3. The numerical analysis will be discussed in chapter 5.

The main objective of this thesis's work is to study the surface energy σ_s for more *complicated* superconductors within the framework of GL theory. In particular, two such problems are studied, namely two-band superconductivity and superconductivity in the presence of antiferromagnetism.

Two-band superconductivity arises when the Fermi surface of a superconductor consists of two or more well separated sheets with different energy gaps.[4, 5] This is the case for many superconductors, including MgB_2 and the recently discovered FeAs superconductors.[6]. Experimental evidence for such superconductors are discussed in chapter 3.

An expansion of the Ginzburg-Landau theory for one-band superconductors can be used to successfully describe two-band superconductors. This is done by describing each band in terms of GL theory separately, while adding a coupling term that links the two bands, as will be discussed in chapter 4. In previous work, see Ref. [7], this coupling term was neglected, which lead to the theoretical prediction of *type-1.5* superconductivity. In this thesis it will be shown that no such state can exist close to the critical temperature. This will again be done by considering the interface energy per unit area. Using the two-band GL theory developed in chapter 4, a functional will be derived from which σ_s for a two-band superconductor can obtained from minimization. It will be shown that the two-band functional is equivalent to the one-band functional near the critical temperature. In other words, it will be shown that the two $\kappa_{i\in\{1,2\}}$ values of the two-band problem, one for each band, will together behave as an effective one-band κ due to the coupling. The specific expression

$$\kappa_{\text{effective}}^{-2} = \kappa_1^{-2} + \kappa_2^{-2} \tag{1.2}$$

will be derived theoretically in chapter 4 and shown to hold numerically in chapter 6. As only type-I and type-II superconductivity exists for one-band superconductors, this means no other states can exist for two-band superconductors.

The second problem presented in this thesis will deal with superconductivity in the presence of anti-ferromagnetism. In many superconductors, amongst others some of the high temperature FeAs superconductors, both superconductivity and anti-ferromagnetism occur and are energetically in close proximity. Specific examples of such superconductors and their respective phase diagrams are discussed in chapter 7.

As in the previous problem, it is possible to extend the one-band Ginzburg-Landau theory to describe a system with these competing phases. Instead of a second band, the theory now includes a second phase, where the two phases are again coupled. Although such systems and the two-band systems differ greatly in terms of the physical behaviour, the Ginzburg-Landau extensions have many similarities. This will be seen in chapter 8 in deriving the Ginzburg-Landau theory for competing phases.

From the new GL theory it is again possible to construct interfaces. In the previous systems the interface occurred between a normal state and a superconducting state. In this problem this is again the case, except that the normal state is now a purely anti-ferromagnetic state. And there are two possible interfaces, not just one as in the previous scenarios. The two possible interfaces are due to the fact that there are now two distinct superconducting states. One is the familiar state with pure superconductivity. The other is a state where superconductivity coexists with anti-ferromagnetism.

Both these interfaces are studied theoretically in chapter 8. Again the boundary between type-I and type-II superconductivity for both scenarios will be considered. A functional will again be derived which, when minimized, will yield the value for the interface energy per unit area. However, unlike in the previous scenarios, this functional will depend on a total of four parameters. This means that one can no longer theoretically derive a boundary condition between type-I and type-II superconductivity in terms of the original one-band problem. By using the assumption that the phase transition between a pure AFM state and a coexisting state, as a function of the external field, is of second-order, it is again possible to derive a theoretical expression for the boundary between type-I and type-II superconductivity. This will be discussed at the end of chapter 8.

The functional for the interface energy will also be analysed numerically. Due to the large phase-space, only specific scenarios will be considered. These will be discussed in chapter 9. It will be shown that there is a discrepancy between the theoretically predicted boundary and the numerically obtained boundary. This shows that the assumption of a second-order phase transition may be incorrect, and that one is instead dealing with a weak first order transition. An outlook on this possibility will be discussed in the conclusion, along with a general overview of both problems considered in this thesis.

CHAPTER 2
Ginzburg-Landau theory

In this chapter a brief overview of the Ginzburg-Landau formalism as applied to superconductors is presented. The aim is to introduce the concepts and formulas that will be used in later sections of this text. For a more complete introduction to Ginzburg-Landau theory a standard text such as Refs. [8] or [9] may be consulted.

This formalism was first proposed by Ginzburg and Landau in 1950[3] seven years before the microscopic theory of Bardeen, Cooper and Schrieffer (BCS). It was originally considered to be a phenomenological description of the superconducting phase transition, but was later derived as a limiting case of BCS theory[10, 11].

Within Ginzburg-Landau theory a description of many well-known superconducting phenomena such as the Meissner effect, the Josephson effect, vortices and vortex lattices etc.[8, 9] is possible. It is however important to stress that the theory is only valid in a region of parameter space which is sufficiently close to the superconducting phase transition.

2.1 Thermodynamic approach to superconductors

Ginzburg-Landau theory successfully describes the free energy of the superconducting state near the transition temperature. Before the explicit expression for the Ginzburg-Landau free energy is given, one should first discuss some general properties of this free energy and of the corresponding enthalpy using thermodynamical arguments.

Consider a macroscopic body in a magnetic field, $\mathbf{H}$, where $\mathbf{H}$ is created by externally applied currents, $\mathbf{j}_{ext}$. From the external sources[1]

$$\nabla \times \mathbf{H} = \frac{4\pi}{c}\mathbf{j}_{ext}. \tag{2.1}$$

As is the case in superconductors, there may also be quantum mechanical currents induced within the macroscopic body[2]. These induced currents, j_{ind}, together with the external currents give rise to another quantity, $\mathbf{B}$

$$\nabla \times \mathbf{B} = \frac{4\pi}{c}\left(\mathbf{j}_{ext} + \mathbf{j}_{ind}\right). \tag{2.2}$$

Thus $\mathbf{B}$ is the macroscopic resultant field averaged over mesoscopic regions, to allow for a con-

[1]Only a stationary system is considered, thus terms like $\frac{1}{c}\partial \mathbf{D}/\partial t$ for $\nabla \times \mathbf{H}$ or the corresponding term $\frac{1}{c}\partial \mathbf{E}/\partial t$ in $\nabla \times \mathbf{B}$ were ignored.

[2]These quantum mechanical currents are also known as supercurrents.

tinuum description[12]. The work done on the magnetic field of this macroscopic body is given by

$$\delta W = \frac{1}{4\pi} \int \mathbf{H} \cdot \mathbf{dB}\, d^3 r. \tag{2.3}$$

In general $\nabla \cdot \mathbf{H} \neq 0$. However, in highly symmetric systems, for instance a cylindrical geometry, symmetry forces $\mathbf{H}$ to be divergenceless. In such cases $\mathbf{H}$ is simply the magnetic field produced by external currents in the absence of a superconductor. In the remainder of this text sufficient symmetry for this to hold is assumed.

From Eqs. (2.1) and (2.2) the following relation holds via the magnetization, $\mathbf{M}$

$$\mathbf{H} = \mathbf{B} - 4\pi \mathbf{M} \tag{2.4}$$

with $\mathbf{j}_{ind} = c\nabla \times \mathbf{M}$.

The relation between free energy and work can be obtained via the expression $F = U - TS$, which is well known in thermodynamics. Here F is the free energy, U is the internal energy, T is the temperature and S is the entropy. In derivative form the expression above reads $dF = dU - TdS - SdT$[12]. Using the fact that $dU = TdS + \delta W$[12] and Eq. (2.3), the expression for the free energy density, f, is therefore

$$df = -sdT + \frac{1}{4\pi}\mathbf{H} \cdot \mathbf{dB}, \tag{2.5}$$

where s is the entropy density.

The minimum of the free energy gives the state of the system at a given temperature and $\mathbf{B}$. However, what is required is the state of the system at a given temperature and $\mathbf{H}$, since it is $\mathbf{H}$, not $\mathbf{B}$, that an experimentalist controls. The appropriate thermodynamic function to minimize is the enthalpy which is obtained from the free energy by means of the Legendre transformation

$$g = f - \frac{1}{4\pi}\mathbf{H} \cdot \mathbf{B} \tag{2.6}$$

which, together with Eq. (2.5), gives

$$dg = -sdT - \frac{1}{4\pi}\mathbf{B} \cdot \mathbf{dH}. \tag{2.7}$$

Integration at a fixed temperature T then yields

$$g\left(T, \mathbf{H}\right) = g\left(T, \mathbf{0}\right) - \frac{1}{4\pi}\int_0^H \mathbf{B}\left(\mathbf{H}'\right) \cdot \mathbf{dH}'. \tag{2.8}$$

Consider now the equations of state in terms of the Meissner effect for the bulk normal and superconducting states. The normal state is characterized by $\mathbf{B}(\mathbf{H}) = \mathbf{H}$. Thus, for the normal state Eq. (2.8) gives

$$g_n(T,\mathbf{H}) = g_n(T,\mathbf{0}) - \frac{1}{8\pi}H^2. \tag{2.9}$$

On the other hand, if the material is in the superconducting state, from the Meissner effect one has that $\mathbf{B}(\mathbf{H}) = \mathbf{0}$. Eq. (2.8) now yields

$$g_s(T,\mathbf{H}) = g_s(T,\mathbf{0}). \tag{2.10}$$

The thermodynamic critical field is the field where both these states are energetically equally favourable. This means

$$g_n(T,\mathbf{H_c}) = g_s(T,\mathbf{H_c}), \tag{2.11}$$

ignoring changes in the volume at the superconducting transition. Thus from Eqs. (2.9) and (2.10) one has that

$$\begin{aligned} \frac{1}{8\pi}H_c^2(T) &= g_n(T,\mathbf{0}) - g_s(T,\mathbf{0}) \\ &= f_n(T,\mathbf{0}) - f_s(T,\mathbf{0}) \end{aligned} \tag{2.12}$$

i.e. from the difference in the free energy density at zero field, one can calculate the critical field.

To show that the superconducting state is energetically favourable for $H < H_c$, one needs to write down the difference in enthalpy in general. Again from Eqs. (2.9) and (2.10)

$$\begin{aligned} g_s(T,\mathbf{H}) - g_n(T,\mathbf{H}) &= g_s(T,\mathbf{0}) - g_n(T,\mathbf{0}) + \frac{1}{8\pi}\mathbf{H}^2(T) \\ &= \frac{1}{8\pi}\left(\mathbf{H}^2 - \mathbf{H}_c^2(T)\right). \end{aligned} \tag{2.13}$$

As expected, for $H < H_c$ one sees that $g_s(T,\mathbf{H}) < g_n(T,\mathbf{H})$, i.e. the superconducting state with $\mathbf{B} = \mathbf{0}$ is indeed energetically favourable with respect to the normal state below the thermodynamical critical field.

2.2 Ginzburg-Landau equations

The form of the free energy as proposed by Ginzburg and Landau was inspired by a combination of the quantum nature of superconductors and the general theory of second-order phase transitions.

Proposed by Landau in 1937[13], the general theory of second-order phase transitions states that for every second-order phase transition there exists an order parameter which goes to zero at the transition. As the order parameter is small in the vicinity of the transition, the free energy can be expanded in terms of the order parameter with all coefficients of the expansion being regular functions. This expansion means that the free energy is only valid close to the transition temperature.

In the superconductivity problem, the transition temperature depends on the externally applied magnetic field or vice versa: the critical magnetic field depends on the temperature of the system. Ginzburg and Landau chose the temperature dependence to describe the superconducting phase transition. Thus, the external magnetic field is specified and the temperature is varied around the transition temperature which is dependent on the chosen external magnetic field. Thus $T_c = T_c(\mathbf{H})$. The expansion coefficients are therefore written as regular functions in temperature.

To account for the quantum behaviour of superconductors, the free energy was constructed as an expansion in a complex order parameter, ψ, and its complex conjugate, ψ^*. As the free energy is a real quantity, Ginzburg and Landau only allowed combinations of ψ and ψ^* which give real values.

2.2.1 The bulk free energy

First consider the bulk of a superconductor in the absence of an external magnetic field, thus $\mathbf{H} = \mathbf{0}$, and $\psi(\mathbf{r})$ is a complex constant since $\psi(\mathbf{r})$ should be translationally invariant in a bulk state. Ginzburg and Landau constructed the free energy as

$$F_s = F_n + \int f(\mathbf{r})\, d^3 r \tag{2.14}$$

where f is the free energy density given by the expansion

$$f = a(T)\,|\psi|^2 + \frac{1}{2} b(T)\,|\psi|^4 + \dots \,. \tag{2.15}$$

As previously discussed, the coefficients, e.g. $a(T)$ and $b(T)$, are regular functions in T and only $\psi^*\psi = |\psi|^2 \in \mathbf{R}$ terms are allowed. This means the expansion only has even powers of $\psi(\mathbf{r})$.

In the normal state, thus above T_c, it is required that the minimum of the free energy occurs at $\psi = 0$, while below T_c in the superconducting state $\psi \neq 0$. To achieve two such stable minima at least a forth order term is required. In the simplest model the series is therefore only truncated after the second term

$$f = a(T)\,|\psi|^2 + \frac{1}{2} b(T)\,|\psi|^4 \,. \tag{2.16}$$

Now, the minimum free energy, hence at $df/d\psi = 0$, for the superconducting state, thus $\psi \neq 0$, occurs at

$$|\psi|^2 = -\frac{a}{b} \equiv \psi_0^2. \tag{2.17}$$

The value of the free energy density for this bulk superconducting state is

$$f|_{\psi_0} = -\frac{1}{2}\frac{a^2}{b} = -\frac{1}{2}b\,|\psi_0|^4\,. \tag{2.18}$$

The second derivative of Eq. (2.16) with respect to $|\psi|$ has to be positive at the stationary points in order for the free energy to be a minimum. Substituting the values for $|\psi|^2$ at the stationary points of f, thus $|\psi|^2 \in \{0, \psi_0^2\}$ into this second derivative, one finds that a must be negative in the superconducting state, but positive in the normal state. This means that a undergoes a sign change when crossing from one state to the other.

On the other hand, b is positive in both states: in order for $\psi = 0$ to be a minimum of Eq. (2.16), b needs to be positive in this equation, and as both the normal state solution and the bulk superconducting state solution is obtained by the minimization of Eq. (2.16), b is positive for both states.

One can expand the coefficients a and b around the transition temperature as the theory is by construction only valid in this region. In order to do so, define

$$\tau = (T - T_c)/T_c \tag{2.19}$$

which is constructed as a dimensionless measure for the distance from the transition with τ negative below T_c, while positive above. Since the Ginzburg-Landau theory is only valid for small $|\tau|$, both a and b can be expressed in terms of τ to first order. This gives $a = a_0\tau$ with $a_0 > 0$ and $b \approx b\,(T_c) > 0$. The latter statement follows from the fact that the finite b does not change sign, and can therefore not have a first order τ dependence.

Consider the total free energy density of the system as obtained via Eq. (2.14):

$$f_s = f_n + f\,(\mathbf{r}) \tag{2.20}$$

Compare this to Eq. (2.12), where the value of $f\,(r)$ for the bulk superconducting state is given by Eq. (2.18). Thus, one obtains for the critical magnetic field

$$f_n - f_s = \frac{H_c^2}{8\pi} = \frac{a_0^2\tau^2}{2b}. \tag{2.21}$$

2.2.2 The Ginzburg-Landau equations at zero external field

In the previous section the external magnetic field was ignored and only the bulk of the superconductor was described. In other words, $\mathbf{H} = \mathbf{0}$, $\mathbf{B} = \mathbf{0}$ due to a complete Meissner effect and no spatial variation in ψ was considered. In order to describe the superconductor outside of its bulk, one must take a spatial variation in $\psi(\mathbf{r})$ into account and allow $\mathbf{B} \neq 0$. In this section this scenario will be considered, still in the absence of an external magnetic field, thus $\mathbf{H} = \mathbf{0}$. $\mathbf{H} = \mathbf{0}$ does not imply $\mathbf{B} = \mathbf{0}$ since the presence of any currents (not due to an external magnetic field) in the superconductor would induce a magnetic field, meaning $\mathbf{B} \neq \mathbf{0}$, see Eq. (2.2).

Assuming that the spatial variation of ψ is slow, meaning only the lowest order in $|\nabla\psi|$ is considered, one has

$$f = a\,|\psi|^2 + \frac{1}{2}b\,|\psi|^4 + \gamma\,|\nabla\psi|^2 + \ldots\,. \tag{2.22}$$

Inspired by the notion that superconductivity is a macroscopic quantum phenomena, Ginzburg and Landau viewed the order parameter as a wave function for a ‘particle’[3] with charge e^* and mass m^*[14]. Thus they postulated that, in the presence of a magnetic field

$$\mathbf{B} = \nabla \times \mathbf{A}, \tag{2.23}$$

Eq. (2.22) becomes

$$f = a_0\tau\,|\psi|^2 + \frac{1}{2}b\,|\psi|^4 + \frac{1}{2m^*}\left|\left(-i\hbar\nabla - \frac{e^*}{c}\mathbf{A}\right)\psi\right|^2 + \frac{B^2}{8\pi}, \tag{2.24}$$

where $B^2/8\pi$ is the magnetic energy per unit volume. In other words the vector potential is added as in the Schrödinger equation, i.e. by means of minimal substitution $-i\hbar\nabla \rightarrow -i\hbar\nabla - e^*\mathbf{A}/c$. Under the gauge transformation $\mathbf{A} \rightarrow \mathbf{A} + \nabla\Lambda$ the order parameter transforms as $\psi \rightarrow \exp(ie^*\Lambda/\hbar c)\psi$ so that f is gauge invariant.

Finally, in order to obtain the Ginzburg-Landau differential equations the total free energy must be stationarized:

$$\delta F = \int d^3r \left\{ \frac{\delta F}{\delta\psi(\mathbf{r})}\delta\psi(\mathbf{r}) + \frac{\delta F}{\delta\mathbf{A}(\mathbf{r})}\cdot\delta\mathbf{A}(\mathbf{r}) \right\} = 0. \tag{2.25}$$

By minimizing the free energy with respect to ψ^* (or ψ - this simply gives the complex

[3]The wave function turned out to be the wave function of a Cooper pair, in which case $e^* = 2e$ and $m^* = 2m$ approximately.

conjugate of the result), one finds in the interior[14]

$$\frac{1}{2m^*}\left(-i\hbar\nabla - \frac{e^*}{c}\mathbf{A}\right)^2\psi + a_0\tau\psi + b\left|\psi\right|^2\psi = 0, \tag{2.26}$$

reminiscent of a Schrödinger equation, but with the important difference that it includes a non-linear term in ψ. On the boundary between the superconductor and vacuum (or an insulator) one finds

$$\mathbf{n}\cdot\left(-i\hbar\nabla - \frac{e^*}{c}\mathbf{A}\right)\psi\Big|_{Surface} = 0, \tag{2.27}$$

where $\mathbf{n}$ is the normal vector to the surface, S.

By minimizing the free energy with respect to $\mathbf{A}$, one finds

$$\nabla\times\mathbf{B} = \frac{4\pi}{c}\mathbf{j}_{ind} \tag{2.28}$$

with gauge invariant current

$$\mathbf{j}_{ind} = \frac{e^*\hbar}{2m^*i}\left(\psi^*\nabla\psi - \psi\nabla\psi^*\right) - \frac{e^{*2}}{m^*c}\left|\psi\right|^2\mathbf{A}, \tag{2.29}$$

and a boundary condition on the surface of the superconductor

$$\mathbf{n}\times\mathbf{B}|_{Surface} = \mathbf{0}. \tag{2.30}$$

From the expression for j_{ind} it is seen that the boundary condition given in Eq. (2.27) ensures that j_{ind} at the boundary does not have a component parallel to $\mathbf{n}$. This means that no currents leave the superconductor and thus the charge associated with j_{ind} is conserved. The second boundary condition corresponds to a continuity-like equation. From standard electrodynamics one has that $\mathbf{B}^{\perp} = 0$ and from Eq. (2.30) one has that $\mathbf{B}^{||} = 0$. Thus, at the boundary of the superconductor the $\mathbf{B}$ field must be equal to zero, which in this case is also the field outside of the superconductor as $\mathbf{H}$ is set to zero. These differential equations are known as the Ginzburg-Landau equations.

In order to obtain the minimum free energy of the system one must substitute the solutions for ψ and $\mathbf{A}$ which minimizes the free energy, back into the expression for the free energy. This was the strategy to obtain Eq. (2.18) for the minimum free energy of the bulk superconducting state. One knows that the solutions for ψ and $\mathbf{A}$ that minimize the free energy must obey Eq. (2.26). One can therefore rather substitute Eq. (2.26) into the expression for the free energy, Eq. (2.24). In doing so one obtains

$$F = F_n + \int \left(\frac{B^2}{8\pi} - \frac{1}{2} b \left|\psi\right|^4 \right) d^3 r. \tag{2.31}$$

The Meissner effect, the phenomenon of a zero magnetic field inside the bulk of the superconductor, can easily be seen in this construction of the free energy density. By comparing Eq. (2.31) to the minimum free energy of the bulk superconducting state as obtained by substituting Eq. (2.18) into Eq. (2.14):

$$F_s = F_n + \int \left(-\frac{1}{2} b \left|\psi_0\right|^4 \right) d^3 r, \tag{2.32}$$

it clearly shows that in the bulk of the superconducting state $\mathbf{B}$ is set to be zero.

2.2.3 The Ginzburg-Landau equations at a finite external field

The Ginzburg-Landau equations can also be constructed for a non-zero external magnetic field: $\mathbf{H} \neq 0$. Now one considers the minimization of the free enthalpy, obtained by performing a Legendre transformation on the free energy

$$G = F - \frac{1}{4\pi} \int d^3 r \mathbf{B}\left(\mathbf{r}\right) \cdot \mathbf{H}\left(\mathbf{r}\right). \tag{2.33}$$

The condition $\delta G = 0$, or $\partial G / \partial \psi = \partial G / \partial a = 0$, yields the same equations for the interior[4] of the superconductor as given by the Ginzburg-Landau differential equations, namely Eqs. (2.26) and (2.28-2.29). The boundary condition from Eq. (2.27) also remains unchanged. However, the continuity-like boundary condition given in Eq. (2.30) does alter in such a way as to remain continuity-like

$$\mathbf{n} \times \left(\mathbf{B} - \mathbf{H}\right)\big|_S = \mathbf{0}. \tag{2.34}$$

This forces $\mathbf{B}^{||} = \mathbf{H}^{||}$, while from standard electrodynamics one has again that $\mathbf{B}^{\perp} = \mathbf{H}^{\perp}$, which means that at the boundary of the superconductor one has indeed that the field is continuous.

Analogous to Eq. (2.31), one has for the free enthalpy

$$G = F_n + \int \left(\frac{\left(\mathbf{B} - \mathbf{H}\right)^2}{8\pi} - \frac{1}{2} b \left|\psi\right|^4 - \frac{H^2}{8\pi} \right) d^3 r, \tag{2.35}$$

from Eq. (2.33).

[4]In the interior of the macroscopic body within the external magnetic field one has $j_{ext} = 0$, which means that $j = j_{ext} + j_{ind} = j_{ind}$.

2.2.4 The natural length scales

In section 2.2.1 one considers only the free energy of the bulk of the superconductor. This corresponds to choosing the order parameter as homogeneous and setting $\mathbf{A} = \mathbf{0}$ in the general expression for the free energy given in Eq. (2.24). In the superconducting state, but outside of the bulk, both the order parameter and $\mathbf{A}$ (and therefore the induced magnetic field, $\mathbf{B}$) are no longer constants. A natural length scale is associated to each of the spatial variations in order parameter and $\mathbf{A}$ respectively, the latter having the same natural length scale as the induced magnetic field, $\mathbf{B}$ by Eq. (2.23).

2.2.4.1 The coherence length

In order to determine the length scale associated with the order parameter, assume that the spatial variation of the order parameter is slow compared to that of $\mathbf{A}$. This implies that at some point one has $\mathbf{A} = \mathbf{0}$, while the order parameter is not yet $\psi = \psi_0$ as given in Eq. (2.17).

Specifically, consider the situation where the order parameter is real and only depends on one coordinate[5], $\psi(\mathbf{r}) = \psi(z)$, and $\mathbf{A} = \mathbf{0}$. Let $z > 0$ be a superconducting half space and $z < 0$ be a normal half space with $\psi(z \leq 0) = 0$. Thus, $\psi(z \to \infty) \to \psi_0$ in the bulk. In order to analyze the order parameter in the superconducting half space, consider the first Ginzburg-Landau equation, Eq. (2.26), which simplifies to give

$$-\frac{\hbar^2}{2m^*}\frac{d^2\psi}{dz^2} + a_0\tau\psi + b|\psi|^2\psi = 0. \tag{2.36}$$

It is easier to solve this differential equation in dimensionless form, thus define $v = \psi/\psi_0$. The above equation now reads, after dividing by $-a_0\tau$ on both sides

$$\frac{\hbar^2}{2m^*a_0\tau}\frac{d^2v}{dz^2} - v + v^3 = 0. \tag{2.37}$$

By redefining the length scale $x = z/\xi$, with

$$\xi = \frac{\hbar}{\sqrt{2m^*a_0|\tau|}} \tag{2.38}$$

one can now write the differential equation in a completely dimensionless form

$$-\frac{d^2v(x)}{dx^2} - v + v^3 = 0, \tag{2.39}$$

where $\psi(z) = \psi_0 v(z/\xi)$.

[5] The validity of this assumption will be discussed in section 2.3

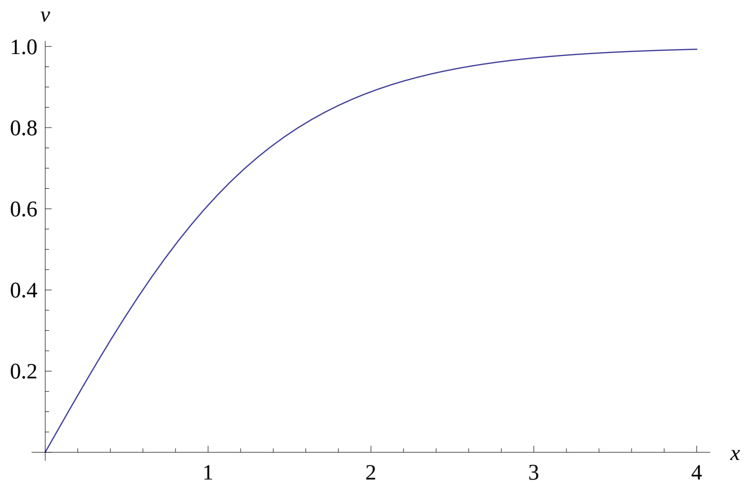

Figure 2.1: The dimensionless order parameter $v = \psi/\psi_0$ as a function of the dimensionless unit $x = z/\xi$ in the superconducting half-space as given by Eq. (2.40).

This differential equation can be solved analytically by keeping in mind that $v\,(x \to \infty) = 1$ and $v'\,(x \to \infty) = 0$, and that one is interested in a solution where $dv/dx > 0$. The solution for v is

$$v\,(x) = \tanh\left(\frac{x}{\sqrt{2}}\right) \tag{2.40}$$

as demonstrated in Fig. (2.1). In the original variables, this then reads

$$\psi\,(z) = \psi_0 \tanh\left(\frac{z}{\sqrt{2}\xi}\right). \tag{2.41}$$

This equation shows explicitly that ψ varies on a natural length scale ξ, which is called the coherence length.

2.2.4.2 The magnetic penetration depth - the London limit

In order to obtain the natural length scale on which $\mathbf{A}$ and also $\mathbf{B}$ vary, one considers the London limit, named after the brothers Fritz and Heinz London who published the work in 1935. The London limit refers to the case where $\psi\,(\mathbf{r}) = \psi_0 = const$, while $\mathbf{A} \neq \mathbf{0}$ in the superconducting half space as defined in the previous section. This corresponds to the opposite scenario as discussed previously: the spatial variation of the order parameter is now considered faster than that of $\mathbf{A}$, meaning that there is a point at which the order parameter has reached its bulk value, but $\mathbf{A}$ is not yet zero.

From the Ginzburg-Landau equations, specifically Eq. (2.29), one has that

$$\mathbf{j}_{ind} = -\frac{e^{*2}}{m^* c}\psi_0^2 \mathbf{A} \tag{2.42}$$

By taking the curl on both sides, this yields

$$\nabla \times \mathbf{j}_{ind} = -\frac{e^{*2}}{m^* c}\psi_0^2 \mathbf{B}, \tag{2.43}$$

which is, from Eq. (2.28), equivalent to

$$\nabla \times \nabla \times \mathbf{B} = -\frac{4\pi e^{*2}}{m^* c^2}\psi_0^2 \mathbf{B}. \tag{2.44}$$

Since $\nabla \cdot \mathbf{B} = \mathbf{0}$, this equation simplifies to the London equation:

$$\nabla^2 \mathbf{B} = \frac{4\pi e^{*2}}{m^* c^2}\psi_0^2 \mathbf{B}. \tag{2.45}$$

This is a well known differential equation and has the solution

$$\mathbf{B}(z) = \mathbf{B}(0) \exp(-z/\lambda) \tag{2.46}$$

with $\lambda^{-2} = \frac{4\pi e^{*2}}{m^* c^2}\psi_0^2$. Thus,

$$\lambda = \sqrt{\frac{m^* c^2 b}{4\pi e^{*2} a_0 |\tau|}}, \tag{2.47}$$

which is known as the penetration depth of the magnetic field into a superconductor. Eq. (2.46) shows the Meissner effect: the magnetic field decays exponentially from the surface of the superconductor to give a zero magnetic field in the bulk of the superconductor, as can be seen from Fig. (2.2).

2.2.4.3 The dimensionless number, κ

In each of the previous two cases a characteristic length scale was defined. The order parameter varies on the length scale $\xi(T)$, while the magnetic field varies on the length scale $\lambda(T)$. The ratio of these two length scales give the dimensionless number

$$\kappa = \frac{\lambda}{\xi} = \sqrt{\frac{b}{2\pi}}\frac{m^* c}{\hbar e^*}. \tag{2.48}$$

In the derivation for ξ, one assumed $\mathbf{A} = 0$ while the order parameter varied. This description

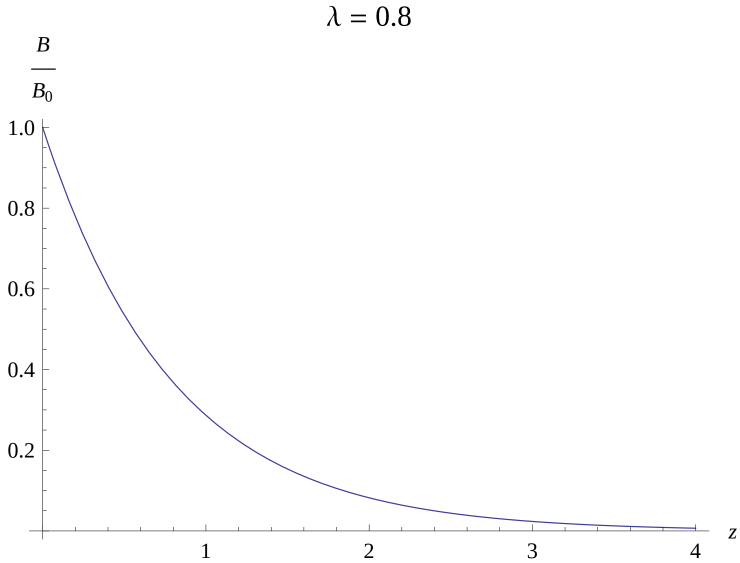

Figure 2.2: The decay of the normalized B field inside the superconducting half-space, as given by Eq. (2.46) with $\lambda = 0.8$.

fits a small κ scenario: at some point the magnetic field would have reached zero while the order parameter is not yet at its bulk value ψ_0. Thus, the order parameter varies on a greater scale than the magnetic field inside the superconductor. The London limit on the other hand corresponds to a large κ value where the penetration depth is greater than the coherence length.

2.3 The interface energy

In the previous section on natural length scales, section 2.2.4, the effect of a adjacent normal state on the induced magnetic field, $\mathbf{B}$, and the order parameter, ψ, in the superconducting state was discussed. In this section, the setup of a coexisting normal state and a superconducting state is formalized and the energy associated to an interface between these two states is discussed.

Consider again the setup as defined previously: let $z > 0$ be the superconducting half space and $z < 0$ be the normal half space. The two states coexist in the presence of a specific external magnetic field, $\mathbf{H}_c$ so that the enthalpies of the two states equate. This was discussed previously in section 2.1. As before one assumes cylindrical symmetry allowing one the following, as demonstrated in Fig. 2.3:

$$\mathbf{B}\left(\mathbf{r}\right) = B\left(z\right)\mathbf{e}_x \tag{2.49}$$

and

$$\psi\left(\mathbf{r}\right) = \psi\left(z\right)e^{i\varphi(\mathbf{r})} \tag{2.50}$$

with real function $\psi\left(z\right)$.

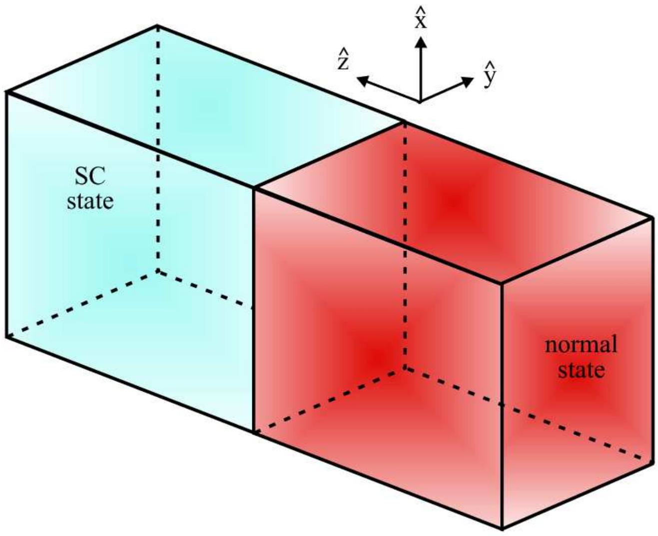

Figure 2.3: Schematic representation of the setup that results in an interface between a normal and a superconducting state.

To determine the current induced, $\mathbf{j}_{ind}$, one can use Eq. (2.28) for the superconducting half space at zero field. This gives

$$\frac{4\pi}{c}\mathbf{j}_{ind} = \nabla \times \mathbf{B} = \mathbf{e}_y \frac{\partial B(z)}{\partial z}. \tag{2.51}$$

The current direction is clearly along the y-axis and only depends on z, thus $\mathbf{j}_{ind}(\mathbf{r}) = j(z)\,\mathbf{e}_y$. This expression for $\mathbf{j}_{ind}$ can be compared with Eq. (2.29) for $\mathbf{j}_{ind}$, which in this symmetrical setup reads

$$\mathbf{j}_{ind} = \frac{e^*\hbar}{m^*}|\psi|^2\left(\frac{\partial\varphi}{\partial x}\mathbf{e}_x + \frac{\partial\varphi}{\partial y}\mathbf{e}_y + \frac{\partial\varphi}{\partial z}\mathbf{e}_z\right) + \frac{e^{*2}}{m^*c}|\psi|^2 A(z)\,\mathbf{e}_y. \tag{2.52}$$

Since $\mathbf{j}_{ind}$ can only be along the y direction, it must hold that $\frac{\partial\varphi}{\partial x} = \frac{\partial\varphi}{\partial z} = 0$, while $\varphi(y)$ must be linear in y to ensure that $\frac{\partial\varphi(y)}{\partial y}$ is independent of y.

This information can be used to eliminate the complex phase of the order parameter in the Ginzburg-Landau equations, which simplifies further analysis of the problem considerably. In order to obtain the Ginzburg-Landau equations with only a real ψ, the following gauge transformation is necessary

$$\mathbf{A}' = \mathbf{A} + \frac{\hbar c}{e^*}\nabla\varphi = \mathbf{A} + \frac{\hbar c}{e^*}\frac{\partial\varphi}{\partial y}\mathbf{e}_y. \tag{2.53}$$

Inserting $\mathbf{A}'$ instead of $\mathbf{A}$ into the Ginzburg-Landau equations, Eqs. (2.26), (2.28) and (2.29), one indeed eliminates φ to obtain the new form of the Ginzburg-Landau equations:

$$\begin{aligned} \frac{\hbar^2}{2m^*}\frac{d^2\psi}{dz^2} &= a_0\tau\psi + b\psi^3 + \frac{e^{*2}}{2m^*c^2}\,A^2\psi \\ \frac{\partial B(z)}{\partial z} &= \frac{4\pi e^{*2}}{m^*c^2}\,|\psi|^2\,A(z) \end{aligned} \tag{2.54}$$

where now $\psi = \psi(z)$ is a real function. The boundary conditions are

$$\psi(z \to -\infty) = 0 \text{ and } \psi(z \to \infty) = \psi_0 \tag{2.55}$$

as well as

$$B(z \to -\infty) = H_c \text{ and } B(z \to \infty) = 0 \tag{2.56}$$

The condition $B(z \to -\infty) = H_c$ ensures that the interface is between two states that have same bulk free energy. The important conclusion here is that the order parameter can be taken as real $\psi(\mathbf{r}) = \psi(z)$ in the specific gauge where $\mathbf{A}$ is in the form $\mathbf{A}(\mathbf{r}) = -A(z)\,\mathbf{e}_y$. Using Eq. (2.23) this means

$$B(z) = \frac{\partial A(z)}{\partial z}. \tag{2.57}$$

The free energy can now also be written as a function of a real ψ. From Eq. (2.14) and Eq. (2.24) one has for the free energy associated with the superconducting state

$$F_s = F_n + L^2\int\left(a_0\tau\psi^2 + \frac{1}{2}b\psi^4 + \frac{\hbar^2}{2m^*}\left(\frac{d\psi}{dz}\right)^2 + \frac{e^{*2}\psi^2}{2m^*c^2}A^2 + \frac{B^2}{8\pi}\right)dz. \tag{2.58}$$

After applying the Legendre transformation to account for the externally applied field, the free enthalpy is given by

$$G_s = F_n + L^2\int\left(a_0\tau\psi^2 + \frac{b}{2}\psi^4 + \frac{\hbar^2}{2m^*}\left(\frac{d\psi}{dz}\right)^2 + \frac{e^{*2}A^2\psi^2}{2m^*c^2} + \frac{(B-H_c)^2}{8\pi} - \frac{H_c^2}{8\pi}\right)dz. \tag{2.59}$$

The free enthalpy for the normal state, where $\psi = 0$ and $\mathbf{B} = \mathbf{H} = \mathbf{H}_c$, is from Eq. (2.35)

$$G_n = F_n - L^2\int\frac{H_c^2}{8\pi}dz. \tag{2.60}$$

The energy associated to the interface between the two states is given by the difference in the enthalpies of the individual states

$$\Sigma\left[\psi, A\right] = \int \left(a_0 \tau \psi^2 + \frac{b}{2}\psi^4 + \frac{\hbar^2}{2m^*}\left(\frac{d\psi}{dz}\right)^2 + \frac{e^{*2}A^2\psi^2}{2m^*c^2} + \frac{(B-H_c)^2}{8\pi} \right) dz. \tag{2.61}$$

As with the free energy expressions, this functional has to be minimized with respect to both functions ψ and $\mathbf{A}$ to yield the value for the interface energy σ_s.

2.3.1 Dimensionless units

In order to simplify the minimization calculation, the functional can be simplified further by writing it in dimensionless form. To do so, define the following dimensionless units

$$v = \frac{\psi}{\psi_0},\ \beta = \frac{B}{\sqrt{2}H_c},\ \text{and } t = \frac{z}{\lambda}, \tag{2.62}$$

with the corresponding dimensionless vector potential

$$\alpha = \frac{A}{\sqrt{2}H_c\lambda}, \tag{2.63}$$

which means $\beta = \partial\alpha/\partial t$.

In these dimensionless units the Ginzburg-Landau equations from Eq. (2.54) now read

$$\begin{aligned} \kappa^{-2}\frac{d^2v}{dt^2} &= -v + v^3 + \alpha^2 v \\ \frac{\partial^2\alpha}{\partial t^2} &= v^2\alpha, \end{aligned} \tag{2.64}$$

while the surface energy functional reads

$$\Sigma\left[v, \alpha\right] = \frac{H_c^2\lambda}{4\pi}\int \left(-v^2 + \frac{1}{2}v^4 + \frac{1}{\kappa^2}\left(\frac{dv}{dt}\right)^2 + v^2\alpha^2 + \frac{1}{2}\left(\sqrt{2}\frac{\partial\alpha}{\partial t} - 1\right)^2 \right) dt. \tag{2.65}$$

This functional and the minimization thereof clearly only depend on a single variable, namely κ. The interface energy, σ_s, will therefore be in the form

$$\sigma_s = \lambda\frac{H_c^2}{4\pi}\Upsilon\left(\kappa\right), \tag{2.66}$$

where $\Upsilon\left(\kappa\right)$ is a dimensionless function that depends only on κ.

The variations $\delta\Sigma/\delta v = 0$ and $\delta\Sigma/\delta\alpha = 0$ again yield the equations Eq. (2.64). By substituting these differential equations back into the interface energy function, one will obtain the actual value for σ_s. Alternatively, one can rewrite the enthalpy at the minimum for both the superconducting state and the normal state in dimensionless units and take the difference. For this problem Eq. (2.35) in dimensionless units reads

$$G_s = F_n + \lambda \frac{H_c^2}{8\pi} L^2 \int dt \left(\sqrt{2}\beta_{min} - 1\right)^2 - v_{min}^4 - 1, \tag{2.67}$$

while Eq. (2.60) for the normal state gives in dimensionless units

$$G_s = F_n - \lambda \frac{H_c^2}{8\pi} L^2 \int 1\, dt. \tag{2.68}$$

The difference then gives

$$\sigma_s = \lambda \frac{H_c^2}{8\pi} \int \left(\left(\sqrt{2}\beta_{min}\left(t\right) - 1\right)^2 - v_{min}\left(t\right)^4 \right) dt, \tag{2.69}$$

where both v_{min} and β_{min} are here the solutions to the differential equations or the minimization of the functional as a function of κ, still to be obtained.

If the value of σ_s is positive it means that energy is required to form these interfaces or domain walls. The lowest energy state of the system would therefore not include any such domain walls. Superconductors with this property are referred to as type-I superconductors. If σ_s is negative however, it would be advantageous for the system to have domain walls as this would lower the total energy. This leads to a vortex lattice within the superconductor[8]. Such superconductors are referred to as type-II superconductors.

At this point it may be worthwhile to make a few remarks regarding geometrical aspects in this theory. In order to derive the expression for the interface energy, Eq. (2.69), the assumption was made that one is dealing with cylindrical geometry. The interface thus corresponds to a separating plane. For a type-I superconductor this assumption is plausible as one is dealing with two adjacent homogeneous states. However, in a type-II superconductor, the mixed state is not homogeneous and the geometry of an interface is much more complex[8]. Even a single vortex - which is in some sence an interface loop - is more involved.

However, the assumption of cylindrical geometry in the GL theory for interfaces serves as an excellent tool in order to classify materials as either type-I or type-II. A method which is in complete agreement with experimental observations.

2.3.2 Analysis of special cases

Obtaining the functions v and β which will minimize the interface functional for any given value of κ is not possible analytically. However, it is possible to minimize $\Sigma[v, \alpha]$ analytically for the two extrema of κ. These calculations will be given in this section along with further properties of σ_s.

2.3.2.1 The limit $\kappa \ll 1$

In the limit $\kappa = \lambda/\xi \ll 1$ the penetration depth, λ, is considered very small and one can therefore assume $a = 0$ in the superconducting half space. The dimensionless Ginzburg-Landau equations, Eqs. (2.64) in this limit give

$$\kappa^{-2}\frac{d^2v}{dt^2} = -v + v^3. \tag{2.70}$$

This is the same problem that was solved in section 2.2.4.1. The solution in dimensionless units is

$$v(t) = \tanh\left(\frac{t\kappa}{\sqrt{2}}\right). \tag{2.71}$$

Defining $s = t\kappa/\sqrt{2}$, the interface energy is given by Eq. (2.69),

$$\begin{aligned}\sigma_s &= \frac{H_c^2}{8\pi}\lambda\frac{\sqrt{2}}{\kappa}\int_0^\infty \left(1 - \tanh^4(s)\right) ds \\ &= \frac{H_c^2}{8\pi}\xi\sqrt{2}\frac{4}{3} \simeq 1.8856 \times \xi\frac{H_c^2}{8\pi}.\end{aligned} \tag{2.72}$$

Thus $\sigma_s(\kappa \ll 1) > 0$, which means type-I behaviour, and the homogeneous solution is stable against domain walls.

2.3.2.2 The limit $\kappa \gg 1$

In the limit $\kappa \gg 1$ the term $\kappa^{-2}d^2v/dt^2$ can be neglected in Eq. (2.64). This gives the dimensionless Ginzburg-Landau equations, from Eqs. (2.64)

$$\begin{aligned}0 &= -v + v^3 + \alpha^2 v \\ \frac{\partial^2\alpha}{\partial t^2} &= v^2\alpha.\end{aligned} \tag{2.73}$$

This limit reminds rather of the London limit, as discussed in section (2.2.4.2), where $v = 1$ was taken as a constant. The London limit is however not completely correct as there is a subtlety that requires some care: v can not be taken as a constant in a region where β changes. A spatial variation in β means a spatial variation in α which in turn requires a spatial variation in v from the first line in Eq. (2.73).

However, even without v as a constant, σ_s can be solved analytically. Rewrite Eq. (2.73) in terms of β using $\beta(t) = \frac{d\alpha}{dt}$. After some simple rearrangement this gives

$$\left(\frac{d\beta}{dt}\right)^2 = v^4\left(1 - v^2\right), \tag{2.74}$$

along with

$$\beta = \frac{d}{dt}\left(v^{-2}\frac{d\beta}{dt}\right) = -\frac{d}{dt}\left(1 - v^2\right)^{1/2}. \tag{2.75}$$

In combination this gives

$$\begin{aligned}\frac{d^2}{dt^2}\left(1 - v^2\right)^{1/2} &= v^2\left(1 - v^2\right)^{1/2} \\ &= \left(1 - v^2\right)^{1/2} - \left(1 - v^2\right)^{3/2},\end{aligned} \tag{2.76}$$

By substituting $u = \left(1 - v^2\right)^{1/2}$, which means $\beta = -\frac{du}{dt}$ from Eq. (2.75), the above equation reads

$$\frac{d^2u}{dt^2} = u - u^3. \tag{2.77}$$

Integrating gives

$$\left(\frac{du}{dt}\right)^2 = u^2 - \frac{u^4}{2} + C \tag{2.78}$$

where $C = 0$ since at $t \to \infty$ one expects $u = 0$ and $du/dt = 0$. Thus

$$\frac{du}{dt} = -u\sqrt{1 - \frac{u^2}{2}} \tag{2.79}$$

since $du/dt < 0$.

This is already sufficient to determine σ_s. Starting from Eq. (2.69), one has

$$\begin{aligned}\sigma_s &= \lambda\frac{H_c^2}{8\pi}\int\left(\left(\sqrt{2}\beta(t) - 1\right)^2 - v(t)^4\right)dt \\ &= \lambda\frac{H_c^2}{4\pi}\int_0^1\left(2u\sqrt{1 - \frac{u^2}{2}} - \sqrt{2}\right)du \\ &= -\frac{8}{3}\left(\sqrt{2} - 1\right)\lambda\frac{H_c^2}{8\pi} \simeq -1.10457\lambda\frac{H_c^2}{8\pi}.\end{aligned} \tag{2.80}$$

This, and not the London limit, is the correct result[6] for the interface energy for large κ.

[6]However, the London limit gives the correct sign as it predicts $\sigma_s = -\frac{3}{2}\lambda\frac{H_c^2}{8\pi}$.

As $\sigma_s (\kappa \gg 1) < 0$ the superconductor is of type-II.

With regards to Eq. (2.66),

$$\sigma_s = \lambda \frac{H_c^2}{4\pi} \Upsilon(\kappa), \tag{2.81}$$

the result from this section together with the result from the previous section yields for $\Upsilon(\kappa)$

$$\Upsilon(\kappa) = \begin{cases} \frac{2^{3/2}}{3}\kappa^{-1} & \text{if } \kappa \ll 1 \\ -\frac{4}{3}\left(\sqrt{2}-1\right) & \text{if } \kappa \gg 1. \end{cases} \tag{2.82}$$

2.3.2.3 The point $\sigma_s = 0$

From the previous two sections it is known that σ_s is positive for small values of κ and negative for large values of κ. In order to identify where the interface energy changes sign, consider the point(s) where $\sigma_s = 0$. Keeping in mind that $\frac{d\beta}{dt} < 0$ and $\frac{dv}{dt} > 0$, Eq. (2.69) gives the following for the null point(s)

$$\beta = \frac{1}{\sqrt{2}}\left(1 - v^2\right). \tag{2.83}$$

Taking derivatives one finds

$$\begin{aligned} \frac{d\beta}{dt} &= -\sqrt{2} v \frac{dv}{dt}, & (2.84) \\ \frac{d^2\beta}{dt^2} &= -\sqrt{2}\left(\frac{dv}{dt}\right)^2 - \sqrt{2} v \frac{d^2 v}{dt^2}. & (2.85) \end{aligned}$$

Substituting the equations above into the two dimensionless Ginzburg-Landau equations, Eqs. (2.64), and using the definition of $\beta = d\alpha/dt$, one obtains two expressions. From the first equation one obtains

$$\begin{aligned} \kappa^{-2}\frac{d^2 v}{dt^2} &= -v + v^3 + v^{-3}\left(\frac{d\beta}{dt}\right)^2 \\ &= -v + v^3 + \frac{2}{v}\left(\frac{dv}{dt}\right)^2, & (2.86) \end{aligned}$$

and from the second

$$\begin{aligned} \beta &= \frac{d}{dt}\left(v^{-2}\frac{d\beta}{dt}\right) \\ &= -\frac{2}{v^3}\frac{dv}{dt}\frac{d\beta}{dt} + \frac{1}{v^2}\frac{d^2\beta}{dt^2}, & (2.87) \end{aligned}$$

which, after substituting away β with Eqs. (2.85), gives

$$2\frac{d^2v}{dt^2} = -v + v^3 + \frac{2}{v}\left(\frac{dv}{dt}\right)^2. \tag{2.88}$$

By comparing the last equation to the first equation obtained, the value for κ_c must be

$$\kappa_c = \frac{1}{\sqrt{2}}. \tag{2.89}$$

2.3.2.4 Proof of $d\sigma_s/d\kappa < 0$.

The result above gives a single value for κ at which the interface energy is zero. In principle more such points could exist between the two κ extremes. By analyzing the gradient of σ_s with respect to κ, it is possible to show that $\kappa_c = 1/\sqrt{2}$ is the only value for which $\sigma_s = 0$.

First consider the variation of κ in the functional $\Sigma\left[v, \alpha\right]$ as given in Eq. (2.65)

$$\frac{d\Sigma}{d\kappa} = -\frac{H_c^2\lambda}{2\pi\kappa^3}\int\left(\frac{dv}{dt}\right)^2 dt + \int dt\left(\frac{\delta\Sigma}{\delta v\left(t\right)}\frac{\partial v\left(t\right)}{\partial\kappa} + \frac{\delta\Sigma}{\delta\alpha\left(t\right)}\frac{\partial\alpha\left(t\right)}{\partial\kappa}\right). \tag{2.90}$$

The second integral vanishes for the minimum of the interface energy, which gives σ_s, thus

$$\frac{d\sigma_s}{d\kappa} = -\frac{H_c^2\lambda}{2\pi\kappa^3}\int\left(\frac{dv}{dt}\right)^2 dt < 0, \tag{2.91}$$

which shows a strictly decreasing trend for the interface energy allowing for only a single value at which $\sigma_s = 0$.

CHAPTER 3
Experimental overview of two-band superconductors

In the previous chapter the Ginzburg-Landau theory as applicable to one-band superconductors was given. Before presenting an extension of the theory which would apply to two-band superconductors, first consider the experimental evidence for the existence of such two-band superconductors.

The Fermi surface of a traditional one-band superconductor consists of only one sheet with a single energy gap, Δ. From BSC theory, a simple relation between the gap[7] 2Δ and the order parameter ψ was found: $\Delta \propto \psi$. Thus, there is a relation between the Fermi surface of a superconductor and the order parameter in the Ginzburg-Landau theory as presented previously.

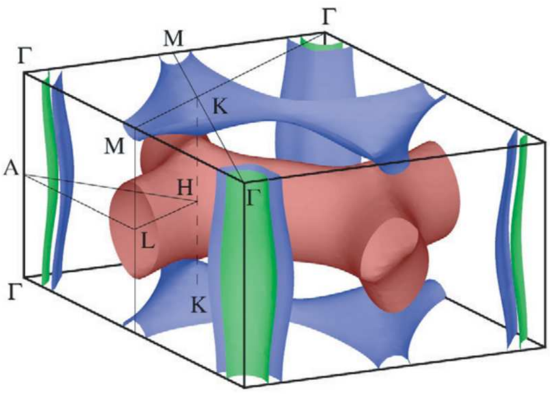

(a) The Fermi surface of MgB_2 from band structure calculation. Green and blue cylinders (hole-like) are the σ bands, and the blue (hole-like) and the red (electron-like) tubular networks are the π bands. A different energy gap is associated to each band. Taken from Kortus *et al.*[15]

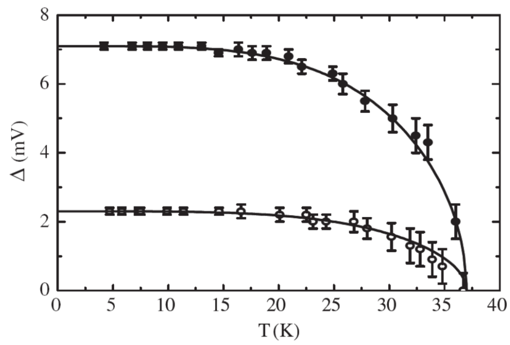

(b) Values for the two gaps in MgB_2 extracted from the scanning tunneling spectroscopy as a function of temperature. The lines are the BCS predictions. Taken from M. Iavarone *et al.*[20].

Figure 3.1: Experimental evidence for MgB_2 as a two-band superconductor.

However, the Fermi surface of many superconductors consists of two or more well separated sheets. Associated to these multiple sheets are multiple bands, with each band in turn corresponding to a different energy gap $2\Delta_i$.[4, 5] As stated before, the gap and the order parameter are closely related, thus in the case of n bands, one needs to include n order parameters in the GL theory.

An example of such separated sheets in the Fermi surface can be seen in the recently discovered

[7] The energy gap refers to the energy required, by convention 2Δ, between the ground state and the first excited states.

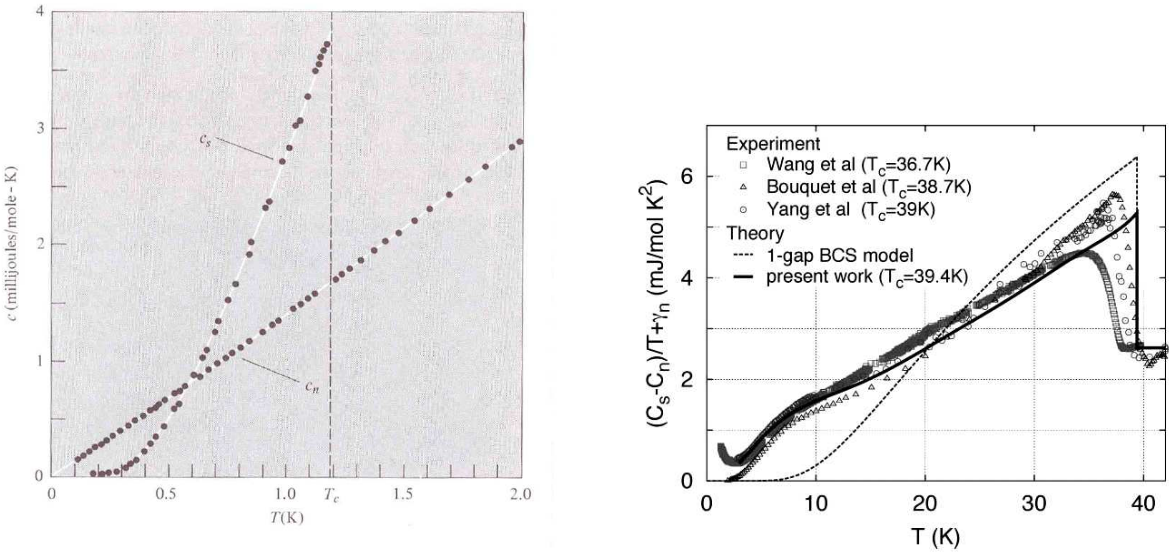

(a) Heat capacity measurements for Aluminium, a one-band superconductor, at low temperature. In the superconducting state, thus below T_c, the heat capacity measurements are denoted by c_s. In the normal state the measurements are denoted by c_n. The normal state below T_c is created by applying a weak magnetic field to destroy the superconducting ordering, but has only a negligible effect on the heat capacity measurements. Taken from Ref. [30].

(b) Heat capacity measurements for MgB_2 as obtained by various research groups, each with different samples of MgB_2. The critical temperatures of all the samples are in close proximity to the theoretically predicted value. The heat capacity data is shown along side the theoretical prediction for heat capacities in a one-band superconductor as well as a two-band superconductor. This clearly shows that MgB_2 has a two-band nature. Taken from Ref. [29].

Figure 3.2: A comparison in experimental heat capacity measurements for MgB_2 and theoretically predicted heat-capacity measurements for both one-band and two-band superconductors.

two-band superconductor MgB_2[15, 16, 17, 18, 19] as illustrated in Fig. 3.1(a). Here there are two distinct bands, each with a unique energy gap, Δ_1 and Δ_2.

The two-band superconducting nature of MgB_2 is also evident from tunneling spectroscopy[20, 21, 22], point contact spectroscopy[23, 24] and heat capacity measurements[25, 26, 27]. All these experiments give clear evidence for two-band superconductivity in MgB_2 with gaps $\Delta_1 \simeq 7.1\,\mathrm{meV}$ and $\Delta_2 \simeq 2.3\,\mathrm{meV}$ as presented in Fig. 3.1(b)[20].[8] (for recent reviews, see Refs. [28] and [29]).

Consider the results of heat capacity experiments on one-band superconductors. Both the analytic and the experimental observations are given in Fig. 3.2(a). From the plot it is clear that above the critical temperature, but still at low temperature, the heat capacity is dominated by a term linear in temperature. Below the critical temperature, and in the superconducting state, one has the form $\exp(-\Delta/k_bT)$. In this region the curve is thus determined by the value

[8] These values are still under some dispute as different values for the gap energy have been obtained in other research groups. However, the values only differ from the second decimal onward.

of the one-band superconducting gap, Δ.

Compare this curve to the results obtained from various research groups for the heat capacity measurements for MgB_2 as given in Fig. 3.2(b). Clearly the curve found in two-band heat capacity experiments no longer has just a single exponential dependency. Instead, the change in gradient at around 8 K suggest that one is dealing with two different exponential decays. This shows that there exists two Δ values, confirming the two-band nature of MgB_2.

Indeed, as one increases the temperature from zero K, there is initially only sufficient thermal energy to create an excitation over the smallest gap. As the temperature increases, so does the thermal energy, leading to a point where an excitation over the larger gap is also possible. Further increasing in temperature eventually leads to a phase transition into the normal state at T_c.

The concept of two-band superconducting behaviour was however known prior to the discovery of the properties of MgB_2. Other superconductors, such as high-purity superconducting Nb, Ta, and V,[31] and Nb-doped $SrTiO_3$[32] already showed evidence for two distinct energy gaps, Δ_1 and Δ_2.

In the case of high-purity Nb, consider the heat capacity measurements as shown in Fig. 3.3(a). Again, the measurements indicate two different rates of exponential decay for each of the two samples, which correspond to two different gap values for each of the two bands in the superconductor.

In the case of Nb-doped $SrTiO_3$, the two-band behaviour is apparent from tunneling experiments, the results of which are presented in Fig. 3.3(b). First consider tunneling in the one-band problem: at a given voltage the tunneling current is proportional to the amount of available states. This is equivalent to saying that the tunneling conductance is proportional to the density of states. Thus, as soon as eV is larger than Δ, there is a sudden peak in the density of states as a large number of states become available for tunneling directly above the gap. This peak is therefore the indication of a gap in the Fermi surface. As can be seen from Fig. 3.3(b) the density of states of Nb shows two such peaks, which indicates two Δ values.

Other systems that have been discussed as two-band superconductors are $R\mathrm{Ni}_2\mathrm{B}_2\mathrm{C}$ with R=Lu,Y,[33, 34] 2H-$NbSe_2$[35] and the recently discovered FeAs superconductors.[6] In all cases the amplitude of the superconducting gap turns out to be different for different sheets of the Fermi surface. Thus each of the two gaps corresponds to a different band in the superconductor, which needs to be accounted for in the theory.

Various theoretical works have followed these clear experimental results to take two bands into consideration. As each band, $\psi_1(\mathbf{r})$ and $\psi_2(\mathbf{r})$, has individually associated to it a length

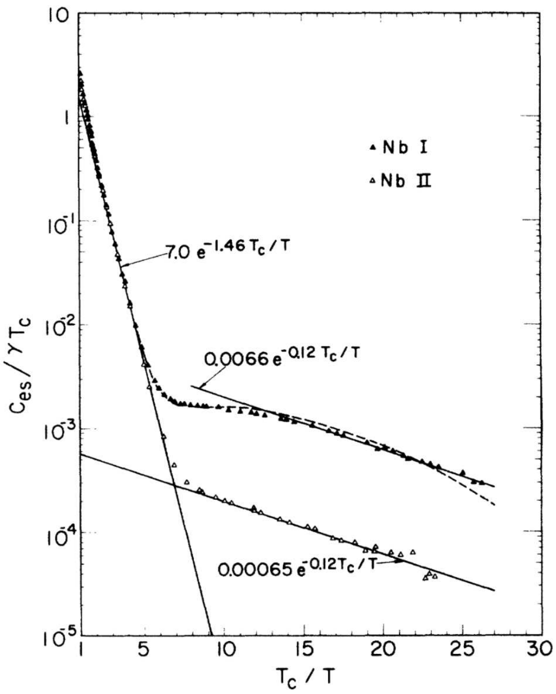

(a) Heat capacity measurements which indicates a two-band structure for two samples of Nb. Taken from L. Y. L. Shen *et al.*[31]

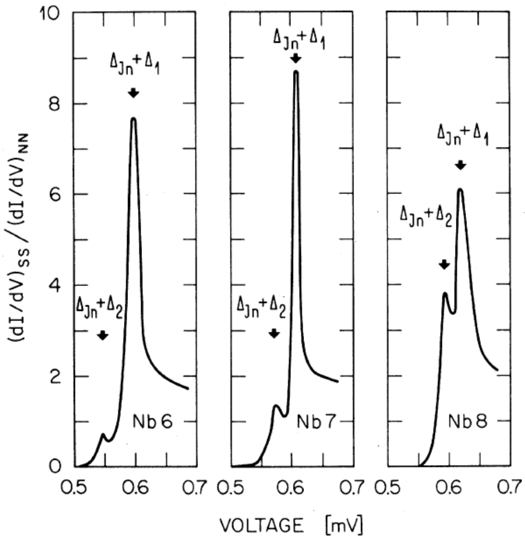

(b) Normalized tunneling conductance of Nb-doped $SrTiO_3$-In junctions in the range of two-band superconductivity measured at T = 100 mK. Taken from G. Binnig *et al.*[32]

Figure 3.3: Experimental evidence for Nb and Nb-doped $SrTiO_3$ as two-band superconductors.

scale, ξ_1 and ξ_2, a state that is intermediate between the two regimes - the normal state and the *doubly* superconducting state - was deemed possible. The term *type-1.5* superconductivity has subsequently been coined.[7] However, a coupling between the two bands, ψ_1 and ψ_2 was neglected in these works. The following chapter therefore deals with the effect of a Josephson type coupling between two order parameters on the length scales ξ_1 and ξ_2, as well as further properties of the coupled system.

CHAPTER 4
Interface energy of a two-band superconductor

In the previous chapter experimental evidence for two-band superconductivity was given and discussed briefly. It is therefore useful to have a theoretical understanding of the behaviour of these two-band superconductors. In this chapter a two-band Ginzburg-Landau theory[36] will be formulated based on the Ginzburg-Landau theory for one-band superconductors as was done in chapter 2.

In the one-band problem the key parameter in describing the system, κ, naturally occurred in the dimensionless form of the energy associated with the interface of a one-band superconductor. In analogy to this, the dimensionless expression for the interface energy of a two-band superconductor will be derived in this chapter in order to find the relevant parameter(s) to describe the two-band problem. Since Ginzburg-Landau theory (GL) is only valid in the vicinity of the transition temperature, this expression will in turn be analyzed around this specific point.

4.1 The free energy of a two-band superconductor

In the microscopic derivation of the GL equations it emerges that the gap Δ is proportional to the order parameter. In a two-band superconductor there are two gaps and hence two order parameters. The two-band Ginzburg-Landau theory will therefore be constructed in terms of two order parameters ψ_i, $i = 1, 2$, each of which satisfies the one-band GL theory, and with a Joshephson-like coupling between the two order parameters.

The expression for the free energy of a two-band system, F, in a zero external magnetic field can now be constructed. It must hold that the functional F depends on both the pairing wave functions ψ_1 and ψ_2 of the two bands and, as before, on the vector potential $\mathbf{A}$ associated with the magnetic field $\mathbf{B} = \nabla \times \mathbf{A}$. Using the free energy for a one-band superconductor in a zero external magnetic field, Eq. (2.14), along with the free energy density of Eq. (2.24), this gives:

$$F\left[\psi_1, \psi_2, \mathbf{A}\right] = \int f\left(\mathbf{r}\right) d^3r, \tag{4.1}$$

with

$$f\left(\mathbf{r}\right) = f_1\left(\mathbf{r}\right) + f_2\left(\mathbf{r}\right) + f_c\left(\mathbf{r}\right) + \frac{B^2\left(\mathbf{r}\right)}{8\pi}. \tag{4.2}$$

The $f_j(\mathbf{r})$ terms, with $j = 1, 2$, are the GL expansions of the two uncoupled bands:

$$f_j = a_j |\psi_j|^2 + \frac{1}{2} b_j |\psi_j|^4 + \frac{1}{2m_j^*} \left| \left(\frac{\hbar}{i} \nabla - \frac{e^*}{c} \mathbf{A} \right) \psi_j \right|^2 . \tag{4.3}$$

By the same argument as in the one-band case, $b_j > 0$. The bands' effective masses are m_j^*, but the charges are equal with $e^* = 2e$. The factor two can be traced back to the fact that a Cooper pair consists of two electrons[9]. The term $f_c(\mathbf{r})$ is the coupling term

$$f_c(\mathbf{r}) = -\eta \left(\psi_1^*(\mathbf{r}) \psi_2(\mathbf{r}) + \psi_2^*(\mathbf{r}) \psi_1(\mathbf{r}) \right) . \tag{4.4}$$

In principle additional coupling terms such as $(\Psi_1^* \Psi_2)^2$ etc. are allowed. For clean multi-band systems a weak coupling expansion yields that the coefficients of such terms vanish due to momentum conservation[37]. In addition, even if present, such terms are sub-leading close to the transition temperature point when compared to $f_c(\mathbf{r})$.

The functions of the order parameters and vector potential that will result in the physical interface energy are determined via $\delta F / \delta \psi_i = \delta F / \delta A_\alpha = 0$ as was done in Eq. (2.25) for one band.

4.1.1 The homogeneous two-band problem with $\mathbf{A} = 0$

First it is necessary to understand the behaviour of the order parameters in the bulk of the superconductor. The bulk of the superconductor is characterized by homogeneous or constant order parameters and by a complete Meissner effect. This means that one has to obtain the order parameter solutions to the minimization of the free energy within these constraints. Clearly a minimization of the sum of Eqs. $(4.3)_{j=1,2}$, and (4.4) for constant order parameters would yield $\mathbf{A} = 0$. Since $\mathbf{B} = \nabla \times \mathbf{A} = \mathbf{0}$, this predicts the Meissner effect. The expression to minimize further is therefore

$$f = a_1 |\psi_1|^2 + \frac{b_1}{2} |\psi_1|^4 + a_2 |\psi_2|^2 + \frac{b_2}{2} |\psi_2|^4 - \eta \left(\psi_1^* \psi_2 + \psi_2^* \psi_1 \right) . \tag{4.5}$$

One can assume that $\eta \geq 0$. If this is not the case, it will be reflected when determining the solution of the ψ_i's: the sign will be absorbed via one of the order parameters, e.g. $\psi_2 \rightarrow -\psi_2$. This sign change of the order parameter will have no effect on the rest of the free energy formulation, since all other terms contain even powers in both ψ's.

Again one can set both ψ_i to real functions by an appropriate gauge transformation on $\mathbf{A}$ as was done in the one-band case.

If the interband coupling f_c is ignored, one finds the usual mean-field equations

$$\begin{aligned} a_1\psi_1 + b_1\psi_1^3 &= 0 \\ a_2\psi_2 + b_2\psi_2^3 &= 0 \end{aligned} \tag{4.6}$$

with, as expected, the usual one-band homogeneous solutions to the order parameters:

$$\begin{aligned} \psi_{i,0}\left(\eta = 0\right) = \sqrt{-a_i/b_i} \quad &\text{for} \quad a_i < 0 \\ \psi_{i,0}\left(\eta = 0\right) = 0 \quad &\text{for} \quad a_i > 0, \end{aligned} \tag{4.7}$$

and $b_i > 0$. This was the assumption of Refs. [38, 39], but in general $f_c \neq 0$. The more general mean-field equations are

$$\begin{aligned} a_1\psi_1 + b_1\psi_1^3 - \eta\psi_2 &= 0 \\ a_2\psi_2 + b_2\psi_2^3 - \eta\psi_1 &= 0. \end{aligned} \tag{4.8}$$

Inserting $\psi_2 = \left(a_1\psi_1 + b_1\psi_1^3\right)/\eta$ from the first equation into the second equation one finds a fourth-order equation for $u = \psi_1^2$

$$\frac{b_2}{\eta^4} u \left(a_1 + b_1 u\right)^3 + \frac{a_2}{\eta^2}\left(a_1 + b_1 u\right) - 1 = 0 \tag{4.9}$$

This fourth-order equation in u can be solved using Mathematica, but the result is a lengthy expression for u in terms of the five parameters. From this expression it is difficult to deduce the behaviour of u analytically or numerically given the large parameter space. An alternative route is to study Eq. (4.9) only in the vicinity of the transition temperature as GL theory essentially only describes superconductivity well in this region.

In order to expand Eq. (4.9) around the transition temperature, one must first calculate the appropriate transition temperature carefully. In previous works where no coupling between the order parameters were considered, e.g. Refs. [38, 39] (for a recent review see [40]), the transition temperature of the two bands were forced to be equal. This ensured a single transformation between the superconducting and the normal state. However, there is no reason that both coefficients $a_i\left(T\right)$ change sign at the same temperature, meaning that the common critical temperature T_c is not necessarily equal to either of $T_{c,j}$.

In the one-band problem, the transition temperature is defined as the point where, in lowering the temperature, one first observes superconductivity. This corresponds to the minimum of the free energy shifting to a point where the homogeneous order parameter is no longer zero, but some finite value. In a one-band superconductor, this occurs where the coefficient $a = a_0\tau$ leading the $|\psi|^2$ term from Eq. (2.24) changes sign, thus at zero. To determine the superconducting transition temperature of the two-band problem, one needs to again consider the coefficients of the terms with dimension of the order parameter squared in the homogeneous zero field scenario, thus Eq. (4.5). In this equation there are three terms with this dimension, which can be written in matrix form

$$\begin{pmatrix} \psi_1 & \psi_2 \end{pmatrix} \begin{pmatrix} a_1 & -\eta \\ -\eta & a_2 \end{pmatrix} \begin{pmatrix} \psi_1 \\ \psi_2 \end{pmatrix}. \tag{4.10}$$

The eigenvalues of the matrix

$$R = \begin{pmatrix} a_1 & -\eta \\ -\eta & a_2 \end{pmatrix} \tag{4.11}$$

are

$$r_\pm = \frac{1}{2}\left(a_1 + a_2 \pm \sqrt{(a_1 - a_2)^2 + 4\eta^2}\right). \tag{4.12}$$

In order to obtain a non-trivial phase, meaning a minimum of the free energy where the order parameter is not zero, one needs at least one of the eigenvalues to be negative. The transition temperature of the two-band problem is therefore defined as the temperature where the smallest of the eigenvalues changes sign. Clearly r_- is always smaller than r_+ and therefore the transition temperature corresponds to $r_- = 0$. This occurs when setting $\eta^2 = a_1a_2$. Since this by definition occurs at the two-band transition temperature, this means that

$$\eta^2 = a_1(T_c)\, a_2(T_c)\,. \tag{4.13}$$

By substituting this into the eigenvalue r_-, one obtains

$$0 = r_- = \frac{1}{2}\left(a_1 + a_2 - |a_1 + a_2|\right), \tag{4.14}$$

which means that $a_1 + a_2 = |a_1 + a_2|$, which in turn means that $a_1 + a_2$ must be positive. Since both the sum and the product, from Eq. (4.13), are positive, it must hold that $a_{1,2}(T_c) > 0$. Thus, the interband coupling increases the transition temperature compared to the largest of the $T_{c,j}$ for the $\eta = 0$ limit.

In order to do Taylor expansions around the critical temperature, the following dimensionless ratio is introduced

$$t \equiv \frac{\eta^2 - a_1a_2}{a_1a_2} \propto \frac{T_c - T}{T_c}, \tag{4.15}$$

which vanishes at T_c. The sign of t is chosen such that it is positive below T_c and switches to negative above T_c. Thus, small positive t naturally corresponds to finite interband coupling η. By doing a Taylor expansion of the eigenvalue r_- in t around $t=0$ it follows that

$$r_- \simeq -\frac{a_1 a_2}{a_1 + a_2} t \tag{4.16}$$

which appropriately changes sign at T_c or $t=0$ as expected. To first order the eigenvalue r_- is therefore analogous to the coefficient of the quadratic order parameter term in the homogeneous one-band problem.

One can also do a Taylor expansion in t around the critical temperature for the function $u=\psi^2$ of Eq. (4.9). Thus

$$u(t) = \sum_{n=1} u_{(n)} t^n. \tag{4.17}$$

Since the order parameter vanishes at $t=0$, one can set $u_0=0$. This expression for u can be substituted back into Eq. (4.9) and after eliminating $\eta^2 = (1+t)\, a_1 a_2$ in favor of t, one finds

$$\frac{b_2 u(t) \left(a_1 + b_1 u(t)\right)^3}{\left(a_1 a_2 (1+t)\right)^2} + \frac{a_2 \left(a_1 + b_1 u(t)\right)}{a_1 a_2 (1+t)} - 1 = 0. \tag{4.18}$$

The left hand side of Eq. (4.18) can be expanded in powers of t. By the right hand side of Eq. (4.18) the coefficients to all these orders in t must vanish. From Mathematica one obtains expressions for these coefficients and by setting them to zero the first two terms in the expansion of u can be solved:

$$\begin{aligned} u_{(1)} &= \frac{a_2^2 a_1}{a_2^2 b_1 + a_1^2 b_2} \\ u_{(2)} &= \frac{a_1^3 a_2^2 b_2 \left(a_1^2 b_2 - 2 b_1 a_2^2\right)}{\left(a_2^2 b_1 + a_1^2 b_2\right)^3}. \end{aligned} \tag{4.19}$$

By definition this means one has to leading order in t

$$\psi_{1,0}^2 = Y_1 t \ \text{ with } Y_1 = \frac{a_2^2 a_1}{a_2^2 b_1 + a_1^2 b_2}, \tag{4.20}$$

$$\psi_{2,0}^2 = Y_2 t \ \text{ with } Y_2 = \frac{a_1^2 a_2}{a_2^2 b_1 + a_1^2 b_2}, \tag{4.21}$$

where the subscript 0 is to denote the zero field solution. The second solution is obtained using the symmetry that exists between ψ_1 and ψ_2.

By consistently analyzing the problem to leading order in t, one simplifies the problem significantly. This simplification is really no limitation as the Ginzburg-Landau theory is not valid for temperatures away from the transition temperature to begin with. An expansion in t to leading order gives for the order parameter

$$\psi_{j,0}^2 \propto t \propto \frac{T_c - T}{T_c} \tag{4.22}$$

(as constructed). Going beyond this leading order behaviour, one would simply enter a regime where the GL theory is not applicable. Away from T_c corrections can be significant, in particular for small η, but those effects require a microscopic approach based on Bogoliubov-de Gennes equations.[41]

4.1.2 The critical magnetic field

The critical magnetic field is the externally applied magnetic field for which neither the superconducting- nor the normal state is energetically favourable. In other words, the enthalpy of both the bulk states are of equal value as derived in section 2.1. By equating these two enthalpies, one can obtain an expression for the critical external magnetic field.

First consider the free energy of the superconducting state with real order parameters

$$f = a_1 |\psi_1|^2 + \frac{b_1}{2} |\psi_1|^4 + a_2 |\psi_2|^2 + \frac{b_2}{2} |\psi_2|^4 - \eta\psi_1\psi_2 - \eta\psi_2\psi_1. \tag{4.23}$$

To obtain the value of the free energy at its minimum, one can substitute the η terms with the expressions obtained in the mean-field equations, as given in Eq. (4.8). By multiplying the mean-field equations by the appropriate order parameter, one obtains the exact η terms required:

$$\begin{aligned} a_1\psi_1^2 + b_1\psi_1^4 &= \eta\psi_2\psi_1 \\ a_2\psi_2^2 + b_2\psi_2^4 &= \eta\psi_1\psi_2. \end{aligned} \tag{4.24}$$

Substituting this into Eq. (4.23) gives the expression for the free energy. Keeping in mind that $\mathbf{B} = 0$ in the bulk of the superconducting state, by Eq. (2.6) the free energy is equal to the enthalpy. The expression for the bulk enthalpy is then

$$g_{\text{bulk SC}} = -\frac{1}{2}\sum_{j=1}^{2} b_j |\psi_j|^4 , \tag{4.25}$$

which is similar to the one-band minimum given in Eq. (2.31). As discussed in the one-band problem, the enthalpy of the normal state is

$$g_{\mathrm{n}} = -\frac{H_c^2}{8\pi}. \tag{4.26}$$

From the homogeneous order parameter solutions in Eqs. (4.20) and (4.21), one can calculate the critical applied magnetic field

$$\frac{H_c^2}{4\pi} = \sum_{j=1}^{2} b_j \left|\psi_j\right|^4 = \frac{a_1^2 a_2^2 t^2}{a_2^2 b_1 + a_1^2 b_2}. \tag{4.27}$$

4.1.3 The London limit

Consider the London limit as was done in the one-band problem. Although the London limit does not yield the correct result for the magnetic field $\mathbf{B}$, it does introduce a useful natural length scale (the magnetic penetration depth) in the problem.

The London limit in the two-band problem would correspond to $\psi_j(\mathbf{r}) = \psi_{j,0} = const$, but $\mathbf{A} \neq \mathbf{0}$ in the superconducting state. The expressions for the current induced by the superconductor in analogy to Eq. (2.29) is now

$$\mathbf{j}_{ind} = -\frac{e^{*2}}{c}\left(\frac{\psi_{1,0}^2}{m_1^*} + \frac{\psi_{2,0}^2}{m_2^*}\right)\mathbf{A}. \tag{4.28}$$

Following the same route as before, one takes the curl on both sides to give

$$\nabla \times \mathbf{j}_{ind} = -\frac{e^{*2}}{c}\left(\frac{\psi_{1,0}^2}{m_1^*} + \frac{\psi_{2,0}^2}{m_2^*}\right)\mathbf{B}. \tag{4.29}$$

By construction $\mathbf{j}_{ind} = -\frac{c}{4\pi}\nabla \times \mathbf{B}$ as shown in Eq. (2.28) which, when substituted into the equation above, yields

$$\nabla \times \nabla \times \mathbf{B} = -\frac{4\pi e^{*2}}{c^2}\left(\frac{\psi_{1,0}^2}{m_1^*} + \frac{\psi_{2,0}^2}{m_2^*}\right)\mathbf{B}. \tag{4.30}$$

Again one uses the fact that $\nabla \cdot \mathbf{B} = \mathbf{0}$ which means that the previous equation simplifies to

$$\nabla^2 \mathbf{B} = \frac{4\pi e^{*2}}{c^2}\left(\frac{\psi_{1,0}^2}{m_1^*} + \frac{\psi_{2,0}^2}{m_2^*}\right)\mathbf{B}. \tag{4.31}$$

Solving this equation in $\mathbf{B}$ yields at an interface between the normal state and the superconducting state

$$\mathbf{B}(z) = \mathbf{B}(0)\exp(-z/\lambda) \tag{4.32}$$

with

$$\begin{aligned}\lambda^{-2} &= \frac{4\pi e^{*2}}{c^2}\left(\frac{\psi_{1,0}^2}{m_1^*}+\frac{\psi_{2,0}^2}{m_2^*}\right)\\ &= \frac{4\pi e^{*2}a_1 a_2 \tau}{c^2}\frac{a_2/m_1^*+a_1/m_2^*}{a_2^2 b_1+a_1^2 b_2}.\end{aligned} \tag{4.33}$$

As stated previously, only the value of λ is useful here, not the expression for $\mathbf{B}$. The two-band penetration depth can be written neatly as

$$\lambda^{-2} = \lambda_1^{-2} + \lambda_2^{-2}, \tag{4.34}$$

where λ_i refers to the penetration depth for each uncoupled band as given in Eq. (2.47).

4.2 The two-band interface energy

The evaluation of the surface energy of the two-band problem closely follows the approach that was used for the single band problem as done in Section 2.3. Thus, again consider the interface between superconducting and normal half-spaces on the z-axis at the plane $z = 0$. The field H is applied along the x axis parallel to the interface and equal to H_c to ensure coexistence of two phases. Then the magnetic induction has only one component $B_x = B(z)$ and the vector potential can be chosen as $A_y = -A(z)$ such that

$$B(z) = A'(z). \tag{4.35}$$

Within this construct, the order parameters can be chosen as real, varying along the z-direction only

$$\psi_j(\mathbf{r}) = \psi_j(z). \tag{4.36}$$

The normal state is chosen for z negative with $\psi_i(z \to -\infty) \to 0$ and $B(z<0) \to H_c$, while the z positive side corresponds to the superconducting state. The bulk of the superconductor therefore corresponds to the limit $z \to \infty$, meaning $B(z \to \infty) \to 0$ and $\psi_i(z \to \infty) \to \psi_{i,0}$ with the homogeneous solutions, $\psi_{i,0}$ as obtained in section 4.1.1.

Consider the full expression for the free energy density of a two-band superconductor as given in Eqs. (4.2)-(4.4) using the constructs for the order parameters and $\mathbf{A}$ and $\mathbf{B}$. In both the uncoupled free energy densities the following expression occurs which, in the new constructs, reads

$$\left(-i\hbar\nabla - \frac{e^*}{c}\mathbf{A}\right)\psi_j = -i\hbar\frac{d\psi_j}{dz}\mathbf{e}_z + \frac{e^*}{c}A(z)\,\mathbf{e}_y \tag{4.37}$$

which means

$$\left|\left(-i\hbar\nabla - \frac{e^*}{c}\mathbf{A}\right)\psi_j\right|^2 = \hbar^2\left(\frac{d\psi_j}{dz}\right)^2 + \frac{e^{*2}}{c^2}A^2\psi_j^2. \tag{4.38}$$

The full expression for the free energy is thus from Eq. (4.1)

$$\begin{aligned} F &= F_n + L^2\int\left(a_1\psi_1^2 + \frac{1}{2}b_1\psi_1^4 + a_2\psi_1^2 + \frac{1}{2}b_2\psi_2^4 + \frac{\hbar^2}{2m_1^*}\left(\frac{d\psi_1}{dz}\right)^2 + \frac{\hbar^2}{2m_2^*}\left(\frac{d\psi_2}{dz}\right)^2\right)dz \\ &\quad + L^2\int\left(-2\gamma\psi_1\psi_2 + \frac{e^{*2}}{2c^2}\left(\frac{\psi_1^2}{m_1^*} + \frac{\psi_2^2}{m_2^*}\right)A^2 + \frac{B}{8\pi}\right)dz. \end{aligned} \tag{4.39}$$

As in the one-band derivation, the interface energy is obtained by minimizing the difference in enthalpy of the superconducting- and the normal state. As given in Eq. (2.6), one has that the Gibbs free energy (per unit area) is

$$G = F - \frac{H_c}{4\pi}\int_{-\infty}^{\infty} dz\, B(z), \tag{4.40}$$

which means the enthalpy of the superconducting state is

$$\begin{aligned} G_{sc} &= F_n + L^2\int\left(a_1\psi_1^2 + \frac{1}{2}b_1\psi_1^4 + a_2\psi_1^2 + \frac{1}{2}b_2\psi_2^4 + \frac{\hbar^2}{2m_1^*}\left(\frac{d\psi_1}{dz}\right)^2 + \frac{\hbar^2}{2m_2^*}\left(\frac{d\psi_2}{dz}\right)^2\right)dz \\ &\quad + L^2\int\left(-2\gamma\psi_1\psi_2 + \frac{e^{*2}}{2c^2}\left(\frac{\psi_1^2}{m_1^*} + \frac{\psi_2^2}{m_2^*}\right)A^2 + \frac{(B-H_c)^2}{8\pi} - \frac{H_c^2}{8\pi}\right)dz. \end{aligned} \tag{4.41}$$

The normal state enthalpy is given by Eq. (2.60) as

$$G_n = F_n - L^2\int\frac{H_c^2}{8\pi}dz. \tag{4.42}$$

The difference in the superconducting state enthalpy and the normal state enthalpy gives the interface energy functional as

$$\begin{aligned} \Sigma[\psi_1,\psi_2,A] &= \int\left(a_1\psi_1^2 + \frac{1}{2}b_1\psi_1^4 + a_2\psi_2^2 + \frac{1}{2}b_2\psi_2^4 + \frac{\hbar^2}{2m_1^*}\left(\frac{d\psi_1}{dz}\right)^2 + \frac{\hbar^2}{2m_2^*}\left(\frac{d\psi_2}{dz}\right)^2\right)dz \\ &\quad + \int\left(-2\gamma\psi_1\psi_2 + \frac{e^{*2}}{2c^2}\left(\frac{\psi_1^2}{m_1^*} + \frac{\psi_2^2}{m_2^*}\right)A^2 + \frac{(B-H_c)^2}{8\pi}\right)dz, \end{aligned} \tag{4.43}$$

which, in order to obtain the value for the interface energy σ_s, must be minimized with respect to the three functions ψ_j and A.

4.2.1 Dimensionless units

It is useful to rewrite Eq. (4.43) in terms of dimensionless quantities. A dimensionless form allows one to work with possibly less parameters, and gives a clearer indication about the dependence of $\Sigma[\psi_1, \psi_2, A]$ on certain quantities. For example, only in the dimensionless form for the one-band problem did κ explicitly appear.

It is convenient to introduce these dimensionless quantities as done in the one-band problem:

$$v_j^2 = \frac{\psi_j^2}{Y_j t}, \quad \beta = \frac{B}{\sqrt{2}H_c}, \quad \text{and } x = \frac{z}{\lambda}, \tag{4.44}$$

with the dimensionless vector potential again at

$$\alpha = \frac{A}{\sqrt{2}H_c\lambda}, \tag{4.45}$$

where λ is now the penetration depth as calculated for the two-band problem from Eq. (4.33).

Substituting these quantities into Eq. (4.43), one can now write the interface functional as

$$\begin{aligned} \Sigma[v_1, v_2, \alpha] &= \lambda\frac{H_c^2}{4\pi}\int\left(\sum_i \Lambda_i v_i^2 + \frac{\delta_i}{2}v_i^4 + \kappa_i^{-2}\left(\frac{dv_i}{dx}\right)^2 + \rho_i v_i^2\alpha^2\right)dx \\ &+\lambda\frac{H_c^2}{4\pi}\int\left(-2\mu v_1 v_2 + \frac{1}{2}\left(\sqrt{2}\beta - 1\right)^2\right)dx \end{aligned} \tag{4.46}$$

where the following abbreviations were used

$$\begin{aligned} \Lambda_i &= \frac{4\pi a_i Y_i t}{H_c^2} \quad \text{and} \quad \delta_i = \frac{4\pi b_i Y_i^2 t^2}{H_c^2} \\ \kappa_i^{-2} &= \frac{4\pi\hbar^2 Y_i t}{2m_i^*\lambda^2 H_c^2} \quad \text{and} \quad \rho_i = \frac{4\pi e^{*2}\lambda^2 Y_i t}{c^2 m_i^*} \\ \mu &= \frac{4\pi\gamma\sqrt{Y_1 Y_2}t}{H_c^2}. \end{aligned} \tag{4.47}$$

These newly defined variables or abbreviations above are not yet in their simplest form. By using the definitions of the following quantities

$$\begin{aligned} \lambda^{-2} &= \frac{4\pi e^{*2}a_1 a_2 t}{c^2}\frac{a_2/m_1^* + a_1/m_2^*}{a_2^2 b_1 + a_1^2 b_2} \quad \text{and} \quad \frac{H_c^2}{4\pi} = \frac{a_1^2 a_2^2 t^2}{a_2^2 b_1 + a_1^2 b_2} \\ Y_1 &= \frac{a_2^2 a_1}{a_2^2 b_1 + a_1^2 b_2} \quad \text{and} \quad Y_2 = \frac{a_1^2 a_2}{a_2^2 b_1 + a_1^2 b_2} \end{aligned} \tag{4.48}$$

from Eqs. (4.33), (4.27), (4.20) and (4.21), and substituting these values into the abbreviations, one finds that

$$\begin{aligned} \Lambda &\equiv \Lambda_1 = \Lambda_2 = t^{-1} \text{ and } \mu = \frac{\sqrt{1+t}}{t} \\ \delta &\equiv \delta_1 = \frac{b_1 a_2^2}{a_2^2 b_1 + a_1^2 b_2} \text{ and } \delta_2 = \frac{b_2 a_1^2}{a_2^2 b_1 + a_1^2 b_2} = 1 - \delta. \end{aligned} \tag{4.49}$$

Thus, the five dimensionless ratios δ_i, Λ_i, and μ are not independent and determined by only two dimensionless numbers t and δ. In addition follows

$$\begin{aligned} \kappa_1^{-2} &= \frac{4\pi e^{*2}\hbar^2}{2c^2} \frac{a_2}{m_1^*} \frac{a_2/m_1^* + a_1/m_2^*}{a_2^2 b_1 + a_1^2 b_2} \\ \kappa_2^{-2} &= \frac{4\pi e^{*2}\ \hbar^2}{2c^2} \frac{a_1}{m_2^*} \frac{a_2/m_1^* + a_1/m_2^*}{a_2^2 b_1 + a_1^2 b_2} \end{aligned} \tag{4.50}$$

as well as

$$\rho_1 = \frac{a_2 m_2^*}{a_2 m_2^* + a_1 m_1^*} \quad \text{and} \quad \rho_2 = \frac{a_1 m_1^*}{a_2 m_2^* + a_1 m_1^*}. \tag{4.51}$$

Another relation emerges: $\rho_1 + \rho_2 = 1$. With the help of the new quantity

$$\zeta = \frac{a_2 m_2^*}{a_1 m_1^*} = \frac{\rho_1}{\rho_2} \tag{4.52}$$

one can write ρ_i in the form

$$\rho_1 = \frac{\zeta}{1+\zeta} \text{ and } \rho_2 = \frac{1}{1+\zeta}. \tag{4.53}$$

It also holds that the quantity ζ is equal to the ratio of the κ_i^2: $\zeta = \kappa_2^2/\kappa_1^2$. One can therefore eliminate ζ and write

$$\rho_1 = \frac{1}{1+\kappa_1^2/\kappa_2^2} \quad \text{and} \quad \rho_2 = \frac{1}{1+\kappa_2^2/\kappa_1^2}. \tag{4.54}$$

Only two out of the four dimensionless rations κ_i and ρ_i are independent. Substituting this information into the expression for the interface energy functional as given in Eq. (4.46), it finally follows that

$$\Sigma[v_1, v_2, \alpha] = \lambda \frac{H_c^2}{4\pi} \int \left(W(v_1, v_2, \alpha) + \kappa_1^{-2} \left(\frac{dv_1}{dx}\right)^2 + \kappa_2^{-2} \left(\frac{dv_2}{dx}\right)^2 + \frac{\left(\sqrt{2}\frac{d\alpha}{dt} - 1\right)^2}{2} \right) dx \tag{4.55}$$

with

$$W(v_1, v_2, \alpha) = \frac{v_1^2 + v_2^2 - 2\sqrt{1+t}\, v_1 v_2}{t} + \frac{\delta}{2} v_1^4 + \frac{1-\delta}{2} v_2^4 + \frac{\kappa_2^2 v_1^2 + \kappa_1^2 v_2^2}{\kappa_1^2 + \kappa_2^2} \alpha^2. \tag{4.56}$$

This minimization only depends on four parameters now.

In order for Σ to be at its minimum, the partial derivatives of Σ with respect to v_i and α must equal zero. Taking these derivatives and substituting the results back into the expression for Σ, one obtains the following value for the interface energy at the minimum

$$\sigma_s = \lambda \frac{H_c^2}{4\pi} \int dx \left(\frac{1}{2} \left(\sqrt{2}\alpha' - 1 \right)^2 - \frac{\delta}{2} v_1^4 - \frac{1-\delta}{2} v_2^4 \right), \tag{4.57}$$

where α' indicates the derivative with respect to x.

4.2.2 The interface energy to leading order in t

The peculiar term in the analysis is the first one in $W(v_1, v_2, \alpha)$ for it seems to be singular as $t \to 0$. This can easily be seen by expanding this term for small t:

$$\frac{v_1^2 + v_2^2 - 2\sqrt{1+t}\, v_1 v_2}{t} \simeq \frac{(v_1 - v_2)^2}{t} - v_1 v_2. \tag{4.58}$$

This means that as one approaches the transition temperature, the term above will diverge. In order for Σ to be at a minimum, one must therefore have $(v_1 - v_2)^2 \to 0$ faster than $1/t \to \infty$ in order to prevent divergence. This implies that $v_1 \to v_2$ in the limit where $t \to 0$. As GL theory is only valid for $t \to 0$, one can therefore set $v_1 = v_2$.

The origin of this peculiar divergence behaviour is the coefficients of the quadratic terms in the GL expansion which do not change sign at the transition temperature of the system. This is caused by the Josephson coupling between the two bands that raises the transition temperature of the coupled system above the transition temperatures of the uncoupled systems (where these coefficients do change sign). This conclusion is confirmed by a direct numerical minimization of the full functional Σ of Eq. (4.55), which will be given in the next chapter.

Introducing $v(x) = v_1(x) = v_2(x)$ one obtains the interface energy functional in the form:

$$\Sigma = \int dx \left(W_0(v, \alpha) + \kappa^{-2} v'^2 + \left(\alpha' - 2^{-1/2} \right)^2 \right), \tag{4.59}$$

with

$$W_0(v, \alpha) = -v^2 + \frac{1}{2} v^4 + v^2 \alpha^2 \tag{4.60}$$

and effective parameter κ given by

$$\kappa^{-2} = \kappa_1^{-2} + \kappa_2^{-2}. \tag{4.61}$$

This functional is in exactly the same form as the functional for the standard one-band surface energy problem given in Eq. (2.65).

It is worth noting that κ_i enter the surface energy only through the combination κ of Eq. (4.61). From this expression of the effective κ one can now obtain an effective correlation length, ξ, for the two-band problem using the definition $\kappa = \lambda/\xi$. This results in the expression

$$\xi = \left(\xi_1^{-2} + \xi_2^{-2}\right)^{-1/2}. \tag{4.62}$$

One concludes that the interface problem for the two-band system is identical to the one of a single band system, as given in Eq. (2.66) with the same function $\Upsilon(\kappa)$. This can be seen by comparing Eq. (4.57) of the two-band problem with $v_1 = v_2$ to Eq. (2.69) of the one-band problem.

4.2.3 The limit $\kappa_1 \ll 1$ and $\kappa_2 \gg 1$

This limit describes the interesting scenario of a two-band superconductor in which one uncoupled band falls under type-I behaviour, while the other uncoupled band falls under type-II behaviour. From the previous analysis the resultant behaviour of this mixed limit should be that of a type-I one-band superconductor due to the coupling of the bands. This can be seen by the relation in κ values from Eq. (4.61), where $\kappa_1 < 1/\sqrt{2}$ while $\kappa_2 > 1/\sqrt{2}$ (or vice versa)

$$\kappa^{-2} = \kappa_1^{-2} + \kappa_2^{-2}. \tag{4.63}$$

It is interesting to note that the effective κ will only result in type-II behaviour if both uncoupled bands are well within the type-II regime. This can be seen in Fig. 4.1.

Consider the functional Σ from Eq. (4.55). At the stationary point of this functional the integrand, L, must satisfy the Euler Lagrange equation

$$0 = \frac{\partial L}{\partial q} - \frac{d}{dt}\frac{\partial \Sigma}{\partial \dot{q}}, \tag{4.64}$$

with $q = v_1, v_2, \alpha$ in this specific case. Thus, the following differential equations are obtained

$$\begin{aligned}
\kappa_1^{-2}\frac{d^2 v_1}{dx^2} &= \frac{1}{2}\frac{\partial W(v_1, v_2, \alpha)}{\partial v_1} \\
\kappa_2^{-2}\frac{d^2 v_2}{dx^2} &= \frac{1}{2}\frac{\partial W(v_1, v_2, \alpha)}{\partial v_2} \\
\frac{d^2 \alpha}{dx^2} &= \frac{1}{2}\frac{\partial W(v_1, v_2, \alpha)}{\partial \alpha}.
\end{aligned} \tag{4.65}$$

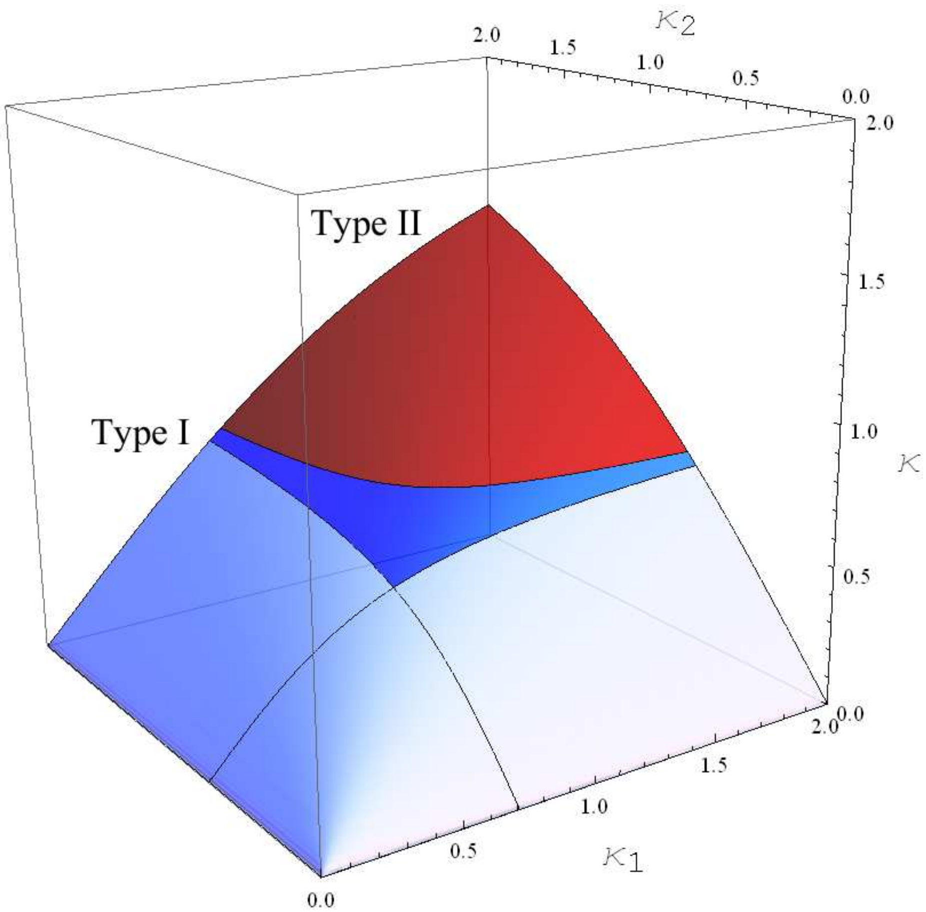

Figure 4.1: The values for κ from Eq. (4.61) as a function of the uncoupled one-band values for κ_1 and κ_2. This figure shows that κ will only result in type-II behaviour (dark red area) if both the κ_i are far enough in the type-II regime individually, meaning $\kappa_i >> 1/\sqrt{2} \approx 0.7$. If either of the κ_i are below $1/\sqrt{2}$, this will result in type-I behaviour (light blue areas). The dark blue area corresponds to an effective type-I behaviour where both κ_i would individually however result in type-II behaviour.

Calculating the partial derivatives on the right side, Eq. (4.65) reads

$$\begin{aligned}
\kappa_1^{-2}\frac{d^2 v_1}{dx^2} &= \frac{v_1 - \sqrt{1+t}v_2}{t} + \delta v_1^3 + \frac{\kappa_2^2 v_1}{\kappa_1^2+\kappa_2^2}\alpha^2 \\
\kappa_2^{-2}\frac{d^2 v_2}{dx^2} &= \frac{v_2 - \sqrt{1+t}v_1}{t} + (1-\delta)\, v_2^3 + \frac{\kappa_1^2 v_2}{\kappa_1^2+\kappa_2^2}\alpha^2 \\
\frac{d^2 \alpha}{dx^2} &= \frac{\kappa_2^2 v_1^2 + \kappa_1^2 v_2^2}{\kappa_1^2+\kappa_2^2}\alpha. \qquad (4.66)
\end{aligned}$$

In the limit $\kappa_1 \ll 1$ and $\kappa_2 \gg 1$ one can simplify these equations by only considering the leading behaviour, thus $\kappa_2^{-2} \approx 0$, $\kappa_1 + \kappa_2 \approx \kappa_2$ and $\kappa_1/\kappa_2 \approx 0$:

$$\begin{aligned}
\kappa_1^{-2}\frac{d^2 v_1}{dx^2} &= \frac{v_1 - \sqrt{1+t}v_2}{t} + \delta v_1^3 + v_1\alpha^2 \\
0 &= \frac{v_2 - \sqrt{1+t}v_1}{t} + (1-\delta)\, v_2^3 \\
\frac{d^2\alpha}{dx^2} &= v_1^2\alpha.
\end{aligned} \tag{4.67}$$

The second equation yields to leading order in t

$$v_2 \simeq v_1 + \left(\frac{v_1}{2} - (1-\delta)\, v_2^3\right) t. \tag{4.68}$$

Substituting this into the remaining equations, it follows to leading order in t

$$\begin{aligned}
\kappa_1^{-2}\frac{d^2 v_1}{dx^2} &= -\frac{v_1}{2} + \delta v_1^3 + v_1\alpha^2 \\
\frac{d^2\alpha}{dx^2} &= v_1^2\alpha.
\end{aligned} \tag{4.69}$$

Those are essentially the equations for the single band problem as given in Eq. (2.64). Although the coefficients do not match perfectly, the form of the differential equations are enough indication that one is dealing with single band behaviour here. Thus, again the two-band problem reduces to a single band problem close to the critical temperature as was expected from the previous analysis.

This theoretical result, supported by the numerical analysis presented in the next two chapters, was subsequently published, see Ref. [42]. Following this publication, a generalization of the theoretical work was published in Ref. [43].

CHAPTER 5
Numerical results for the interface energy in the one-band problem

In section 2.3 the expression for the interface energy of the one-band problem in dimensionless units was derived:

$$\sigma_s = \min_{v,\,\alpha} \Sigma\left[v,\, \alpha\right], \tag{5.1}$$

where Σ is the functional from Eq. (2.65). The minimization of Σ is only dependent on a single variable, κ, and the resulting values for the interface energy can be written as a function, $\Upsilon\left(\kappa\right)$, which has the following limits, as shown in section 2.3.2.1 and section 2.3.2.2:

$$\Upsilon\left(\kappa\right) = \begin{cases} \frac{2^{3/2}}{3}\kappa^{-1} & \text{if} \quad \kappa \ll 1 \\ -\frac{4}{3}\left(\sqrt{2}-1\right) & \text{if} \quad \kappa \gg 1. \end{cases} \tag{5.2}$$

Apart from these limits and the zero point (where $\sigma_s = 0$) there is no analytic description for $\Upsilon\left(\kappa\right)$, nor has it been numerically computed and published[9].

In this chapter $\Upsilon\left(\kappa\right)$ is numerically computed in order to determine the values for the one-band interface energy for all κ-values. This not only gives the interface energy for κ-values which falls outside the theoretically calculated regions, but also shows to which extend the theoretical limits of Eq. (5.2) are correct.

5.1 The Numerical Method

The functional to be minimized, Σ, is given by Eq. (2.65) as

$$\Sigma = \int \left(-v^2 + \frac{1}{2}v^4 + \frac{1}{\kappa^2}\left(\frac{dv}{dt}\right)^2 + v^2\alpha^2 + \frac{1}{2}\left(\sqrt{2}\frac{\partial\alpha}{\partial t} - 1\right)^2\right) dt. \tag{5.3}$$

In order to minimize this numerically, the interval $t = [0, L]$ is divided into N equidistant steps ($t_i = iL/N$). Here $L = 5\max(1, 1/\sqrt{2}\kappa)$, which is five[10] times the maximum between the penetration depth and the coherence length as measured in dimensionless units. Σ is then minimized with respect to v and α, subject to the boundary conditions:

$$v\left(0\right) = 0, \tag{5.4}$$

[9] Until the publication of this exact work, see Ref. [42]

[10] This is an arbitrary number! The reason for the multiplication is to ensure the interface is completely within the range of t.

$$v(L) = 1, \tag{5.5}$$

$$\alpha(L) = 0, \tag{5.6}$$

and an arbitrary value for κ. The first condition requires the left-most side of the t-range to be in the normal state since the normalized order parameter is forced to be zero here. The second and third boundary condition require the right-most side of the t-range to be in the superconducting state where the order parameter takes on the value of the bulk-superconducting state order parameter, thus giving $v = 1$, and where the Meissner effect is complete. The boundary condition on α for the normal side stems from minimizing $\Sigma[0, \alpha]$. Since one already enforces $v = 0$ at the left-most side, this boundary condition is automatically fulfilled when minimizing the Σ-functional.

In the limit $L \to \infty$, the position of the interface between the normal and the superconducting state is arbitrary . By setting the constraint

$$v\left(\left\lceil \frac{L}{2} \right\rceil\right) = 0.5 \tag{5.7}$$

on the system, one only pins the position of the interface energy to a specific value of t. This has no effect on the actual value of the interface energy. This specific constraint is chosen such that in the limit $\kappa >> 1$, it shifts the interface to exactly $\lceil \frac{L}{2} \rceil$.

5.2 The Results

The numerical results for $\Upsilon(\kappa)$ are given in Fig. 5.1 (a duplication of Fig. 1.3).

Each minimization for a different value of κ is represented by a diamond in Fig. 5.1. In these minimizations various values for N were used, with N ranging between $N = 400$ and $N = 800$. The difference in value for Υ is not very significant for N in this range, even so $N = 800$ was used.

These numerical results were found to be in good agreement with the theoretical predictions. From section 2.3.2.3 it is known that the interface energy at $\kappa = 1/\sqrt{2} \approx 0.707$ must give $\sigma_s = 0$. The numerical results show the same behaviour: the numerically obtained value for $\kappa = 0.7$ was $\Upsilon(0.7) \approx 0.002$.

Also, from section 2.3.2.4 it must hold that for all $\kappa < 1/\sqrt{2}$, the interface energy must be strictly positive and for all $\kappa > 1/\sqrt{2}$, the interface energy must be strictly negative, which is clearly in agreement to the numerical results. The theoretical limiting cases for $\kappa >> 1$ and $\kappa << 1$, as given in Eq. 5.2, are accurately portrayed by the numerical results.

The fact that the numerical results are in such good agreement with the theoretical predictions

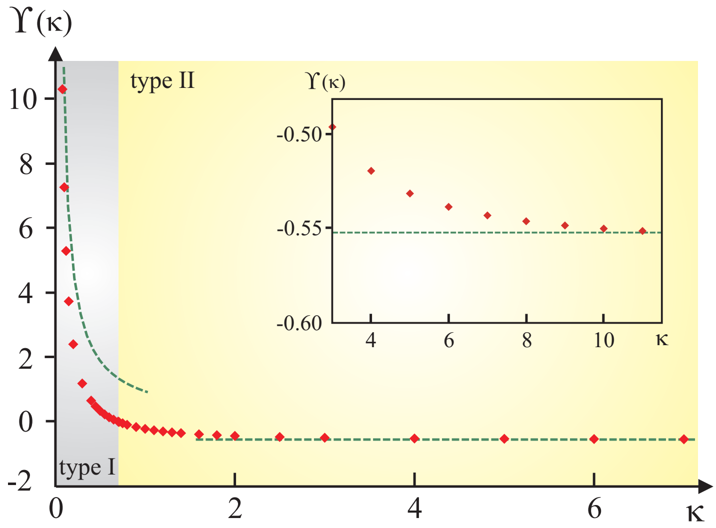

Figure 5.1: The numerical results for $\Upsilon(\kappa)$ are shown by the red diamonds and compare well to the theoretical limits, which are shown by the green dashed lines. The inset shows an enlargement of the large κ domain.

inspires confidence in the computational calculation of the interface energy of a single band superconductor. The same minimization method will thus be used to determine the interface energy for the two-band problem in the next chapter.

CHAPTER 6
Numerical results for the interface energy of the two-band problem

In Chapter 4 it was shown that the interface energy of the two-band problem can be written in the form

$$\sigma_s = \min_{v_1,\, v_2,\, \alpha} \Sigma\left[v_1,\, v_2,\, \alpha\right], \tag{6.1}$$

where Σ is the dimensionless functional as given in Eq. (4.55).

This expression was subsequently analyzed to leading order in t in section 4.2.2. These theoretical results showed that close to the transition temperature both v_1 and v_2 follow the same spatial dependence and that the interface energy of the system can be written as an effective single band interface energy.

These conclusions will now be tested numerically. In this chapter curves for v_1, v_2 and α which minimizes Σ will be computed from which the spatial dependence of the v_i can be deduced and compared to the theoretical model. From these curves one will also be able to calculate the interface energy of the two-band problem. This can then be compared to the numerical value obtained for the interface energy of the one-band problem at the predicted effective κ in order to confirm the theoretical analysis of section 4.2.2.

6.1 The Numerical Method

The dimensionless form for the Σ functional which needs to be minimized with respect to v_i and α from Eq. (4.55) is

$$\Sigma\left[v_1, v_2, \alpha\right] = \lambda\frac{H_c^2}{4\pi}\int\left(W\left(v_1, v_2, \alpha\right) + \kappa_1^{-2}\left(\frac{dv_1}{dx}\right)^2 + \kappa_2^{-2}\left(\frac{dv_2}{dx}\right)^2 + \frac{\left(\sqrt{2}\frac{d\alpha}{dt}-1\right)^2}{2}\right)dx \tag{6.2}$$

with

$$W\left(v_1, v_2, \alpha\right) = \frac{v_1^2 + v_2^2 - 2\sqrt{1+t}v_1v_2}{t} + \frac{\delta}{2}v_1^4 + \frac{1-\delta}{2}v_2^4 + \frac{\kappa_2^2v_1^2 + \kappa_1^2v_2^2}{\kappa_1^2+\kappa_2^2}\alpha^2. \tag{6.3}$$

In order to minimize this functional numerically, the interval $s = [0, 2L]$, where L is again specified as in section 5.1, is discretized into N equidistant steps ($s_j = 2jL/N$). Σ is then minimized with respect to $v_1\left(s_j\right)$, $v_2\left(s_j\right)$ and $\alpha\left(s_j\right)$, subject to the boundary conditions

$$v_i\left(0\right) = 0, \tag{6.4}$$

$$v_i\left(2L\right) = v_{i,0}, \tag{6.5}$$

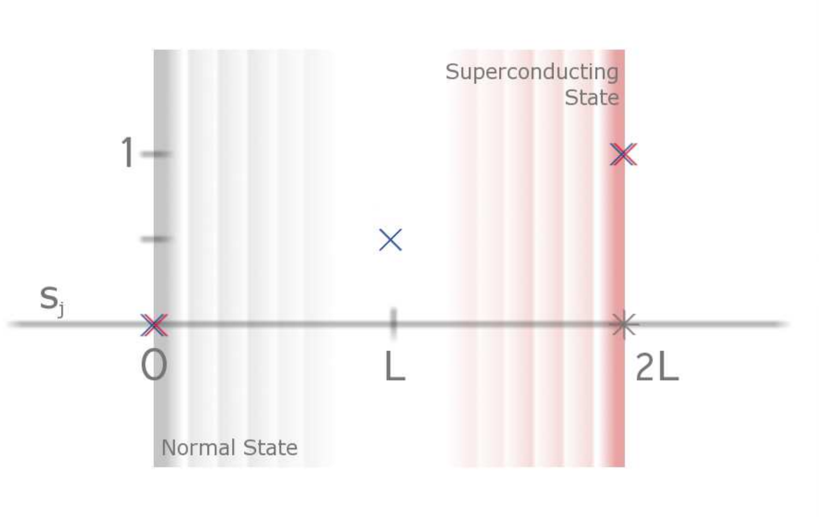

Figure 6.1: Schematic representation of the numerical constraints in the minimization problem. The blue and red crosses represent the order parameter constraints, while the grey star represent the constraint on α.

$$\alpha\,(2L) = 0, \tag{6.6}$$

and arbitrarily chosen values for κ_i, δ and t.

The first boundary condition on the left-most side of t corresponds to a normal state solution for the order parameters. The last two boudary conditions stem from a purely superconducting state far from the interface, thus the right most spectrum of t, in the limit $L \to \infty$ which corresponds to the homogeneous zero field solution. The homogeneous bulk solutions for $v_{i,0}$ approach the value $v_{i,0} = 1$ close to the transition temperature by Eq. (4.44).

From symmetry one would expect a further boundary condition on α at $L = 0$, but this is not necessary. The constraint,

$$\alpha'\,(0) = 2^{-1/2}, \tag{6.7}$$

can be obtained from setting both order parameters to zero in Eq. (6.2) and Eq. (6.3) and minimizing the remaining term with respect to α, but this is exactly the function of the numerical minimization method, which means it is redundant to specify this boundary condition. This equation can however be used as a quick guide to check the correctness of the numerical minimization result for α in the vicinity where the order parameters are close to zero.

Finally, since in the limit $2L \to \infty$ the interface position is arbitrary, at $z = L$ we assumed $v_1\,(L) = \frac{1}{2}$, which centers the interface position in the large κ limit. See Fig. 6.1 for a schematic representation for all the boundary conditions.

6.2 The Results

The numerical optimization for v_i and α was computed with various values of κ_1, κ_2, δ and t, all with $N = 400$. The results for $v_i = \psi_i/\psi_{i,0}$ and $\sqrt{2}\,\beta = B/H_c = \sqrt{2}\,d\alpha/dt$ for different values of κ_i, δ and t are shown in Figs. 6.2 and 6.3.

Consider Fig. 6.2. The values chosen for κ_i correspond to the scenario where the individual bands, v_i, are respectively of type-I and type-II. Specifically $\kappa_1 = 0.45 < 2^{-1/2} < \kappa_2 = 5$. Naively, one could therefore expect v_1 to change on distances of the order $\xi_1 > \sqrt{2}\lambda$ - type-I behavior, while $\xi_2 < \sqrt{2}\lambda$ suggests type-II behavior for v_2. Contrary to this the order parameters have increasingly similar spatial variation as t decreases, in other words when the critical temperature is approached. Thus, as t decreases both order parameters approach identical spatial variation as a result of the strong Joshepson coupling between them. The value of δ does not effect this behaviour.

The same behaviour for the spatial dependence of the order parameters can be seen for a different set of variables. In Fig. 6.3 the fixed values for κ_i both correspond to type-II superconducting behaviour, specifically $\kappa_1 = 3$ and $\kappa_2 = 4$. Again only t is allowed to vary. The results here also indicate that the order parameters approach identical spatial variation as t decreases .

In each of these cases above the value for Σ was calculated. The results are given in table 6.1 and table 6.2.

Consider table 6.1 which corresponds to Fig. 6.2. Firstly, the numerically obtained interface energy for this set of variables is positive, meaning that the system behaves as a type-I superconductor. This is in agreement with the theory of section 4.2.2 where the effective κ from Eq.(4.61) is dominated by the smallest of the two κ_i,

$$\kappa = \sqrt{\frac{1}{(\kappa_1 = 0.45)^{-2} + (\kappa_2 = 5)^{-2}}} \approx 0.448 \; < \frac{1}{\sqrt{2}}, \tag{6.8}$$

which corresponds to type-I behaviour. Secondly, as t decreases, the value of the minimized functional, Eq.(6.2), approaches the value of the function $\Upsilon(\kappa)$ of the single band problem with κ as given above. The value of δ does not influence the two-band interface energy value apart from a small contribution due to a non-zero t.

Now consider table 6.2 which corresponds to Figs. 6.3. The interface energy is shown to be negative, which means the system behaves like a type-II superconductor. Again this is in

	Σ_{min}	%-difference w.r.t. $\Upsilon(\kappa_{\text{eff}}) = 0.479$
$t = 0.07$	0.530	$\sim 11\%$
$t = 0.01$	0.488	$\sim 2\%$

Table 6.1: The values of Σ_{min} for different values of t when $\kappa_1 = 0.45,\ \kappa_2 = 5,\ \delta = 0.6$ along side the percentage difference between Σ_{min} and $\Upsilon(\kappa_{\text{eff}})$ where the value for $\Upsilon(\kappa_{\text{eff}})$ comes from the one-band numerical minimization with $\kappa_{\text{eff}} = 0.448$ as determined by Eq. (4.61).

	Σ_{min}	%-difference w.r.t. $\Upsilon(\kappa_{\text{eff}}) = -0.47$
$t = 0.2$	-0.275	$\sim 42\%$
$t = 0.01$	-0.459	$\sim 2\%$

Table 6.2: The values of Σ_{min} for different values of t when $\kappa_1 = 3,\ \kappa_2 = 4,\ \delta = 0.6$ along side the percentage difference between Σ_{min} and $\Upsilon(\kappa_{\text{eff}})$ where the value for $\Upsilon(\kappa_{\text{eff}})$ comes from the one-band numerical minimization with $\kappa_{\text{eff}} = 2.4$ as determined by Eq. (4.61).

accordance with section 4.2.2 as the effective κ

$$\kappa = \sqrt{\frac{1}{(\kappa_1 = 3)^{-2} + (\kappa_2 = 4)^{-2}}} \approx 2.4 \ > \frac{1}{\sqrt{2}}. \tag{6.9}$$

corresponds to type-II behaviour. As before, the value of the minimized functional of Eq. (6.2) approaches the value of the function $\Upsilon(\kappa)$ of the single band problem with κ equal to the value above. A change in δ again only results in a negligable change in the interface energy.

In conclusion, the numerical results for the two-band problem are in complete agreement with the theoretically obtained results in chapter 4. As stated previously, these numerical results were subsequently published along with the theoretical analysis in Ref. [42].

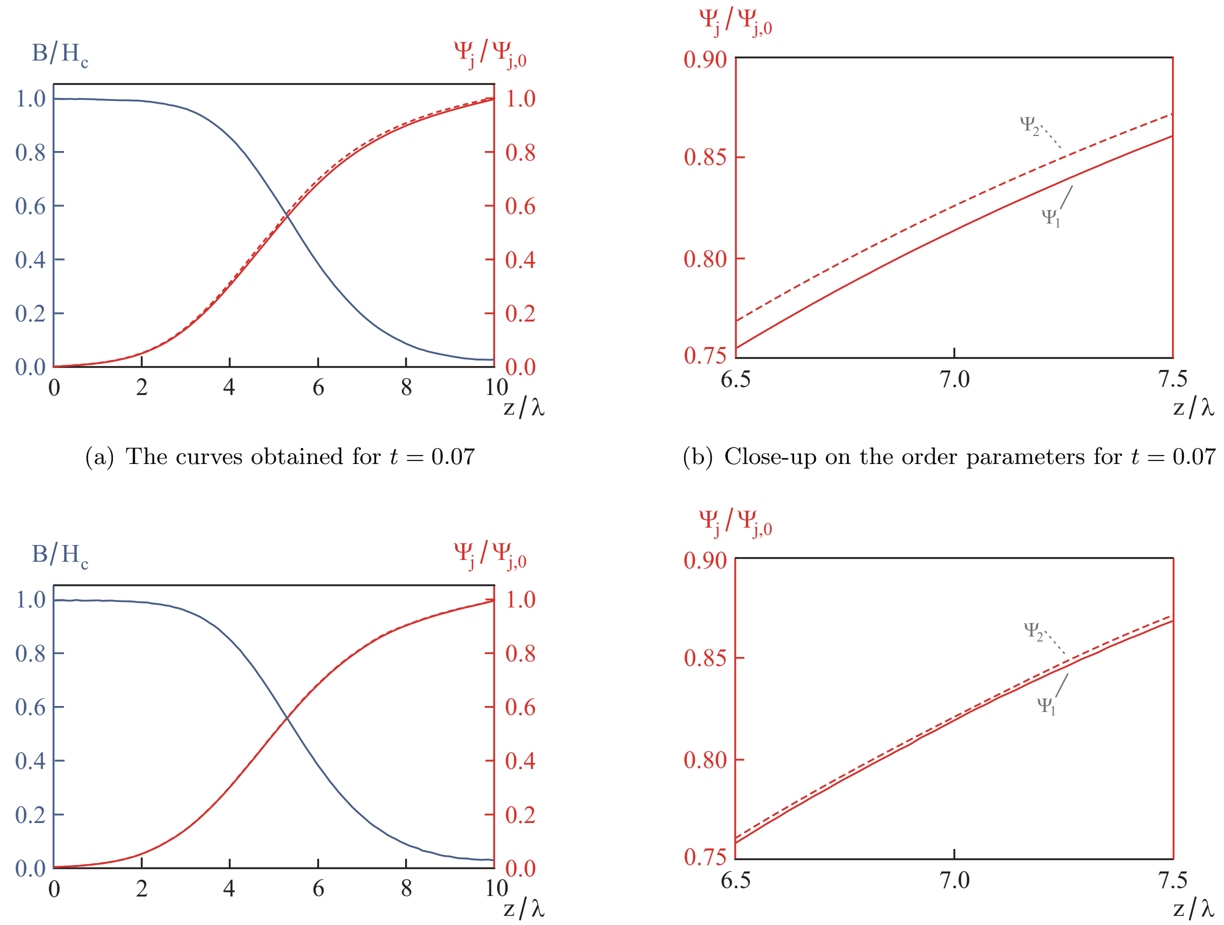

(a) The curves obtained for $t = 0.07$

(b) Close-up on the order parameters for $t = 0.07$

(c) The curves obtained for $t = 0.01$

(d) Close-up on the order parameters for $t = 0.01$

Figure 6.2: On the left is the normalized field and order parameters obtained numerically by minimizing the interface energy functional, Σ, for $\kappa_1 = 0.45$, $\kappa_2 = 5$, $\delta = 0.6$ and for $t = \{0.07, 0.01\}$. The reduced order parameter v_1 is shown by a solid red line, the dashed red line is v_2. The normalized magnetic field is shown by the solid blue line. On the right is a corresponding close-up of the order parameters for $6.5 < z/\lambda < 7.5$.

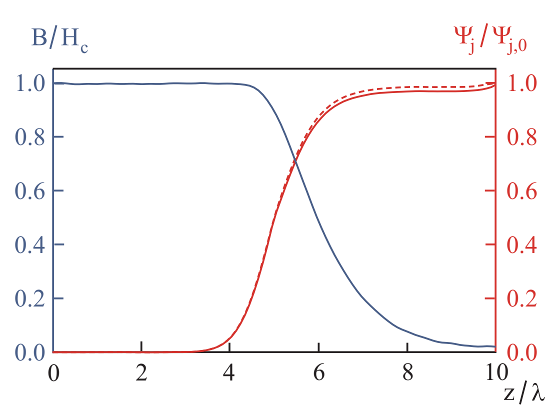

(a) The curves obtained for $t = 0.2$

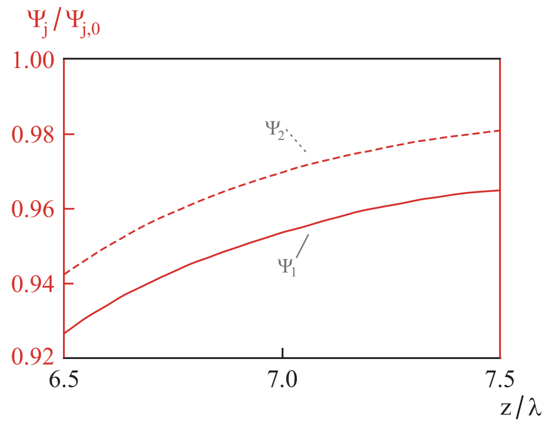

(b) Close-up on the order parameters for $t = 0.2$

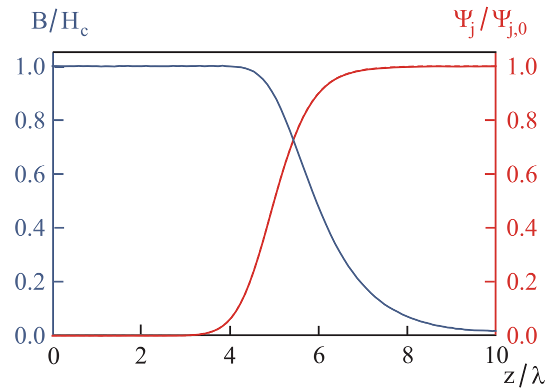

(c) The curves obtained for $t = 0.01$

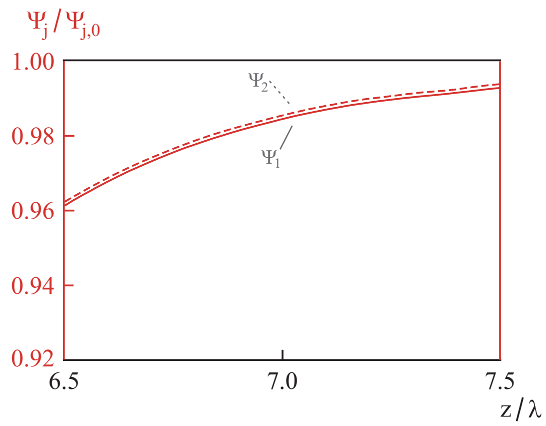

(d) Close-up on the order parameters for $t = 0.01$

Figure 6.3: On the left is the normalized field and order parameters obtained numerically by minimizing the interface energy functional, Σ, for $\kappa_1 = 3$, $\kappa_2 = 4$, $\delta = 0.6$ and for $t = \{0.2, 0.01\}$. The reduced order parameter v_1 is shown by a solid red line, the dashed red line is v_2. The normalized magnetic field is shown by the solid blue line. On the right is a corresponding close-up of the order parameters for $6.5 < z/\lambda < 7.5$.

CHAPTER 7
Experimental evidence for multiphase superconducting and anti-ferromagnetic systems

Before starting on the next problem, a quick summary for the work presented thus far: first the Ginzburg-Landau theory for a one-band superconductor as developed in 1950 was given in chapter 2. This theory was then successfully adapted to describe experimentally observed two-band superconductors with the use of two order parameters in chapter 4. In the next problem, the one-band theory will again be adapted to describe a system with two order parameters, but where the order parameters couple differently. The coupling now describes a system with competing phases, specifically a superconducting phase and an anti-ferromagnetic phase. In this chapter experimental evidence for such multi-phase systems will be given.

Although the next problem deals only with competing anti-ferromagnetism and superconductivity, consider first any material that has a complex phase diagram due to the competing

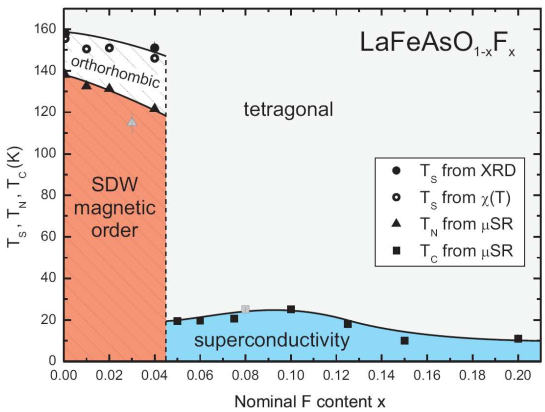

(a) The phase diagram of $\mathrm{LaFeAsO}_{1-x}\mathrm{F}_x$. This phase diagram shows that this material can either exhibit spin density wave (SDW) magnetic order or superconducting order. A state of coexistence between these two phases does however not exist. A structural phase transition from tetragonal to orthorhombic crystal structure is also indicated. References to different experimental techniques to obtain the various critical temperatures are given in the legend. Taken from Ref. [44].

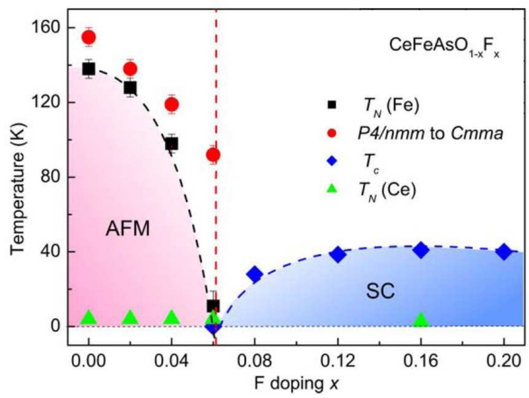

(b) The phase diagram of $\mathrm{CeFeAsO}_{1-x}\mathrm{F}_x$. This phase diagram shows that the material can be in a magnetically order state, specifically an anti-ferromagnetic (AFM) state, or in a superconducting (SC) state, but not in a state where both these orders coexist. A structural phase transition from tetragonal to orthorhombic crystal structure ($P4/nmm$ to $Cmma$) is also indicated in the diagram. Taken from Ref. [45].

Figure 7.1: The phase diagrams of the Ln-FeAsO$_{1-x}$F$_x$ superconductors for Ln = La, Ce, indicating the onset of superconductivity at T_c, and magnetic order at T_N, or a change in the crystal structure at T_s.

interactions. This means that the material undergoes multiple phase transitions to magnetic, superconducting or charge ordered states. Competing phases demonstrate that distinct orders are close in energy and that the material is easily tunable between magnetically responsive to non-responsive or conducting and insulating etc.

As examples of such materials, consider the high-T_c iron arsenide superconductors discovered in 2008. Amongst these superconductors there are two main families, namely the Ln-1111 family of materials and the Ba-122 compounds that become superconducting under doping. The Ln-1111 family of superconductors is short for Ln-FeAsO or Ln-FeAsF. The former under fluoride doping, Ln-FeAsO$_{1-x}$F$_x$, becomes superconducting with T_c's up to 56 K. The specific lanthanoids experimented with thus far include Ln = La, Ce, Pr, Nd, Sm. Ba-122 refers to the compound BaFe$_2$As$_2$ where the iron can be replaced with cobalt, Ba(Fe$_{1-x}$Co$_x$)$_2$As$_2$, in order to give a superconducting material with T_c up to 38 K.

The phase diagrams of some of the Ln-FeAsO$_{1-x}$F$_x$ superconductors are given in Figs 7.1 and 7.2. In all these phase diagrams there are three important transitions, namely a structural transition, a phase transition to a superconducting state and a phase transition to a magneti-

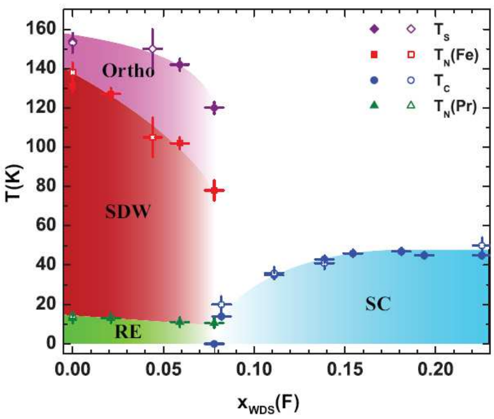

(a) The phase diagram of PrFeAsO$_{1-x}$F$_x$. This phase diagram shows that there is no overlap in the superconducting (SC) and the magnetically ordered spin density wave (SDW) state. The structural phase transition from tetragonal to orthorhombic is also indicated on the diagram. Taken from Ref. [46].

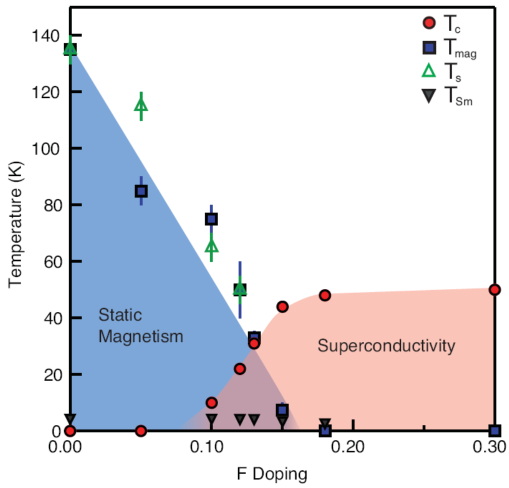

(b) The phase diagram of SmFeAsO$_{1-x}$F$_x$. The phase diagram clearly indicates an overlap between the superconducting state and the magnetically ordered state, resulting in a coexisting state. Two structural transition lines are also indicated where the crystal structure changes from tetragonal to orthorhombic. Taken from Ref. [47].

Figure 7.2: The phase diagrams of the Ln-FeAsO$_{1-x}$F$_x$ superconductors for Ln = Pr, Sm, indicating the onset of superconductivity at T_c, and magnetic order at T_N, or a change in the crystal structure at T_s.

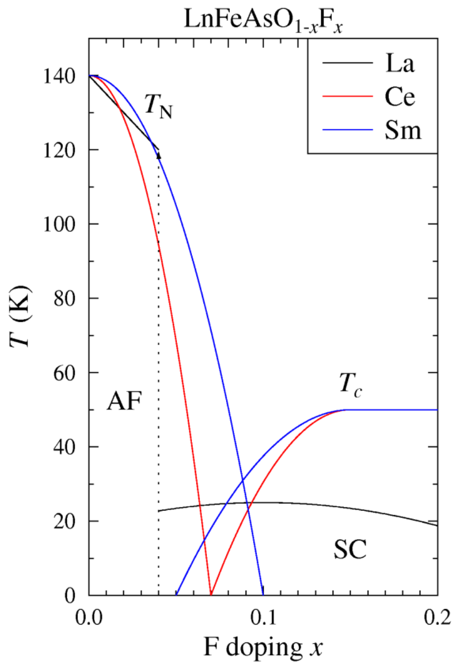

Figure 7.3: A summary of the possible phase diagrams of Ln-FeAsO$_{1-x}$F$_x$. This figure shows three different scenarios in these transitions. For CeFeAsO$_{1-x}$F$_x$ there is no overlap between the superconducting and the anti-ferromagnetic (AF) phase. In LaFeAsO$_{1-x}$F$_x$ the magnetic ordered state is suppressed by the onset of superconductivity. Yet, in SmFeAsO$_{1-x}$F$_x$ coexistence of a static AF order with superconductivity is found.

cally ordered state. The structural transition occurs when the crystal structure changes from a tetragonal structure to an orthorhombic structure, thus $P4/nmm$ to $Cmma$. The critical temperature at which this transition occurs is denoted by T_s. As one reduces the temperature, this transition occurs before the onset of a magnetically ordered state in all these materials. The critical temperatures of the magnetic ordered state is denoted by T_{Neel} or T_N and the critical temperature of the superconducting state by T_c as before. In the case of Ln = Ce, Pr the values for T_c and T_N are such that the superconducting and the magnetically ordered states never overlap, but this is not generally the case. For Ln = La superconductivity is suppressed by the anti-ferromagnetism, while for Ln = Sm a state of coexistence results. Fig. 7.3 summarizes these transitions to magnetic and superconducting order to show the possible phase diagrams of Ln-FeAsO$_{1-x}$F$_x$.

Coexistence of anti-ferromagnetism and superconductivity can also be found in the Ba-122 family of superconductors. The phase diagram of Ba(Fe$_{1-x}$Co$_x$)$_2$As$_2$ is given in Fig. 7.4. Again there is also a structural transition from tetragonal to orthorhombic structure, which occurs before the onset of anti-ferromagnetism.

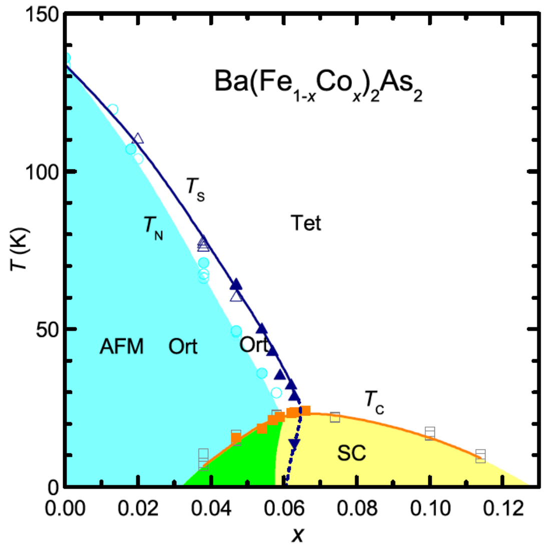

Figure 7.4: The phase diagram of Ba(Fe$_{1-x}$Co$_x$)$_2$As$_2$ obtained experimentally. This phase diagram shows that three possible states occur in this material. They are a superconducting state (SC), an anti-ferromagnetic state (AFM) and a coexisting state where the previously mentioned states overlap. The transitions between these states occurs at various critical temperatures: T_c for the SC state and T_N for the AFM state. There is also a structural transition from tetragonal to orthorhombic crystal structure occurring at T_s. Taken from Ref [48].

From these phase diagrams it is clear that there is an interplay between anti-ferromagnetism and superconductivity. It would therefore be useful to describe these systems within the context of Ginzburg-Landau theory. It would specifically be useful to revisit type-I and type-II superconductivity within this framework. This can be done by considering the interface energy which occurs in systems with both superconductivity and anti-ferromagnetism. This has already been studied in a specific limiting case by [49]. However, it is possible to determine the interface energy for the full spectrum of scenarios as will be shown in the next chapter.

CHAPTER 8
Interface energy of a multi-phased anti-ferromagnetic and superconducting system

In the previous chapter evidence for a coexisting phase in various materials or systems have been discussed. In this chapter the Ginzburg-Landau theory describing these competing phases will be developed. Ginzburg-Landau theory is by construction only valid in a region close to a critical temperature. In this problem there are however two relevant critical temperatures, the superconducting critical temperature T_c and the anti-ferromagnetic critical temperature T_{Neel}. By adjusting for example the doping levels of the systems, one can tune the two critical temperatures to be equal. See Fig. (8.1).

From here the theory will be developed following the same path as in the one-band case: first the free energy for the homogeneous problem at zero field will be discussed; thereafter an external field will be added, and finally the full inhomogeneous case will be developed. This will then set the background for defining various interfaces of the system and calculating the energy associated to these interfaces as well as the critical points between type-I and type-II superconductivity.

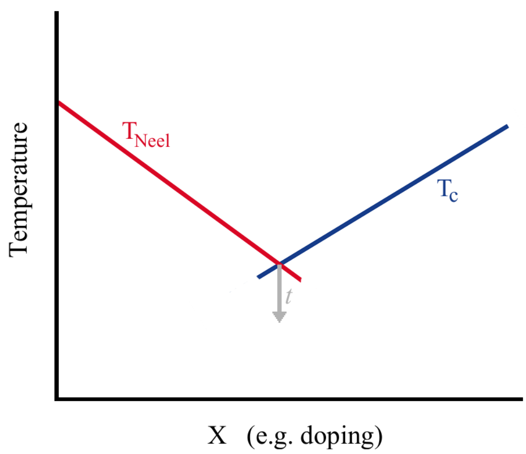

Figure 8.1: A basic schematic representation of how e.g. doping could be used to find a simultaneous or multicritical transition point. To note: the phase lines are not necessarily linear (See. Fig. 7.4). A complete phase diagram will be given further below in Figs. 8.5 and 8.7. The grey arrow and t shows the line along which the theory will be developed.

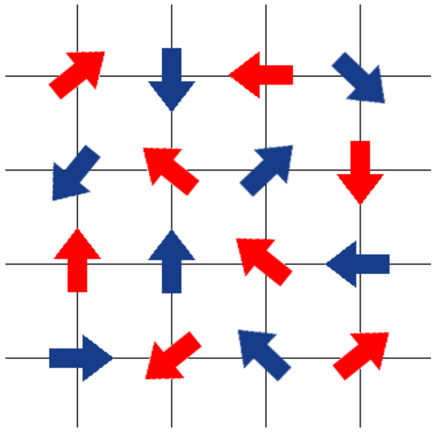

Figure 8.2: A schematic representation of magnetic moments on a bipartite lattice. The magnetic moments are represented by coloured arrows. The two colours distinguish the two sublattices from one another.

8.1 The homogeneous free energy for the coexistence problem

The aim of this section is to obtain and fully understand the expression for the homogeneous free energy of a coexisting superconducting and anti-ferromagnetic state within the context of Ginzburg-Landau theory. In order to do so, first the zero field expression for the free energy of a homogeneous coexisting state, as given in Ref. [50], will be introduced. The solutions of this expression will be discussed after which an external field will be included. The section will end off with the calculation of the critical external magnetic fields at which the various phases are energetically equal.

8.1.1 The staggered magnetization

The free energy functional of the homogeneous coexisting state depends on two functions[50], the superconducting order parameter, ψ, and the staggered magnetization, $\mathbf{M}_s$. The order parameter is already a familiar concept. The aim of this section is to now also introduce the staggered magnetization.

Staggered magnetization is defined on a bipartite lattice. It is the sum of every magnetic moment associated to one lattice, minus the sum of the magnetic moments associated to the other lattice. See Fig. 8.2, where the red arrows indicate one lattice, while blue arrows indicate the other.

In other words, if the sublattices have magnetization $\mathbf{M}_1$ and $\mathbf{M}_2$, the uniform magnetization would be $\mathbf{M} = \mathbf{M}_1 + \mathbf{M}_2$, while the staggered magnetization is $\mathbf{M}_s = \mathbf{M}_1 - \mathbf{M}_2$. In the case of anti-ferromagnetism, as illustrated in Fig. 8.3, one therefore has $\mathbf{M} = \mathbf{0}$, while $\mathbf{M}_s \neq \mathbf{0}$.

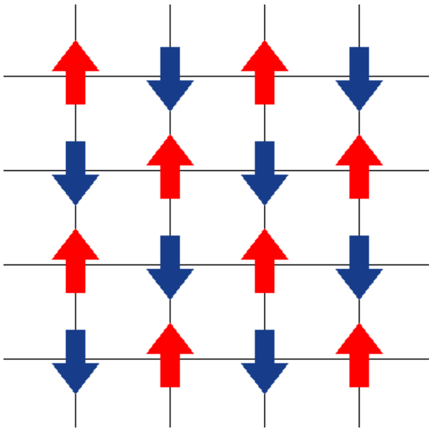

Figure 8.3: A bipartite lattice where the magnetic moments are orientated to give an anti-ferromagnetic state.

8.1.2 The homogeneous coexistence problem with $\mathbf{A} = \mathbf{0}$

As before, it is useful to first consider the simple case of the homogeneous problem without external magnetic field. This section deals with the free energy density of this scenario and the solutions to the minimization thereof. In consequence to these solutions, the various phases of the system are then discussed. The section will be concluded with a brief look at the theoretically predicted reentrant behaviour. Even though this does not fit directly into the overall interface problem, its importance lies in the fact that this behaviour has been observed experimentally, allowing for confidence in the theory.

The expression for the free energy of a coexisting state at zero field, in analogy to Eqs. (2.14) and (2.16), is[50]

$$\Phi = \Phi_0 + \int \phi(\mathbf{r})\, d^3r \tag{8.1}$$

with

$$\phi = -a_s t\,|\psi|^2 + \frac{1}{2}b_s\,|\psi|^4 + \gamma\,|\psi|^2\,\mathbf{M}_s^2 - a_m t\mathbf{M}_s^2 + \frac{1}{2}b_m\mathbf{M}_s^4, \tag{8.2}$$

where the coefficients a_s, b_s, a_m, b_s and γ are positive constants. Again,

$$t = \frac{T_c - T}{T_c} \tag{8.3}$$

is a dimensionless measure for the distance from the transition, with t positive below the transition temperature, T_c. It is extremely important to note that the assumption here is $T_c = T_{Neel}$. See Fig. 8.1. A single critical temperature is necessary as Ginzburg-Landau theory is only valid in this one vicinity. As mentioned earlier, the condition $T_c = T_{Neel}$ can be achieved by eg. doping or pressure adjustments. Unless otherwise stated, this will be the assumption throughout the rest of the chapter.

The key difference between this free energy expression and that of the two-band superconductor, see Eqs. (4.1) - (4.4), lies in the coupling of the two order parameters. In the two-band problem the coupling term was effectively quadratic, while in this problem the coupling gives a fourth-order term. Also note that a positive γ means that the coupling increases the free energy in the coexisting state. Thus, if the value for γ is too large, a minimization of the coupling term will result in a suppression of coexistence. One therefore expects to find certain conditions on γ, and possibly on the coefficients a_s, b_s, a_m, b_s as well, in order to allow for coexistence in the system. These conditions will be derived and discussed later in the section.

Consider the minimum free energy of this homogeneous system. Taking the derivatives, $\partial\phi/\partial\psi$ and $\partial\phi/\partial\mathbf{M}_s$, and setting them to zero yields

$$\begin{aligned} -a_s t\psi + b_s \left|\psi\right|^2 \psi + \gamma\psi\mathbf{M}_s^2 &= 0 \\ -a_m t\mathbf{M}_s + b_m\mathbf{M}_s^2\mathbf{M}_s + \gamma\left|\psi\right|^2\mathbf{M}_s &= 0. \end{aligned} \tag{8.4}$$

Above the critical temperature, thus $t < 0$, there is only one solution, namely the trivial solution where $|\psi|^2 = \mathbf{M}_s^2 = 0$. If $t > 0$, there are four possible solutions for these equations:

$$\begin{array}{lll} & |\psi|^2 & \mathbf{M}_s^2 \\ \text{solution 1} & 0 & 0 \\ \text{solution 2} & \frac{a_s}{b_s}t & 0 \\ \text{solution 3} & 0 & \frac{a_m}{b_m}t \\ \text{solution 4} & \frac{a_s-\frac{\gamma}{b_m}a_m}{b_s\left(1-\frac{\gamma^2}{b_s b_m}\right)}t & \frac{a_m-\frac{\gamma}{b_s}a_s}{b_m\left(1-\frac{\gamma^2}{b_s b_m}\right)}t \end{array} \tag{8.5}$$

The first three solutions are easy to obtain and are clearly in coherence with previous theory where only one order parameter was considered. Solution 4, the coexisting solution, can be obtained by dividing the second equation of Eq. (8.4) by $\mathbf{M}_s$, which now is assumed non-zero, and rewriting this to give an expression for $\mathbf{M}_s^2$:

$$\mathbf{M}_s^2 = -\frac{\left(-a_m t + \gamma\left|\psi\right|^2\right)}{b_m}. \tag{8.6}$$

One must be careful here as this expression implies a condition on $|\psi|^2$. Since $\mathbf{M}_s^2$ must be positive and real, $\left(-a_m t + \gamma\left|\psi\right|^2\right)$ must be negative. In other words there is an upper limit for $|\psi|^2$ in the coexisting regime. Substituting the expression above back into the free energy of Eq.

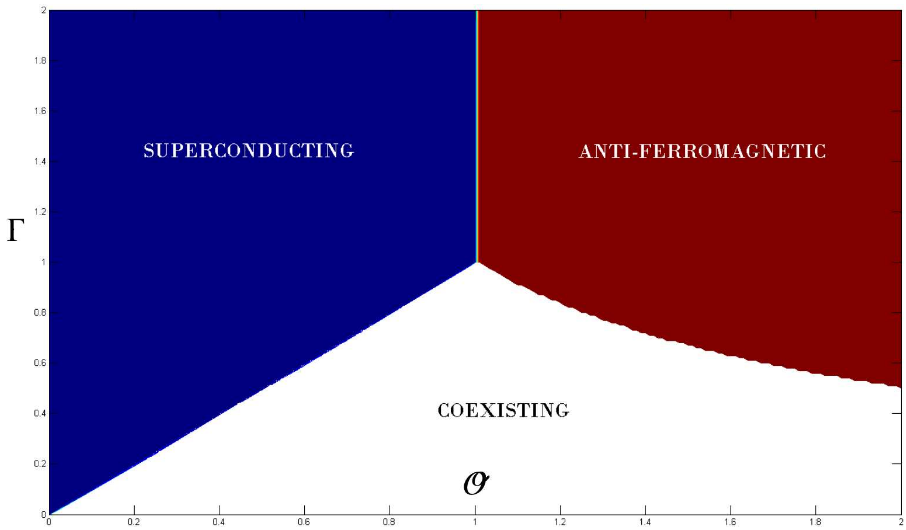

Figure 8.4: The phase diagram in Γ, a measure of the strength of the interaction between ψ and $\mathbf{M}_s$, and θ, a ratio between free energies of the individual uncoupled homogeneous states at zero external magnetic field. At $\theta = 1, \Gamma \geq 1$ the superconducting state and the anti-ferromagnetic state are both possible.

(8.2), and rearranging the terms, one obtains

$$\phi_\psi \equiv \phi(\psi)|_{\mathbf{M}_s = \text{ Eq. (8.6)}} = \left(-a_s + \frac{a_m \gamma}{b_m}\right) t\,|\psi|^2 + \frac{1}{2}\left(b_s - \frac{\gamma^2}{b_m}\right)|\psi|^4 - \frac{a_m^2}{2b_m}t^2. \tag{8.7}$$

The minimum, $\partial\phi_\psi/\partial\psi = 0$, occurs at $|\psi|^2 = \frac{a_s - \frac{\gamma}{b_m}a_m}{b_s\left(1-\frac{\gamma^2}{b_s b_m}\right)}t$. The calculation can be repeated to find $\phi_{\mathbf{M}_s}$, defined in the same manner as above, from which the solution for $\mathbf{M}_s^2$ in the coexisting state can be obtained. However, from the symmetry between ψ and $\mathbf{M}_s$ in the free energy density expression, the solution for $\mathbf{M}_s^2$ must be exactly symmetric to that of $|\psi|^2$.

8.1.2.1 The conditions on coexistence

As mentioned in the previous section, certain conditions must be met in order for a coexisting state to be stable. The aim of this section is to determine and discuss these conditions, which can then be mapped onto a phase diagram.

In order to determine the conditions for coexistence, first consider the actual values for the free energy density of each possible state below the multicritical temperature. In keeping with the order of Eq. (8.5), substituting the solutions into the free energy density, Eq. (8.2), yields

$$\begin{aligned}
\phi_1 &= 0, \\
\phi_2 &= -\frac{a_s^2}{2b_s}t^2, \\
\phi_3 &= -\frac{a_m^2}{2b_m}t^2, \\
\phi_4 &= -\frac{a_m^2 b_s + a_s^2 b_m - 2\gamma a_m a_s}{2\left(b_m b_s - \gamma^2\right)}t^2.
\end{aligned} \tag{8.8}$$

Clearly ϕ_1 has the largest value and is therefore never the stable solution below the multicritical point. Consider the dimensionless ratio:

$$\theta^2 := \frac{\phi_3}{\phi_2} = \frac{a_m^2 b_s}{a_s^2 b_m} \ . \tag{8.9}$$

If $\theta > 1$, it means ϕ_3 is smaller than ϕ_2. In other words, the homogeneous anti-ferromagnetic-only state is lower in energy than the homogeneous superconducting-only state. Clearly if $\theta < 1$ the opposite is true. The question that remains is when ϕ_4 is stable. To this end the following dimensionless quantity is introduced

$$\Gamma = \frac{\gamma}{\sqrt{b_m b_s}} \ . \tag{8.10}$$

One finds that if $\Gamma \geq 1$ simultaneous order is not allowed. This can be deduced from the expression for ϕ as given in Eq. (8.2). In order for ϕ to have a minimum for a non-zero $|\psi|^2$ and a non-zero $\mathbf{M}_s^2$, the Hessian must be positive definite. Thus:

$$\begin{vmatrix} \frac{\partial\phi}{\partial|\psi|^2\partial|\psi|^2} & \frac{\partial\phi}{\partial|\psi|^2\partial\mathbf{M}^2} \\ \frac{\partial\phi}{\partial\mathbf{M}^2\partial|\psi|^2} & \frac{\partial\phi}{\partial\mathbf{M}^2\partial\mathbf{M}^2} \end{vmatrix} > 0, \tag{8.11}$$

which gives

$$\begin{vmatrix} b_s & \gamma \\ \gamma & b_m \end{vmatrix} = b_s b_m - \gamma^2 > 0. \tag{8.12}$$

In the original variables, this means a necessary, yet not sufficient (as will be shown next), condition for coexistence is $\Gamma < 1$. In other words, if $\Gamma \geq 1$ a coexisting state is not possible. The stable state is then either ϕ_2 or ϕ_3, whichever is lower, as determined by $\theta \lesseqgtr 1$.

Further constraints for the coexisting state can be found by considering the values for the order parameter and the staggered magnetization in solution 4, Eq. (8.5). As one is dealing with squares, both values must be positive. For coexistence one already has that $\Gamma < 1$, which means $\gamma^2 < b_m b_s$. Therefore it must hold that $a_s > \frac{\gamma}{b_m} a_m$ and $a_m > \frac{\gamma}{b_s} a_s$. These two conditions can be

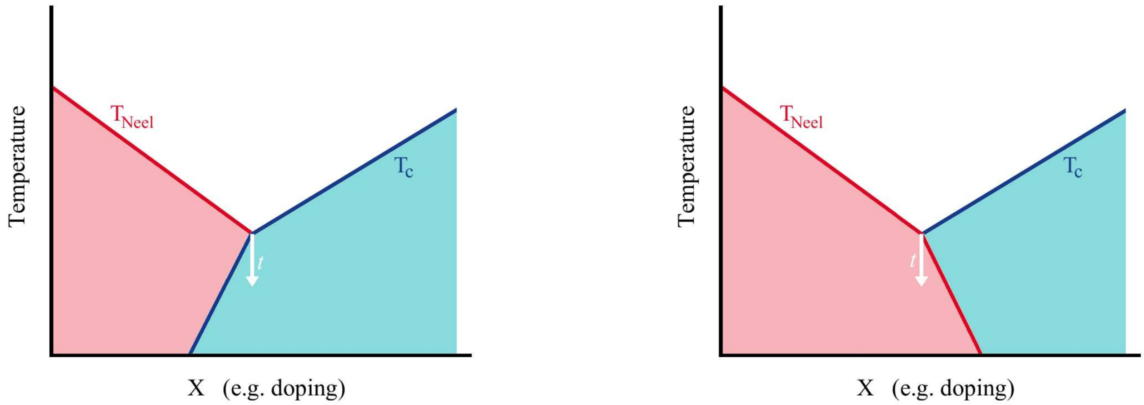

(a) The full phase diagram for $\Gamma \geq 1$, $\theta < 1$.

(b) The full phase diagram for $\Gamma \geq 1$, $\theta > 1$.

Figure 8.5: The possible phase diagrams for $\Gamma \geq 1$. The superconducting state is given in blue, with the anti-ferromagnetic state in red. The white region indicates a normal state. The line along which the theory is developed is indicated by the white arrow. To note: the phase boundaries are not necessarily linear (See. Fig. 7.4).

written as

$$\Gamma < \theta < \Gamma^{-1}, \tag{8.13}$$

which implies $\Gamma < 1$ in order to find a valid θ.

These conditions are in accordance with the condition arising from Eq. (8.6). The calculation showing this agreement, along with another cross-check of the conditions can be found in Appendix A. A summary of the conditions for coexistence is given in Fig. 8.4.

8.1.2.2 A different context for Γ and θ

Both Γ and θ have been defined as useful dimensionless quantities to determine the conditions for a coexisting state at zero field. The resulting phase diagram was given in Fig. 8.4. In this section the effect of varying Γ and θ within the context of the phase diagram given in Fig. 8.1 will be shown.

Consider first the scenario where $\Gamma \geq 1$. As stated before, this means that a coexisting state is not stable, which in turns means that one is dealing with a first order phase transition between the superconducting and the anti-ferromagnetic state. There are two possibilities for the full phase diagram (as compared to Fig. 8.1) which are given in Fig. 8.5.

From the previous section one knows that θ determines which of the two states is energetically favourable directly below the multicritical point, or in other words, which of these two states

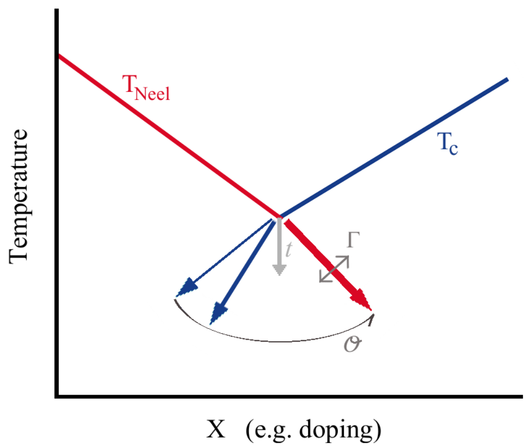

Figure 8.6: The effect of varying Γ and θ on the phase diagram for $\Gamma \geq 1$. This corresponds to first order phase transitions. θ determines the angle, while Γ determines the first order discontinuity jump size which is indicated by the thickness of the arrow. To note: the phase boundaries are not necessarily linear (See. Fig. 7.4).

the system is in at a temperature below T_c (given the critical level of doping). The angle (or if preferred, the gradient, Δ) of the separation line therefore uniquely fixes the value of θ or vice versa. For $\theta = \phi_3/\phi_2 = 1$, the two states are equal in energy, which means $\Delta \to \infty$. For $\theta = \phi_3/\phi_2 < 1$, the superconducting state is stable, which corresponds to Fig. 8.5(a). For $\theta > 1$, the anti-ferromagnetic state is stable, which corresponds to Fig. 8.5(b). The value of Γ determines the magnitude of the discontinuity in the order parameter value and the staggered magnetization value across the separation line. All these properties are summarized in Fig. 8.6. Now consider the scenario where $\Gamma < 1$. The phase transitions are now of second-order, allowing for three different cases of phase diagrams as shown in Fig. 8.7.

As in the previous case, θ rotates the coexisting region, while Γ determines the width of the coexisting state. This is summarized in Fig. 8.8.

8.1.3 The homogeneous coexistence problem with $\mathbf{A} \neq 0$

Consider now the effect of placing the system in an external magnetic field, $\mathbf{H}$. The resultant field in the system is again denoted by $\mathbf{B}$. As before (see section 2.1) the free energy now has an additional term

$$\phi = -a_s t \left|\psi\right|^2 + \frac{1}{2} b_s \left|\psi\right|^4 + \gamma \left|\psi\right|^2 \mathbf{M}_s^2 - a_m t \mathbf{M}_s^2 + \frac{1}{2} b_m \mathbf{M}_s^4 + \frac{\mathbf{B}^2}{8\pi}. \tag{8.14}$$

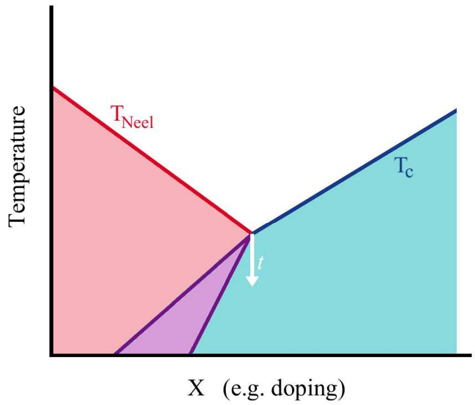

(a) The full phase diagram for $\Gamma < 1$, $\theta < \Gamma$.

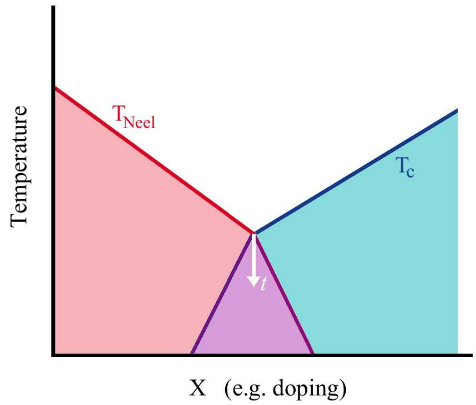

(b) The full phase diagram for $\Gamma < 1$, $\Gamma < \theta < \Gamma^{-1}$.

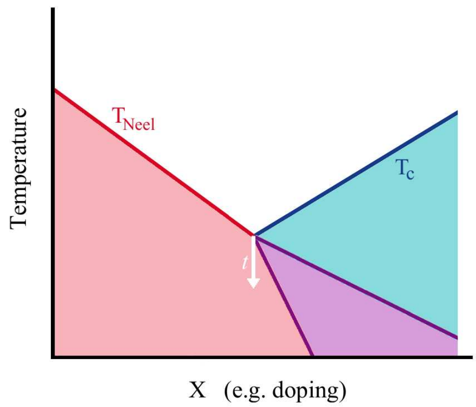

(c) The full phase diagram for $\Gamma < 1$, $\theta < \Gamma$.

Figure 8.7: The possible phase diagrams for $\Gamma < 1$. The superconducting state is given in blue, with the anti-ferromagnetic state in red and the coexisting state in purple. The white region indicates a normal state. The line along which the theory is developed is indicated by the white arrow. To note: the phase boundaries are not necessarily linear (See. Fig. 7.4).

However, the homogeneous superconducting states are characterized by the Meissner effect where $\mathbf{B} = \mathbf{0}$. Thus, both the bulk superconducting-only and the bulk coexisting state have the same free energy as given in Eq. (8.8). Only the free energy for the AFM-only state needs to be recalculated[11]. As no superconductivity is present in this state, one has $\mathbf{B} = \mathbf{H}$, so now

$$\phi_3 = -\frac{a_m^2}{2b_m}t^2 + \frac{H^2}{8\pi}. \tag{8.15}$$

[11]The external magnetic field adds the same value in free energy to both ϕ_1 and ϕ_3, so ϕ_1 always has a higher value than ϕ_3 and is therefore never stable.

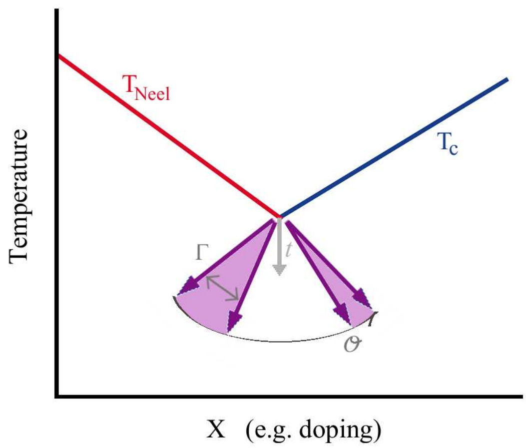

Figure 8.8: The effect of varying Γ and θ on the phase diagram for $\Gamma < 1$. This corresponds to second-order phase transitions. θ determines the angle, while Γ determines the region of coexistence which is indicated in purple. To note: the phase boundaries are not necessarily linear (See. Fig. 7.4).

All that remains now is to calculate which value of the external magnetic field results in two specific states having the same homogeneous free energy.

8.1.3.1 The critical external magnetic fields

The calculation of the interface energy requires that the two states between which an interface occurs be energetically equally favourable. This can be achieved by setting the external magnetic field to a critical magnetic field H_c, where H_c depends on the two states under consideration.

As only the free energy of the homogeneous AFM-only state can be tuned by varying H, there are only two sensible interfaces: one between an AFM-only and a SC-only state and one between an AFM-only and a coexisting state. In this section these two critical fields will be calculated.

Eq. (2.12) gives an expression for the critical external magnetic field

$$\frac{1}{8\pi}H_c^2\left(T\right) = f_n\left(T,\mathbf{0}\right) - f_s\left(T,\mathbf{0}\right), \tag{8.16}$$

where f denotes the free energy density. Using this expression and the conditions from Eq. (8.13), one obtains

$$\frac{1}{8\pi}H_c^2 = \begin{cases} \phi_3 - \phi_4 = \frac{a_m^2}{2b_m}\frac{\left(\gamma - \frac{a_s b_m}{a_m}\right)^2}{\left(b_m b_s - \gamma^2\right)}t^2 & \text{if } \Gamma < \theta < \Gamma^{-1} \\ \phi_3 - \phi_2 = \frac{1}{2}\left(\frac{a_s^2}{b_s} - \frac{a_m^2}{b_m}\right)t^2 & \text{if } \theta < \min\left(1,\Gamma\right) \end{cases} \tag{8.17}$$

This can be rewritten in terms of the dimensionless ratios Γ and θ so that

$$H_c^2(T) = H_{c,0}^2(T)\,\rho(\Gamma,\theta) \tag{8.18}$$

where

$$H_{c,0}^2(T) = 4\pi\frac{a_s^2}{b_s}t^2 \tag{8.19}$$

is the critical field without competing anti-ferromagnetism and

$$\rho(\Gamma,\theta) = \begin{cases} \frac{(1-\theta\Gamma)^2}{1-\Gamma^2} & \text{if } \Gamma < \theta < \Gamma^{-1} \\ 1-\theta^2 & \text{if } \theta < \min(1,\Gamma) \end{cases} \tag{8.20}$$

characterizes the change in the critical field due to the phase competition. In both cases $\rho < 1$ i.e. $H_c(T) < H_{c,0}(T)$. Thus, the competing phases result in a lowering of the external field needed to obtain equal free energies.

8.2 The inhomogeneous free energy for the coexistence problem

In this section an extension to the more general inhomogeneous system will be developed, along with expressions for the coherence lengths and penetration depth, the three natural length scales of the problem. Altogether, this sets the background against which the interface energy functional will be obtained.

The full free energy density expression is obtained by extending Eq. (8.14) to allow for inhomogeneous order parameters

$$\begin{aligned} \phi \;=\; & -a_s t\,|\psi|^2 + \frac{1}{2}b_s|\psi|^4 + \frac{1}{2m^*}\left|\left(-i\hbar\nabla - \frac{e^*}{c}\mathbf{A}\right)\psi\right|^2 + \frac{B^2}{8\pi} \\ & -a_m t\mathbf{M}_s^2 + \frac{1}{2}b_m\mathbf{M}_s^4 + d\,(\nabla\mathbf{M}_s)^2 + \gamma\,|\psi|^2\,\mathbf{M}_s^2, \end{aligned} \tag{8.21}$$

both these new terms are constructed so that the free energy is gauge invariant.

In order to highlight the difference between the two inhomogeneous terms, consider again[12] the familiar '$\nabla\psi$' term. This term originates from the fact that neither ψ nor the vector potential $\mathbf{A}$ is a physical quantity of the system. In fact, there is no unique $\mathbf{A}$ since it relates to the induced magnetic field $\mathbf{B}$, which is a physical quantity, by $\nabla\times\mathbf{A} = \mathbf{B}$.

Unlike with $\mathbf{B}$, a gauge transformation $\mathbf{A} \to \mathbf{A} + \nabla\Lambda$ will alter the value of the free energy density. But as the free energy density is also a physical quantity of the system, it should not depend on the choice of $\mathbf{A}$. In order to compensate for this choice, the spatial variation in ψ is

[12] This was previously discussed in section 2.2.2.

therefore linked to $\mathbf{A}$ as given in the equation above. Thus, under the further transformation $\psi \rightarrow \exp(ie^*\Lambda/\hbar c)\psi$ one obtains a gauge invariant free energy.

In contrast to this, the magnitude of the staggered magnetization, M_s, is in itself a physical quantity of the system. It is therefore fixed and cannot be subject to a gauge transformation. For this reason there is only the term $d\left(\nabla\mathbf{M}_s\right)^2$, where the square ensures a real number as opposed to a vector quantity.

From Eq. (8.21) one can determine the Ginzburg-Landau equations that follow from a minimization of $\Phi\left[\psi, \mathbf{A}, \mathbf{M}_s\right]$:

$$\begin{aligned}
\frac{1}{2m^*}\left(-i\hbar\nabla - \frac{e^*}{c}\mathbf{A}\right)^2\psi - a_s\tau\psi + b_s\left|\psi\right|^2\psi + \gamma\psi\mathbf{M}_s^2 &= 0 \\
-d\nabla^2\mathbf{M}_s - a_m\tau\mathbf{M}_s + b_m\mathbf{M}_s^2\mathbf{M}_s + \gamma\left|\psi\right|^2\mathbf{M}_s &= 0 \\
\nabla\times\mathbf{B} &= \frac{4\pi}{c}\mathbf{j}_{ind}
\end{aligned} \tag{8.22}$$

with gauge invariant current

$$\mathbf{j}_{ind} = \frac{e^*\hbar}{2m^*i}\left(\psi^*\nabla\psi - \psi\nabla\psi^*\right) - \frac{e^{*2}}{m^*c}\left|\psi\right|^2\mathbf{A}. \tag{8.23}$$

8.2.1 The penetration depth

The penetration depth is the natural length scale of the induced magnetic field, $\mathbf{B}$. To obtain this scale, consider, as done in section 2.2.4.2, the London limit where $\psi\left(\mathbf{r}\right) = \psi_0 = const$, but $\mathbf{A} \neq \mathbf{0}$. In other words, consider the limit where the order parameter is constant, but the magnetic field still varies.

From Eq. (8.23) it follows that the current is given by

$$\mathbf{j}_{ind} = -\frac{e^{*2}}{m^*c}\psi_0^2\mathbf{A}. \tag{8.24}$$

From here the calculation follows the same path as done in the one-band scenario given in section 2.2.4.2. The only difference is the value for ψ_0, which differs for the coexisting state. This only comes into play at the end of the derivation. Shortly restating the derivation, one has from Eq. (8.24) $\nabla\times\mathbf{j}_{ind} = -\frac{e^{*2}}{m^*c}\psi_0^2\mathbf{B}$, which yields $\nabla\times\nabla\times\mathbf{B} = -\frac{4\pi e^{*2}}{m^*c^2}\psi_0^2\mathbf{B}$, and since $\nabla\cdot\mathbf{B} = \mathbf{0}$, this equation simplifies to

$$\nabla^2\mathbf{B} = \frac{4\pi e^{*2}}{m^*c^2}\psi_0^2\mathbf{B}. \tag{8.25}$$

The solution for $\mathbf{B}$ is then $\mathbf{B}\left(z\right) = \mathbf{B}\left(0\right)\exp\left(-z/\lambda\right)$ with $\lambda^{-2} = \frac{4\pi e^{*2}}{m^*c^2}\psi_0^2$.

Substituting the values for ψ_0 from Eq. (8.5) into the above equation now yields for the penetration depth

$$\lambda^{-2} = \begin{cases} \frac{4\pi e^{*2}}{m^* c^2} \frac{a_s - \frac{\gamma}{b_m} a_m}{b_s\left(1 - \frac{\gamma^2}{b_s b_m}\right)} t & \text{if} \quad \Gamma < \theta < \Gamma^{-1} \\ \frac{4\pi e^{*2}}{m^* c^2} \frac{a_s}{b_s} t & \text{if} \quad \theta < \min(1, \Gamma) . \end{cases} \tag{8.26}$$

For convenience, this can be written in terms of Γ and θ only:

$$\lambda^{-2} = \lambda_0^{-2} \varphi(\Gamma, \theta) \tag{8.27}$$

where λ_0 is the penetration depth of a purely superconducting state,

$$\lambda_0^{-2} = \frac{4\pi e^{*2}}{m^* c^2} \frac{a_s}{b_s} t, \tag{8.28}$$

and φ is a dimensionless quantity, from Eqs. (8.9) and (8.10)

$$\varphi(\Gamma, \theta) = \begin{cases} \frac{1 - \theta\Gamma}{1 - \Gamma^2} & \text{if} \quad \Gamma < \theta < \Gamma^{-1} \\ 1 & \text{if} \quad \theta < \min(1, \Gamma) . \end{cases} \tag{8.29}$$

This shows that the penetration depth only changes when one considers the coexisting state, not in the pure superconducting state, exactly as expected.

8.2.2 The coherence length

In this section the natural length scales of the order parameter and the staggered magnetization, the respective coherence lengths, will be determined. To do so, the limit where the induced magnetic field is zero, but the order parameters are finite will be discussed.

First, consider the case without competition, thus $\gamma = 0$. The Ginzburg-Landau equations, specifically line 1 in Eq. (8.22), is now in exactly the same form as the London limit for the one-band scenario as done in section 2.2.4.1. Thus, without competition the natural length scale of the superconducting order parameter is already determined

$$\xi_{s,0}^2 = \frac{\hbar^2}{2m^* a_s t}. \tag{8.30}$$

From the symmetry between line 1 and line 2 of Eq. (8.22) at zero field, it is clear that the natural length scale of the magnetic order parameter is

$$\xi_{m,0}^2 = \frac{d}{a_m t}. \tag{8.31}$$

The question is how these length scales behave when $\gamma \neq 0$. For this purpose, consider small spatial deviations from the homogeneous order, i.e, analyze line 1 and 2 of Eq. (8.22)

$$\begin{aligned} -\frac{\hbar^2}{2m^*}\nabla^2\psi - a_s t\psi + b_s\left|\psi\right|^2\psi + \gamma\psi\mathbf{M}_s^2 &= 0 \\ -d\nabla^2\mathbf{M}_s - a_m t\mathbf{M}_s + b_m\mathbf{M}_s^2\mathbf{M}_s + \gamma\left|\psi\right|^2\mathbf{M}_s &= 0 \end{aligned} \tag{8.32}$$

for $\psi(\mathbf{r}) = \psi_0 + \chi(\mathbf{r})$ and $\mathbf{M}_s(\mathbf{r}) = \mathbf{M}_{s,0} + \mu(\mathbf{r})$, with small $\chi(\mathbf{r})$ and $\mu(\mathbf{r})$.

Using Eq. (8.4), this yields

$$\begin{aligned} -\frac{\hbar^2}{2m^*}\nabla^2\chi + \left(3b_s\psi_0^2 - a_s t + \gamma M_{s,0}^2\right)\chi + 2\gamma\psi_0 M_{s,0}\mu &= 0 \\ -d\nabla^2\mu + \left(3b_m M_{s,0}^2 - a_m t + \gamma\psi_0^2\right)\mu + 2\gamma\psi_0 M_{s,0}\chi &= 0, \end{aligned} \tag{8.33}$$

where $M_{s,0}$ is the magnitude of the vector $\mathbf{M}_{s,0}$.

8.2.2.1 The coherence length in the superconducting-only regime

First consider Eqs. (8.33) for the superconducting-only regime $\theta < \min(1, \Gamma)$ where $M_0 = 0$ and $\psi_0^2 = \frac{a_s}{b_s}t$. These equations then read

$$\begin{aligned} -\frac{\hbar^2}{2m^*}\nabla^2\chi + 2a_s t\chi &= 0 \\ -d\nabla^2\mu + a_m t\left(\Gamma/\theta - 1\right)\mu &= 0 \end{aligned} \tag{8.34}$$

By solving for x in an expression with the form

$$-\xi^2\nabla^2 x + x = 0, \tag{8.35}$$

one finds that the natural length scale associated to the variable x is ξ. This means that

$$\begin{aligned} \xi_s^2 &= \frac{\hbar^2}{2m^* 2a_s t} = \frac{1}{2}\xi_{s,0}^2 \\ \xi_m^2 &= \frac{d}{a_m t\left(\Gamma/\theta - 1\right)} = \frac{1}{\Gamma/\theta - 1}\xi_{m,0}^2. \end{aligned} \tag{8.36}$$

These length scales behave as expected for the superconducting-only region. This can be seen by considering the two limits $\theta \to 1$ for $\Gamma > 1$ and $\Gamma \to \theta + 0^+$ corresponding to the two borders of the superconducting-only region, see Fig. 8.4.

The former limit, $\theta \to 1$ for $\Gamma > 1$, corresponds to the border between the two pure states. In this limit one has first order transitions for both order parameters, from $\psi \neq 0$ and $M_s = 0$ to $\psi = 0$ and $M_s \neq 0$. This means that there should be no divergence in the length scales, which is indeed the case for both ξ_s^2 and ξ_m^2.

In contrast, the limit $\Gamma \to \theta + 0^+$, corresponding to the border between a pure superconducting state and a coexisting state, deals with a second-order transition for the magnetic order parameter. Therefore the magnetic correlation length should diverge, which is indeed the case for ξ_m^2 in this limit.

8.2.2.2 The coherence length in the coexisting regime

Next one can analyze Eqs. (8.33) in the regime $\Gamma < \theta < \Gamma^{-1}$ with M_0^2 and ψ_0^2 of Eq. (8.5) (solution 4). This yields

$$
\begin{aligned}
-r_s\nabla^2\chi + \chi + \Gamma\varepsilon\mu &= 0 \\
-r_m\nabla^2\mu + \mu + \Gamma/\varepsilon\chi &= 0
\end{aligned}
\tag{8.37}
$$

where

$$
\begin{aligned}
r_s &= \frac{\hbar^2}{2m^* 2a_s t\frac{1-\Gamma\theta}{1-\Gamma^2}} \\
r_m &= \frac{d}{2a_m t\frac{1-\Gamma/\theta}{1-\Gamma^2}} \\
\varepsilon &= \sqrt{\frac{a_m}{a_s}}\sqrt{\frac{1-\Gamma/\theta}{1-\Gamma\theta}}.
\end{aligned}
\tag{8.38}
$$

The fact that these equations are coupled implies that there is not one single length scale for the decay of the superconducting and magnetic degrees of freedom.

One can however analyze the limits for which these equations decouple. For $\Gamma \to \theta - 0^+$ or $\Gamma \to \theta^{-1} - 0^+$, ε either vanishes or diverges, which decouples the equations. In these limits one finds respectively

$$
\begin{aligned}
\xi_s^2 &= \frac{1}{2}\xi_{s,0}^2\frac{1-\Gamma^2}{1-\Gamma\theta}, \\
\xi_m^2 &= \xi_{m,0}^2\frac{1-\Gamma^2}{1-\Gamma/\theta}.
\end{aligned}
\tag{8.39}
$$

Thus, in the limit $\Gamma \to \theta - 0^+$ where $\psi \to 0$ the natural length scale of the magnetic order parameter is fixed, while ξ_s^2diverges. And in the limit $\Gamma \to \theta^{-1} - 0^+$ where $\mathbf{M}_s \to 0$ the natural length scale of the superconducting order parameter is fixed, while ξ_m^2 diverges.

Although the limit $\Gamma \to 1$ and $\theta \to 1$ does not decouple the system, it is still possible to analyze the equations in this limit too. Consider for example the case $\theta = 1$ and $\Gamma \to 1 - 0^+$. It holds

$$\begin{aligned} -\frac{\hbar^2}{2m^* a_s \tau}\nabla^2\chi + \chi + \sqrt{\frac{a_m}{a_s}}\mu &= 0 \\ -\frac{d}{a_m \tau}\nabla^2\mu + \mu + \sqrt{\frac{a_m}{a_s}}\chi &= 0. \end{aligned} \tag{8.40}$$

This implies that both length scales remain finite in this limit.

8.2.2.3 The final result

Based on the previous results on the natural length scales, it seems sensible to introduce

$$\xi_s^2 = \begin{cases} \frac{1}{2}\xi_{s,0}^2 \frac{1-\Gamma^2}{1-\Gamma\theta} & \Gamma < \theta < \Gamma^{-1} \\ \frac{1}{2}\xi_{s,0}^2 & \theta < \min\left(1, \Gamma\right). \end{cases} \tag{8.41}$$

Although this does not give the precise values for the natural length scales in the interior region of the coexisting regime, this expression does captures all the relevant limits for ξ_s^2. The same can clearly be done for ξ_m^2.

8.3 The coexistence interface energy

All the necessary concepts have been discussed or developed now in order to formulate the interface problem for a system with coexistence. The overall concept of an interface has already been discussed in section 2.3. The novel aspect of this problem is that the interface now occurs between an homogeneous AFM-only state and either a coexisting state or a SC-only state. This section deals with constructing the correct functional $\Sigma\left[\psi, \mathbf{M_s}, \mathbf{A}\right]$ and deriving its dimensionless version for the purpose of numerical calculation. As in the previous interface problem, a key aspect is to determine the critical ratio of relevant length scales, κ_c, which shows the border between type-I and type-II behaviour. This section will end off with an analytical derivation of this κ_c, while the numerical results for κ_c will be given and discussed in the next chapter.

8.3.1 Formulation of the functional

The construct used in this interface problem is similar to that of the one-band scenario discussed in section 2.3 and of the two-band problem as done in section 4.2. Again, by taking the cylindrical symmetry of the interface problem into account, the equations can be rewritten in a one-dimensional form. This will be done first, followed by the derivation of the interface functional itself.

Along the same construct as shown in Fig. 2.3, take the magnetic field $\mathbf{B}\left(\mathbf{r}\right) = B\left(z\right)\mathbf{e}_x$

to point in the x-direction and depend on the z-coordinate. Using the crossproduct definition $B_\alpha = \varepsilon_{\alpha\beta\gamma}\frac{\partial A_\gamma}{\partial x_\beta}$ yields for the vector potential $\mathbf{A}(\mathbf{r}) = -A(z)\,\mathbf{e}_y$ where

$$B(z) = \frac{\partial A(z)}{\partial z}. \tag{8.42}$$

From the cylindric symmetry assumption both order parameters only depend on z. As in the one-band scenario this gives

$$\left|\left(-i\hbar\nabla - \frac{e^*}{c}\mathbf{A}\right)\psi\right|^2 = \hbar^2\left(\frac{d\psi}{dz}\right)^2 + \frac{e^{*2}}{c^2}A^2\psi^2 \tag{8.43}$$

The overall free energy of the coexisting state is therefore

$$\begin{aligned} F &= F_n + L^2\int\left(-a_s t\psi^2 + \frac{1}{2}b_s\psi^4 + \frac{\hbar^2}{2m^*}\left(\frac{d\psi}{dz}\right)^2 + \frac{e^{*2}}{2m^*c^2}A^2\psi^2\right)dz \\ &\quad + L^2\int\left(-a_m t M_s^2 + \frac{1}{2}b_m M_s^4 + d\left(\frac{dM_s}{dz}\right)^2 + \gamma\,|\psi|^2 M_s^2 + \frac{B^2}{8\pi}\right)dz. \end{aligned} \tag{8.44}$$

However, it is the free enthalpy that is the more useful quantity. By Eq. (2.33)

$$\begin{aligned} G &= F_n + L^2\int\left(-a_s t\psi^2 + \frac{b_s}{2}\psi^4 + \frac{\hbar^2}{2m^*}\left(\frac{d\psi}{dz}\right)^2 + \frac{e^{*2}A^2\psi^2}{2m^*c^2} - a_m t M_s^2\right)dz \\ &\quad + L^2\int\left(\frac{1}{2}b_m M_s^4 + d\left(\frac{dM_s}{dz}\right)^2 + \gamma\,|\psi|^2 M_s^2 + \frac{(B-H_c)^2}{8\pi} - \frac{H_c^2}{8\pi}\right)dz. \end{aligned} \tag{8.45}$$

In order to write down the interface energy functional

$$\Sigma = (G - G_{bulk})/L^2, \tag{8.46}$$

the enthalpy of the bulk state - the AFM-only state - must be calculated. The enthalpy of the pure AFM state can be determined by setting $\psi = 0$, $\mathbf{B} = \mathbf{H_c}$ and $\mathbf{M}_s = \mathbf{M}_{s,0}$ in the expression for the coexisting enthalpy, Eq. (8.45)

$$\begin{aligned} G_{bulk} &= -L^2\int\frac{H_c^2}{8\pi}dz + L^2\int\left(-a_m t M_{s,0}^2 + \frac{1}{2}b_m M_{s,0}^4\right)dz \\ &= -L^2\int\left(\frac{H_c^2}{8\pi} + \frac{a_m^2}{2b_m}t^2\right)dz \end{aligned} \tag{8.47}$$

This result can be checked. By construction of $\mathbf{H}_c$, one must have that the free enthalpy of the bulk normal state (the pure AFM state) of Eq. (8.47) be equal to the free enthalpy of the other bulk state in question, thus the lower of ϕ_2 and ϕ_4 from Eq. (8.8). This is certainly the case. From Eqs. (8.47), (8.8) and (8.16)

$$\begin{aligned} G_{bulk} &= -L^2 \int \frac{H_c^2}{8\pi} dz + L^2 \int \phi_3 dz \\ &= -L^2 \int (\phi_3 - \phi_\alpha)\, dz + L^2 \int \phi_3 dz = L^2 \int \phi_\alpha dz \end{aligned} \tag{8.48}$$

where ϕ_α is either ϕ_2 or ϕ_4, whichever is lower as determined by the values of Γ and θ.

Thus by Eq. (8.46) the interface functional is

$$\begin{aligned} \Sigma = & \int \left(-a_s t \psi^2 + \frac{b_s}{2}\psi^4 + \frac{\hbar^2}{2m^*}\left(\frac{d\psi}{dz}\right)^2 + \frac{e^{*2}A^2\psi^2}{2m^*c^2} + \frac{(B-H_c)^2}{8\pi} \right) dz \\ & + \int \left(-a_m t M_s^2 + \frac{1}{2} b_m M_s^4 + d\left(\frac{dM_s}{dz}\right)^2 + \gamma\,|\psi|^2 M_s^2 + \frac{a_m^2}{2b_m}t^2 \right) dz. \end{aligned} \tag{8.49}$$

The two different interfaces, one between a coexisting and a pure AFM state and the other between a pure SC and a pure AFM state, are enforced by the boundary conditions. These are in turn determined by the values chosen for Γ and θ. For both the interfaces one has the normal state on the right so that

$$\begin{aligned} \psi^2 (z \to \infty) &= 0 \\ \mathbf{M}_s^2 (z \to \infty) &= \frac{a_m}{b_m} t. \end{aligned} \tag{8.50}$$

The boundary conditions for $t \to -\infty$ determines whether one is considering the interface with a coexisting state or a pure SC state on the left. For the former solution 4 of Eq. (8.5) is used, and for the latter solution 2. The choice is of course made by the values given for Γ and θ. Thus

$$\begin{aligned} \psi^2 (z \to -\infty) &= \begin{cases} \frac{a_s}{b_s} t & \theta < \min(1,\Gamma) \\ \frac{a_s - \frac{\gamma}{b_m} a_m}{b_s\left(1 - \frac{\gamma^2}{b_s b_m}\right)} t & \Gamma < \theta < \Gamma^{-1} \end{cases} \\ \mathbf{M}_s (z \to -\infty) &= \begin{cases} 0 & \theta < \min(1,\Gamma) \\ \frac{a_m - \frac{\gamma}{b_s} a_s}{b_m\left(1 - \frac{\gamma^2}{b_s b_m}\right)} t & \Gamma < \theta < \Gamma^{-1} \end{cases} \end{aligned} \tag{8.51}$$

In both these cases the boundary conditions on $\mathbf{A}$ are $\mathbf{A}(z \to -\infty) = 0$. This can easily be deduced in the dimensionless form and will therefore be discussed in the next section.

Together with the boundary conditions, the minimization of $\Sigma[M_s, \psi, A]$ from Eq. (8.49) with respect to $\mathbf{M_s}$, ψ and $\mathbf{A}$ will give the interface energy, σ_s. The expressions for the functional and boundary conditions can still be simplified by rewriting them in dimensionless form.

8.3.1.1 Dimensionless units

The dimensionless form of the interface functional and boundary conditions is simpler, and therefore preferable for numerical calculations. To this end one introduces the following dimensionless units

$$v = \frac{\psi}{\sqrt{\frac{a_s}{b_s}t}}, \quad \beta = \frac{B}{\sqrt{2}H_c}, \; s = \frac{z}{\lambda}, \quad m = \frac{M_s}{\sqrt{\frac{a_m}{b_m}t}}. \tag{8.52}$$

The dimensionless vector potential is chosen as

$$\alpha = \frac{A}{\sqrt{2}H_c\lambda}, \tag{8.53}$$

so that $\beta = d\alpha/ds$. A further dimensionless quantity is given by the ratio of the two coherence lengths, see Eqs. (8.30) and (8.31),

$$\begin{aligned} \xi_{m,0}^2 &= \frac{d}{a_m t} \\ \xi_{s,0}^2 &= \frac{\hbar^2}{2m^* a_s t}, \end{aligned} \tag{8.54}$$

which gives

$$\eta = \frac{\xi_{m,0}}{\xi_{s,0}}. \tag{8.55}$$

The final dimensionless variable is given by the familiar ratio

$$\widetilde{\kappa} = \frac{\lambda}{\xi_{s,0}}. \tag{8.56}$$

It may be more appropriate to introduce the ratio $\kappa = \lambda/\xi_s$ or $\kappa_0 = \lambda_0/\xi_{s,0}$, this comment will be returned to in section 8.3.2.

All these dimensionless quantities, plus Γ and θ and the resulting φ and ρ, see Eqs. (8.20) and (8.29), are used to give the dimensionless form of the interface energy functional

$$\begin{aligned} \Sigma \;=\; & \frac{H_c^2\lambda}{4\pi}\int\left(-\frac{1}{\rho}v^2 + \frac{1}{2\rho}v^4 + \frac{1}{\rho\widetilde{\kappa}^2}\left(\frac{dv}{ds}\right)^2 + \frac{1}{\varphi}\alpha^2 v^2 + \frac{\left(\sqrt{2}\beta - 1\right)^2}{2}\right) ds \\ & + \frac{H_c^2\lambda}{4\pi}\int\left(-\frac{\theta^2}{\rho}m^2 + \frac{\theta^2}{2\rho}m^4 + \frac{\theta^2\eta^2}{\rho\,\widetilde{\kappa}^2}\left(\frac{dm}{ds}\right)^2 + \frac{\Gamma\theta}{\rho}\left|v\right|^2 m^2 + \frac{\theta^2}{2\rho}\right) ds. \end{aligned} \tag{8.57}$$

This functional must now be minimized with respect to v, m and α subject to the dimensionless form of the boundary conditions of Eqs. (8.50) and (8.51)

$$\begin{aligned} v\left(s \to \infty\right) &= 0 \\ m\left(s \to \infty\right) &= 1, \end{aligned} \tag{8.58}$$

and

$$\begin{aligned} v\left(s \to -\infty\right) &= \begin{cases} 1 & \theta < \min\left(1, \Gamma\right) \\ \sqrt{\frac{1-\Gamma\theta}{1-\Gamma^2}} & \Gamma < \theta < \Gamma^{-1} \end{cases} \\ m\left(s \to -\infty\right) &= \begin{cases} 0 & \theta < \min\left(1, \Gamma\right) \\ \sqrt{\frac{1-\Gamma/\theta}{1-\Gamma^2}} & \Gamma < \theta < \Gamma^{-1} \end{cases} \end{aligned} \tag{8.59}$$

to give the interface energy.

As this is a minimization process, specifying the boundary conditions on v and m fixes the boundary conditions on α. In other words, specifying the boundary conditions on α too does not add information to the system. It is however easy to calculate what they should be.

Consider only a single state scenario, thus either a SC state, an AFM state or a coexisting state, with the appropriate homogeneous solutions to v and m. Clearly for a single state the interface energy functional, Eq. (8.57), must yield zero as there should be no difference in energy between two regions of the same state. For a pure AFM state, this means that $\beta = 1/\sqrt{2}$. For both the homogeneous coexisting and superconducting state, this yields $\alpha = 0$. As the boundary conditions are just the homogeneous solutions, this fixes the boundary conditions of α to $\alpha\left(s \to -\infty\right) = 0$ and $\left(d\alpha/ds\right)\left(s \to \infty\right) = 1/\sqrt{2}$.

8.3.2 The critical kappa

The question which must still be answered is where the minimization of the interface energy functional as given in the previous section is zero. The zero point(s) give(s) the border between type-I and type-II behaviour of the superconductor. In the one-band problem only one zero point exists, namely at $\kappa = 1/\sqrt{2} \equiv \kappa_c$, see section 2.3.2.3. In this problem there will be several zero points, at least one for every value of Γ and θ. The aim of this section is to obtain an analytic expression for these zero points.

Key to this derivation is the concept of the upper critical magnetic field in type-II superconductivity. This upper critical field, H_{c2}, is defined as the first onset of superconductivity as the external magnetic field is lowered. In traditional one-band superconductivity, this phase transition from a normal state to a type-II superconducting state is of second-order. Thus, just below

H_{c2} the superconducting order parameter is no longer zero, but has some small finite value and the magnetic field penetrates the system in the form of a vortex lattice. If the external field is lowered even further, one reaches H_{c1}, the onset of superconductivity with a complete Meissner effect.

The important assumption for this analysis, where anti-ferromagnetism is included, is that one is again dealing with a second-order phase transition at H_{c2}. This means that just below H_{c2} the order parameter can be linearized while the induced field B can still be taken as H_{c2}. Plugging this information into the Ginzburg-Landau equation (8.22) for this coexistence problem, one obtains

$$\frac{1}{2m^*}\left(-i\hbar\nabla - \frac{e^*}{c}\mathbf{A}\right)^2 \psi = a_s t\psi \; - \gamma\psi\mathbf{M}_s^2. \tag{8.60}$$

Close to this upper critical field $\mathbf{M}_s^2$ can be taken as the homogeneous normal state value $\mathbf{M}_s^2 = \frac{a_m}{b_m}t$ since the superconducting order parameter is small and therefore doesn't suppress the AFM order parameter through competition. This yields

$$\begin{aligned}\frac{1}{2m^*}\left(-i\hbar\nabla - \frac{e^*}{c}\mathbf{A}\right)^2 \psi &= a_s\left(1 \; - \gamma\frac{a_m}{b_m a_s}\right) t\psi \\ &= a_s\left(1 - \Gamma\theta\right) t\psi. \end{aligned}\tag{8.61}$$

This equation is in the form of a Schrödinger equation in an external magnetic field, $H\psi = E_n\psi$, with known eigenvalues

$$E_n = a_s\left(1 - \Gamma\theta\right) t = \frac{\hbar^2}{2m^*}k_z^2 + \left(n + \frac{1}{2}\right)\frac{\hbar e^* B}{m^* c} \tag{8.62}$$

where $n \geq 0$ labels the Landau levels. In this scenario B can be replaced by H_{c2}. By definition H_{c2} is the largest field which still allows for a solution to the above Schrödinger equation. The largest solution for H_{c2} is when $k_z = 0$ and $n = 0$, which yields

$$H_{c2} = \frac{2a_s m^* c}{\hbar e^*}\left(1 - \Gamma\theta\right) t. \tag{8.63}$$

At the border of type-I and type-II superconductivity one expects the critical external magnetic field associated to the type-I superconductivity, H_c, be equal to both H_{c1} and H_{c2}. This means that the ratio of the fields must equal 1, thus $H_{c2}/H_c = 1$. In the coexistence problem, H_c is given by $H_c^2\left(T\right) = H_{c,0}^2\left(T\right)\rho\left(\Gamma,\theta\right)$ with ρ given in Eq. (8.20). Equating H_c and H_{c2} gives the following expression

$$\frac{2a_s m^* c}{\hbar e^*}\left(1 - \Gamma\theta\right) = \sqrt{4\pi}\frac{a_s}{\sqrt{b_s}}\sqrt{\rho\left(\Gamma,\theta\right)}. \tag{8.64}$$

Thus, on the border between type-I and type-II superconductivity the ratio $\kappa_0 = \lambda_0/\xi_{s,0}$ is

$$\frac{\lambda_0}{\xi_{s,0}} = \frac{m^* c\sqrt{b_s}}{\sqrt{2\pi}\hbar e^*} = \frac{1}{\sqrt{2}}\frac{\sqrt{\rho(\Gamma,\theta)}}{(1-\Gamma\theta)}. \tag{8.65}$$

Formally this can be written as

$$\begin{aligned}\kappa_{0,c} &= \frac{\lambda_0}{\xi_{s,0}} = \frac{1}{\sqrt{2}}\frac{\sqrt{\rho(\Gamma,\theta)}}{(1-\Gamma\theta)} \\ &= \begin{cases} \frac{1}{\sqrt{2}}\frac{1}{\sqrt{1-\Gamma^2}} & \text{if } \Gamma < \theta < \Gamma^{-1} \\ \frac{1}{\sqrt{2}}\frac{\sqrt{1-\theta^2}}{1-\Gamma\theta} & \text{if } \theta < \min(1,\Gamma). \end{cases}\end{aligned} \tag{8.66}$$

This result is also in accordance with the traditional one-band problem. Ignoring the AFM energy contribution, thus setting $\theta = 0$, one finds the correct prediction $\kappa_c = 1/\sqrt{2}$ for the one-band problem.

However, in the formulation of the interface functional of section 8.3.1.1 it was not κ_0, but rather $\widetilde{\kappa} = \frac{\lambda}{\xi_{s,0}}$ that was used. Using the expression $\lambda^{-2} = \lambda_0^{-2}\varphi(\Gamma,\theta)$ one can also write down the critical $\widetilde{\kappa_c}$

$$\begin{aligned}\widetilde{\kappa_c} &= \frac{\lambda}{\xi_{s,0}} = \frac{1}{\sqrt{2}}\frac{\sqrt{\rho(\Gamma,\theta)}}{(1-\Gamma\theta)}\frac{1}{\sqrt{\varphi(\Gamma,\theta)}} \\ &= \begin{cases} \frac{1}{\sqrt{2}}\frac{1}{\sqrt{1-\theta\Gamma}} & \text{if } \Gamma < \theta < \Gamma^{-1} \\ \frac{1}{\sqrt{2}}\frac{\sqrt{1-\theta^2}}{1-\Gamma\theta} & \text{if } \theta < \min(1,\Gamma). \end{cases}\end{aligned} \tag{8.67}$$

This is then the analytically predicted behaviour for the critical κ value between type-I and type-II superconductivity as a function of Γ and θ. The same analytical result for the limiting case where $\Gamma = 1$, $0 < \theta < 1$ was found in Ref. [49], also under the assumption that a second-order phase transition occurs at $\mathbf{H}_{c2}$.

CHAPTER 9
Numerical results for the interface energy in the coexisting problem

In this chapter the numerical analysis and results of the interface energy of the coexistence problem are reported. The minimization method is similar to the one used in the previous two numerical studies. This will be recapped, followed by various case studies of specific interface energy calculations. These calculations are divided into two sections.

The first section deals with interfaces between a pure AFM and a pure superconducting state. In this section the limit studied in Ref. [49] is also included. The second deals with interfaces occurring between a coexisting state and a pure AFM state. Here only preliminary results will be given.

In both scenarios the curves for the different order parameters and external field are discussed, see sections 9.2.1 and 9.3.1. Also the numerical results for $\widetilde{\kappa}_c$, the critical $\widetilde{\kappa}$ marking the boundary between type-I and type-II superconductivity, are given in each case. These are discussed and compared to the theoretical prediction in sections 9.2.2 and 9.3.2.

9.1 The setup

In order to minimize the functional, Eq. (8.57)

$$\begin{aligned}\Sigma &= \frac{H_c^2\lambda}{4\pi}\int\left(-\frac{1}{\rho}v^2+\frac{1}{2\rho}v^4+\frac{1}{\rho\widetilde{\kappa}^2}\left(\frac{dv}{ds}\right)^2+\frac{1}{\varphi}\alpha^2v^2+\frac{\left(\sqrt{2}\beta-1\right)^2}{2}\right)ds \\ &\quad+\frac{H_c^2\lambda}{4\pi}\int\left(-\frac{\theta^2}{\rho}m^2+\frac{\theta^2}{2\rho}m^4+\frac{\theta^2\eta^2}{\rho\,\widetilde{\kappa}^2}\left(\frac{dm}{ds}\right)^2+\frac{\Gamma\theta}{\rho}\left|v\right|^2m^2+\frac{\theta^2}{2\rho}\right)ds. \qquad (9.1)\end{aligned}$$

with respect to v, m and α, it must again be discretized over an interval $2L$. The boundary conditions must also be specified to the end points of this interval:

$$\begin{aligned}v\,(s=2L) &= 0 \\ m\,(s=2L) &= 1, \qquad (9.2)\end{aligned}$$

and

$$v\,(s=0) \;=\; \begin{cases} 1 & \theta < \min(1,\Gamma) \\ \sqrt{\frac{1-\Gamma\theta}{1-\Gamma^2}} & \Gamma < \theta < \Gamma^{-1} \end{cases}$$
$$m\,(s=0) \;=\; \begin{cases} 0 & \theta < \min(1,\Gamma) \\ \sqrt{\frac{1-\Gamma/\theta}{1-\Gamma^2}} & \Gamma < \theta < \Gamma^{-1}. \end{cases} \tag{9.3}$$

Although it is not necessary in principle, the condition

$$\alpha\,(s=0) = 0 \tag{9.4}$$

was also specified in the numerical method.

In the coming sections, the large $\widetilde{\kappa}$ limit of the interface energy will be referred to, which results in two terms in Eq. (9.1) effectively being zero. In this limit the interface energy functional reads

$$\begin{aligned}\Sigma \;=\; & \frac{H_c^2\lambda}{4\pi}\int\left(-\frac{1}{\rho}v^2+\frac{1}{2\rho}v^4+\frac{1}{\varphi}\alpha^2v^2+\frac{\left(\sqrt{2}\beta-1\right)^2}{2}\right)ds \\ & +\frac{H_c^2\lambda}{4\pi}\int\left(-\frac{\theta^2}{\rho}m^2+\frac{\theta^2}{2\rho}m^4+\frac{\Gamma\theta}{\rho}\left|v\right|^2m^2+\frac{\theta^2}{2\rho}\right)ds.\end{aligned} \tag{9.5}$$

Again, this functional needs to be minimized subject to the same boundary conditions.

9.2 The pure-state interface results for $\Gamma = 1,\ 0 < \theta < 1$

The general theoretical derivation of the interface energy presented in chapter 8 is not yet found in the literature[13]. However, a specific case of the interface energy where $\Gamma = 1$, $0 < \theta < 1$ and $\eta^2 = 1/\theta$ was studied previously in Ref. [49]. In this section the same line in the $\Gamma\theta$-phase space will be considered, which of course corresponds to an interface between pure states. However, the choice $\eta^2 = 1/\theta$, as used in Ref. [49], will be compared to the cases where $\eta^2 = 1$ and $\eta^2 = 1/\theta^3$ respectively. The specific choices of η^2 will become clear later in this section.

9.2.1 The profiles of the order parameters and induced magnetic field

From the numerical minimization of the interface energy, the profiles of the superconducting order parameter, the staggered magnetization and the induced magnetic field were found. In this specific case $\eta^2 = 1$. As the other choices of η^2 exhibit the same general behaviour, only the case where $\eta^2 = 1$ is given in Fig. 9.1. The boundary values seen in Fig. 9.1 show that these profiles correspond to an interface between the two pure states. As expected from the form of

[13] To the date of submitting this work

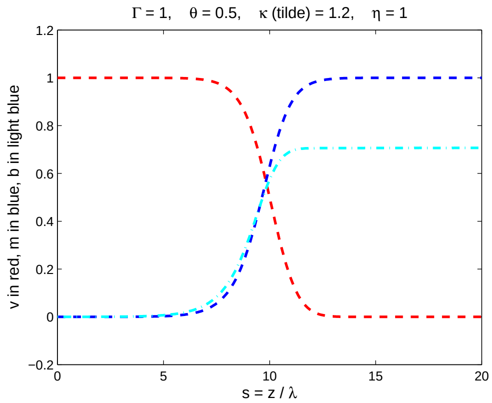

(a) The profiles for $\widetilde{\kappa} = 1.2$.

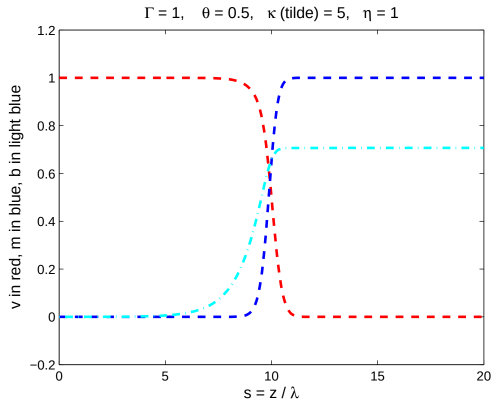

(b) The profiles for $\widetilde{\kappa} = 5$.

Figure 9.1: The $\Gamma = 1, \theta = 0.5$ and $\eta^2 = 1$ curves as a general example of the profiles of the dimensionless order parameters and induced field for different values of $\widetilde{\kappa}$.

the functional, an increase in the value of $\widetilde{\kappa}$ allows the rate of change for the order parameters to increase.

In the large $\widetilde{\kappa}$ limit one obtains the profile plot given in Fig. 9.2. The profiles of the large $\widetilde{\kappa}$ limit show that both the induced magnetic field and the superconducting order parameter vary on the same length scale, while the staggered magnetization varies on an extremely short length scale. This behaviour can be understood as follows. In Eq. (9.5) there is only one term that determines a rate of change, namely the term containing $\beta = d\alpha/ds$. As this term always results in a positive contribution to the interface energy, the minimization of this term leads to a slower (than instantaneous) rate of change for the induced magnetic field. As the superconducting order parameter is coupled to the induced magnetic field, and as there are no other constraints on its rate of change, v will also vary on the same length scale. However, the staggered magnetization is not coupled to the induced magnetic field, only to the superconducting order parameter in a term which gives a positive contribution to the interface energy. That is, of course, unless either one of v or m is zero, see Eq. (9.5). Indeed, this term is zero for every value of s in this pure states interface scenario. From the boundary conditions one has that on one side of the interface $m = 0$, while on the other $v = 0$. In order to minimize the functional, the system therefore keeps either one of m or v at zero which results in the instantaneous leap between $m = 0$ and $m = 1$. Thus, the key why the staggered magnetization does not vary on the same length scale as the superconducting order parameter and induced field, is the boundary conditions.

From the minimization, a specific value for the interface energy is obtained for each set of the profiles associated to a specific $\widetilde{\kappa}$ and η. Ranging $\widetilde{\kappa}$ between 1 and the large $\widetilde{\kappa}$ limit for a

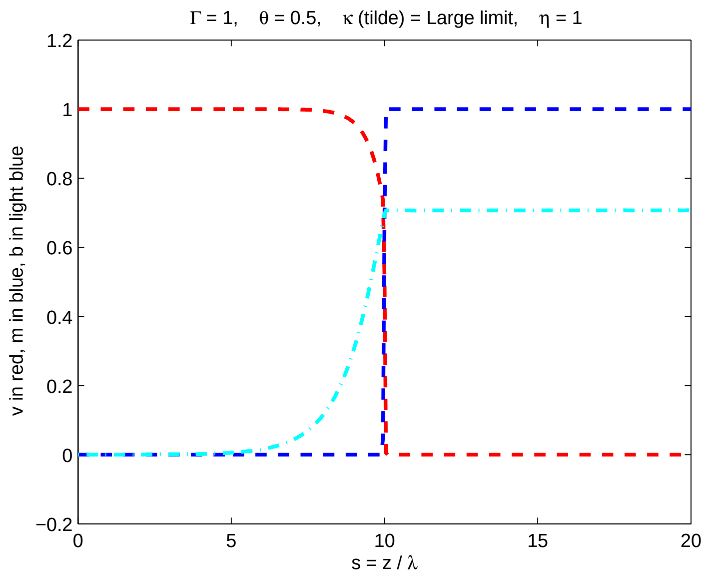

Figure 9.2: The dimensionless order parameters and induced field profiles in the large $\widetilde{\kappa}$ limit for $\Gamma = 1, \theta = 0.5$ and $\eta^2 = 1$.

specific set of Γ, θ and η, one obtains a plot like the one given in Fig. 9.3. Although this curve is specifically obtained with $\Gamma = 1$ and $\theta = 0.5$, neither a change in these values, nor a change in η^2 results in huge difference in the behaviour of the interface energy vs. $\widetilde{\kappa}$.

Compare this curve to the one-band case as given in Fig. 5.1. Although the curves have the same profile, the range of $\widetilde{\kappa}$ differs greatly. Also, in the one-band problem the $\kappa << 1$ limit does not describe the point where $\sigma_s = 0$. In the new problem, this limit would give a good approximation to $\sigma_s = 0$.

From the curves, such as the one given in Fig. 9.3, one can now determine the point where the interface energy crosses the zero line for the specific choice of Γ, θ and η. In other words, the value of $\widetilde{\kappa}_c$ at which the interface energy switches from type-I behaviour to type-II behaviour.

9.2.2 The critical $\widetilde{\kappa}$'s for $\Gamma = 1$, $0 < \theta < 1$

As stated in the beginning of this section, $\widetilde{\kappa}_c$ had previously been studied in [49] for $\eta^2 = 1/\theta$. In Ref. [49] the numerical results were obtained using an integration technique to solve the Ginzburg-Landau differential equations. As the numerical results here are obtained using a minimization technique, the calculations for $\Gamma = 1$, $0 < \theta < 1$ were repeated. The values for $\widetilde{\kappa}_c$ for two other cases, namely, $\eta^2 = 1$ and $\eta^2 = 1/\theta^3$ were also calculated.

Consider first the finite size effects. To this end $\widetilde{\kappa}_c$ was numerically calculated using four s-increment sizes for $\Gamma = 1; \theta = 0.4$ in each of the η^2-scenarios. The increment size started at

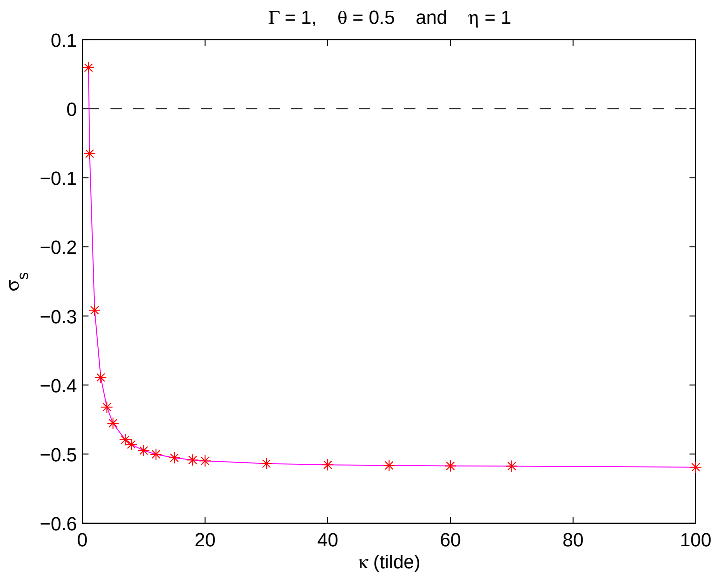

Figure 9.3: The interface energy, σ, in units of $H_c/4\pi$ as a function of $\widetilde{\kappa}$ for $\Gamma = 1, \theta = 0.5$ and $\eta^2 = 1$.

$\Delta s = 0.2$ and was halved repeatedly to give $\Delta s = \{0.1, 0.05, 0.025\}$. The results are given in Fig. 9.4.

In all three η cases the value for $\widetilde{\kappa}_c$ is strictly increasing as the increment size is reduced. From Fig. 9.4 one can also see that the results will converge for each choice in η^2. However, not in any of the choices of η^2 does the result converge to the theoretically predicted value as given in Eq. (8.67).

This is not just the case for $\theta = 0.4$. Consider the results obtained with $\Delta s = 0.025$ for various values of θ; $\Gamma = 1$ in Fig. 9.5. From this figure it is clear that the numerical results of Ref. [49] using an integration technique correspond well to the minimization technique used in the present thesis.

From these curves it is also clear that the choice of η^2 does have an effect on the value of $\widetilde{\kappa}_c$. Here none of the choices for η^2 completely agrees with the theoretical $\widetilde{\kappa}_c$, which is given by the solid line. The current choices in η show that the value of $\widetilde{\kappa}_c$ can be below or above the theoretical value.

The difference between the various η^2-scenarios, as well as the theoretical prediction, is most noticeable when the actual value for $\widetilde{\kappa}_c$ is relatively small, as shown in the inset. As this actual value of $\widetilde{\kappa}_c$ increases, the differences become smaller, falling away completely in the large $\widetilde{\kappa}$ limit. As the interface energy functional in the large $\widetilde{\kappa}$ limit, Eq. (9.5), does not depend on η, it is to be expected that η does not play a role in this limit.

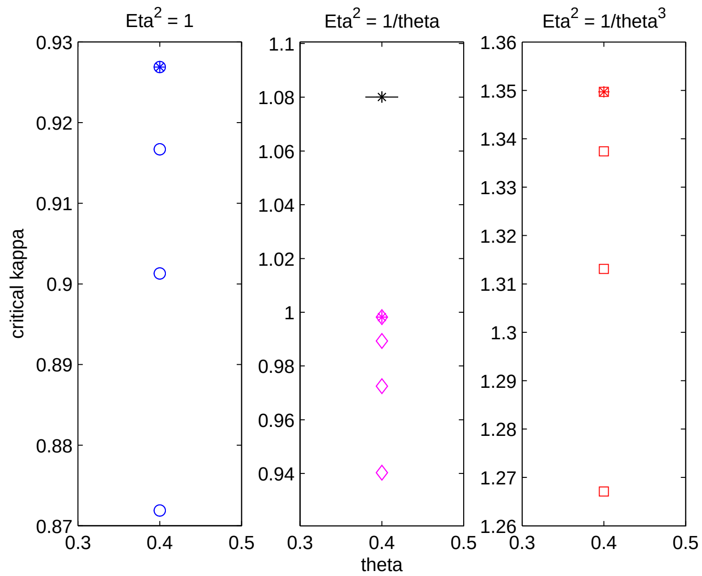

Figure 9.4: The value of $\widetilde{\kappa}_c$ at $\Gamma = 1, \theta = 0.4$ in each of the η^2 scenarios for the increment sizes $\Delta s = \{0.2, 0.1, 0.05, 0.025\}$. The values obtained for $\widetilde{\kappa}_c$ are strictly increasing as the increment size is reduced. The results for $\Delta s = 0.025$ is indicated with an extra star. The line with star in the $\eta^2 = 1/\theta$ plot shows the theoretically predicted value.

This result indicates that the assumption of a second-order phase transition occurring at the upper critical field may not be true in general. Since the numerical results and the theoretical prediction does show the same, this will be discussed in the next chapter.

9.3 The preliminary results for the coexisting state interface for $\Gamma = 0.5$, $0.5 < \theta < 2$

In the previous section it was found that the numerical results do not completely agree with the theoretical prediction for the pure state interface. It was shown that $\widetilde{\kappa}_c$ depends on the choice of η^2. This dependency will again be considered for the interface between a coexisting state and the pure anti-ferromagnetic state. Due to a lack of computing resources, only preliminary results, where the increment size is not yet sufficiently small, were obtained.

9.3.1 The profiles of the order parameters and induced magnetic field

Consider the numerically obtained profiles for the dimensionless order parameters and induced field. In section 9.2.1 this was done for the pure states interface, with the results shown in Fig. 9.1. For the pure states interface an adjustment in Γ and θ does not change the profiles significantly. This is not the case for the interface between a coexisting state and a pure AFM state. For

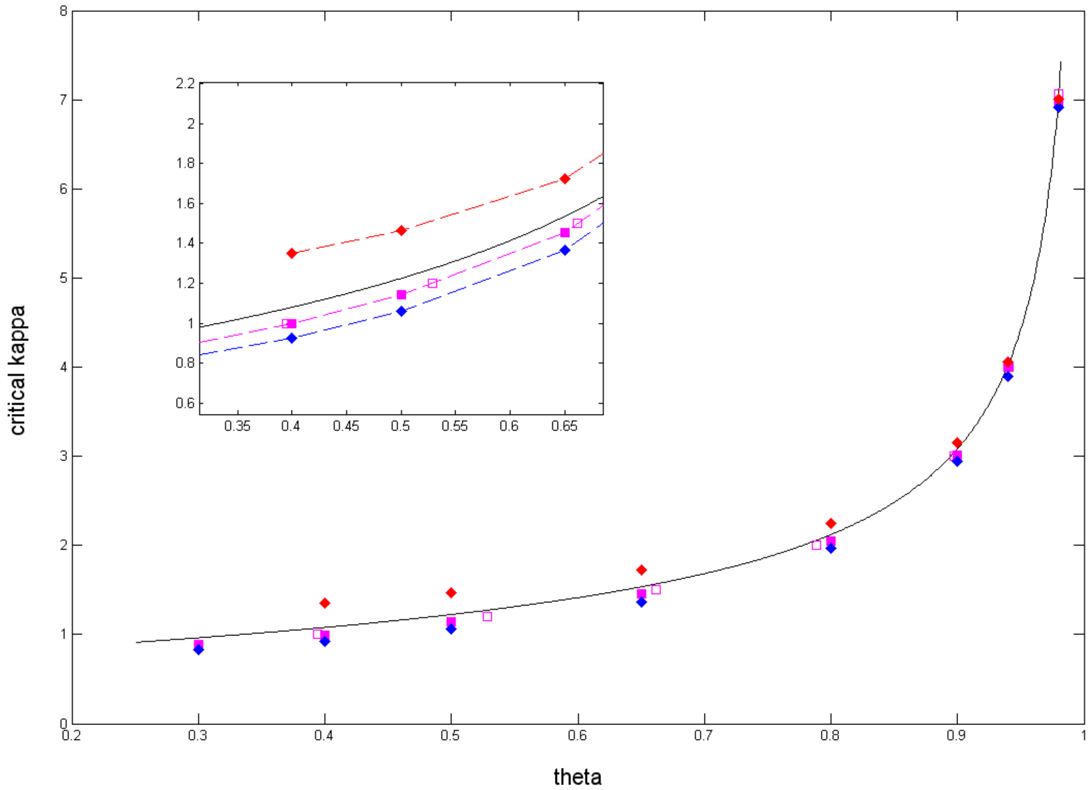

Figure 9.5: The values of $\widetilde{\kappa}_c$ as a function of θ ($\Gamma = 1$) as determined theoretically (the black line) and numerically with $\eta^2 = 1$ (the blue diamonds) , $\eta^2 = 1/\theta$ (all the pink squares) and $\eta^2 = 1/\theta^3$ (the red diamonds). The solid pink square data points were newly determined, while the pink border squares are from Ref. [49]. The inset shows a close-up of the region where the values of κ_c are relatively small. The data points are connected by linear dashed lines to show the general tendency of each curve more clearly.

such an interface Γ and θ play an important role since the boundary conditions depend on these quantities.

Consider $\Gamma = 0.5$ and the three cases where $\theta \in \{0.6, 1, 1.2\}$. The profiles for these cases at $\widetilde{\kappa} = 5$ and $\eta = 1$ are all given in Fig. 9.6, on the left hand side. On the right hand side the same cases are given, but for the large $\widetilde{\kappa}$ limit. $\eta = 1$ remains.

From the boundary values in these figures it is clear that one is considering an interface between a coexisting and a pure AFM state. Again, in the large $\widetilde{\kappa}$ limit one finds that the induced magnetic field and the superconducting order parameter vary on the same length scale. The reason here is the same as discussed in section 9.2.1. In contrast to the previous pure state scenario, the staggered magnetization no longer varies instantaneously. This is also to be

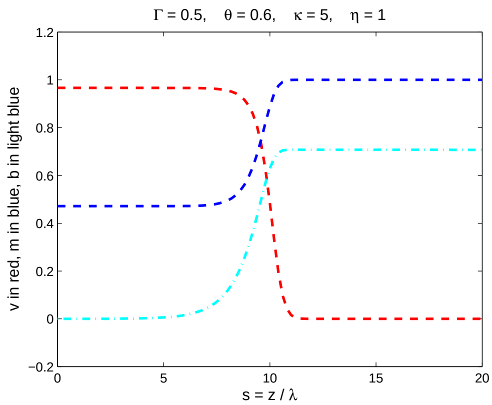

(a) The profiles at $\theta = 0.6$ for $\widetilde{\kappa} = 5$.

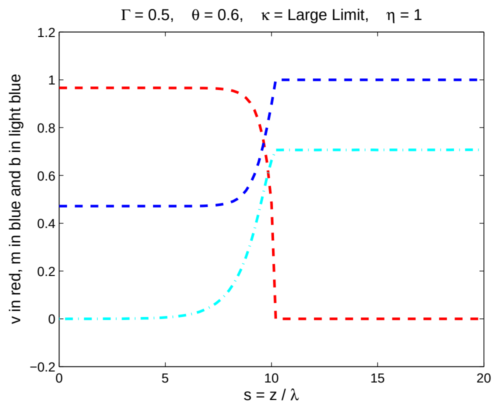

(b) The profiles at $\theta = 0.6$ for large $\widetilde{\kappa}$ limit.

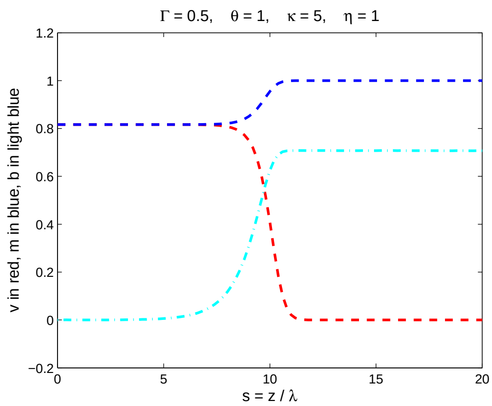

(c) The profiles at $\theta = 1$ for $\widetilde{\kappa} = 5$.

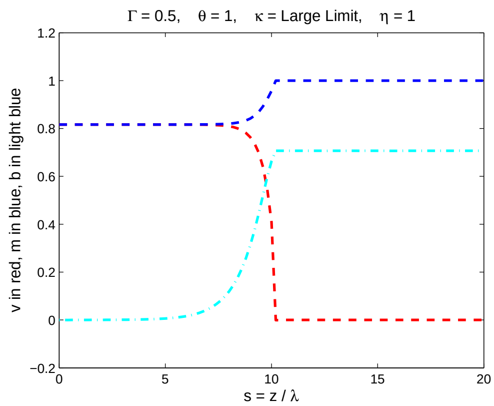

(d) The profiles at $\theta = 1$ for large $\widetilde{\kappa}$ limit.

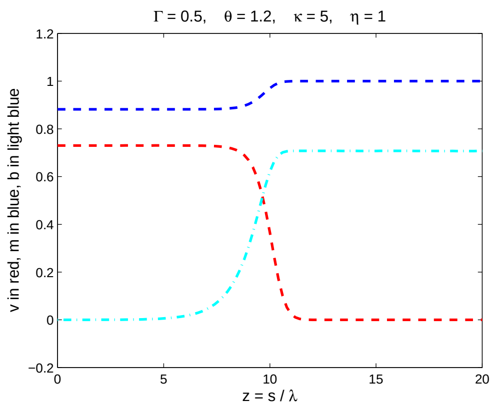

(e) The profiles at $\theta = 1.2$ for $\widetilde{\kappa} = 5$.

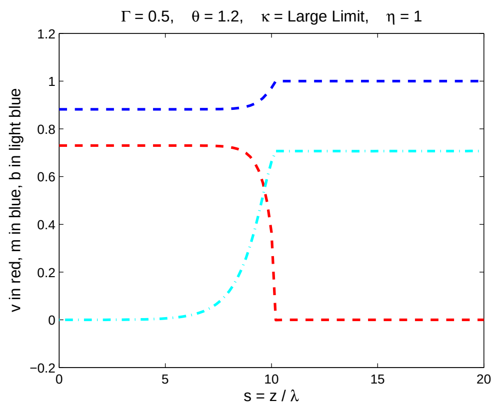

(f) The profiles at $\theta = 1.2$ for large $\widetilde{\kappa}$ limit.

Figure 9.6: Three examples of profiles in the interface between a pure AFM state and a coexisting state. The dimensionless order parameter, v, is in red, the dimensionless staggered magnetization, m, is in blue and the dimensionless induced field, b, is in light blue.

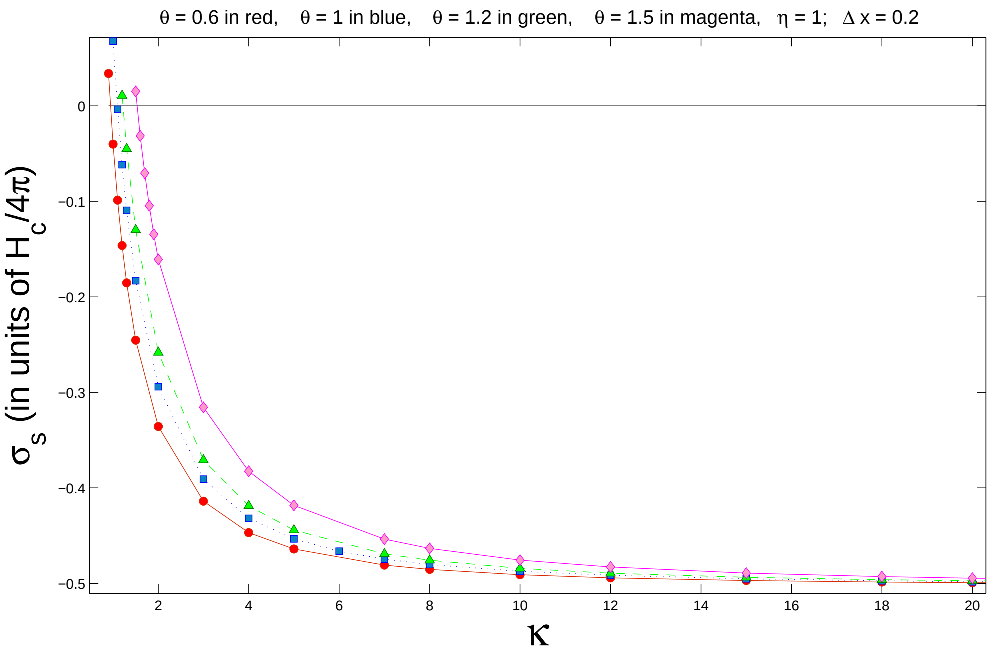

Figure 9.7: The interface energy, σ_s, in units of $H_c/4\pi$ as a function of $\widetilde{\kappa}$ for various points associated to the interface between a coexisting and a pure AFM state.

expected as the boundary conditions differ from the previous scenario. Here one no longer has that either m or v is zero at the boundaries which means that the coupling term between the two order parameters will no longer be zero throughout. This means that the magnetic order parameter now also varies on the same scale as the superconducting order parameter and induced magnetic field.

For various points in the $\Gamma\theta$-phase space one can now determine the $\widetilde{\kappa}$ dependency of the interface energy at a fixed η value. This is given in Fig. 9.7 where $\eta = 1$. Again, these plots give the values of $\widetilde{\kappa}_c$ for any set of Γ, θ and η values.

9.3.2 The critical $\widetilde{\kappa}$'s for $\Gamma = 0.5$, $0.5 < \theta < 2$

The increment size used in this thesis was not sufficiently small to determine the critical $\widetilde{\kappa}$ value accurately. However, the numerical results do give an indication regarding the extent to which the theoretical and numerical results agree. The results for $\eta = 1$ given in Fig. 9.8 show good agreement since the values of $\widetilde{\kappa}_c$ are expected to decrease as the increment size increases. In previous plots the value of $\widetilde{\kappa}_c$ increased with smaller increment size. This change in behaviour is due to a switch in sides of the pure AFM state (left or right) and is discussed in more detail in Appendix B.

In the previous work on the pure states interface one found that $\widetilde{\kappa}_c$ depends on the choice of

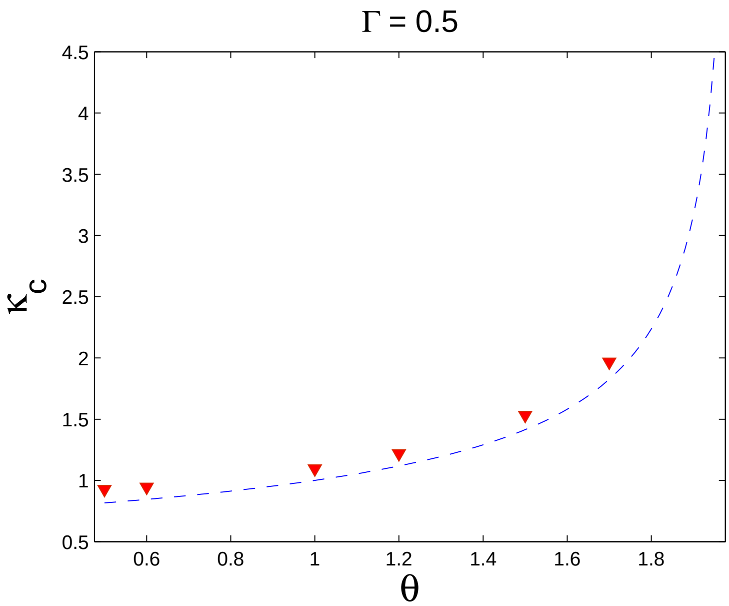

Figure 9.8: The $\widetilde{\kappa}_c$ values as a function of θ, $\Gamma = 0.5$. The blue line gives the theoretical value. The red marks indicate the numerical solutions for $\eta = 1$. Take note: the numerical values for $\widetilde{\kappa}_c$ should drop as one decreases the increment size. In all previous figures it was the other way around.

η. It was also found that the differences between the various $\widetilde{\kappa}_c$'s (due to the choice for η) was most prominent when $\widetilde{\kappa}_c$ was relatively small. For this reason only the point $\Gamma = 0.5, \theta = 0.6$ will be tested for η dependency. The results are given in Fig. 9.9.

From Fig. 9.9 it can be seen that each choice of η yields a different value for $\widetilde{\kappa}_c$. This is the same behaviour found in the pure states interface. Again $\eta^2 = 1/\theta^3$ yields the largest result and $\eta = 1$ the smallest, where $\theta < 1$ in both scenarios.

Due to the insufficient increment size it is not clear to which specific values $\widetilde{\kappa}_c$ will converge. It is therefore not possible to know if any of the chosen η values will converge to the theoretical prediction.

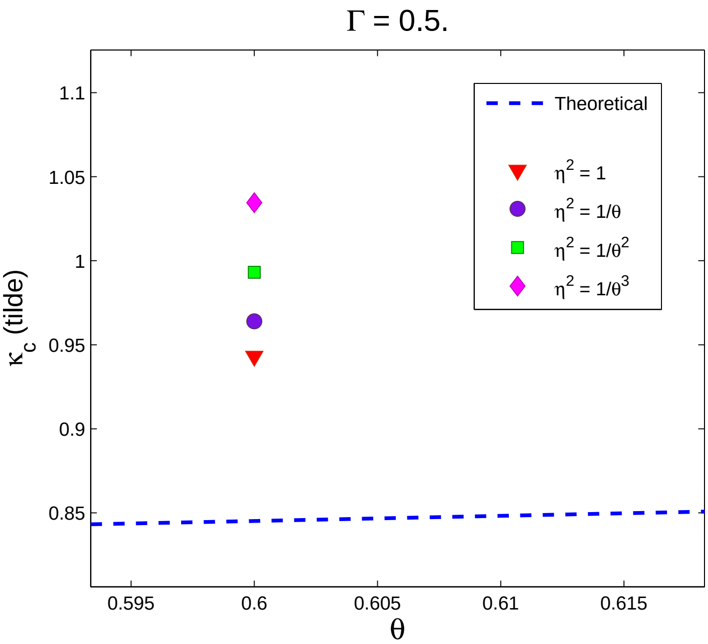

Figure 9.9: The $\widetilde{\kappa}_c$ values for $\Gamma = 0.5$, $\theta = 0.6$ for various values of η. Take note: the numerical values for $\widetilde{\kappa}_c$ will drop considerably in this figure as one decreases the increment size. One expects at least one data point on/below the theoretical prediction.

CHAPTER 10
Conclusions

The aim of this thesis was to study superconducting interface problems with multiple order parameters. Two such problems were investigated theoretically. The first was the interface between a two-band superconductor and a normal state. The second problem was an interface between regions with competing superconductivity and anti-ferromagnetism. Both these scenarios have been shown to occur in physical systems. For example, the superconductor MgB_2 has been experimentally observed to be a two-band superconductor, and the Ln-$FeAsO_{1-x}F_x$ superconductors have experimentally shown competing anti-ferromagnetism and superconductivity.

The theoretical basis for the investigations of these interfaces was Ginzburg-Landau (GL) theory. GL theory has proved to be very consistent with experimental results of the traditional one-band superconductor. The theory is however only valid close to the critical temperature, marking the phase transition between superconductivity and no superconductivity. Within GL theory, emphasis was placed on the interface energy between regions with a zero and a non-zero superconducting order parameter.

The distinction or border between type-I and type-II superconductivity was specifically considered in each problem. This was studied by calculating the interface energy. In type-I superconductivity the interface energy is positive, which results in a complete Meissner effect. In type-II superconductivity the interface energy is negative, which allows for a vortex lattice. The boundary between the two types of superconductivity is thus defined by the zero point of the interface energy. In a traditional one-band superconductor the interface energy only depends on a single dimensionless parameter, namely κ, which is the ratio of magnetic penetration depth to the coherence length of the superconducting order parameter. In the one-band superconductor the zero point of the interface energy occurs at $\kappa = \kappa_c = 1/\sqrt{2}$.

For a two-band superconductor it was found that close to the critical temperature, T_c, the two-band problem reduces to an effective one-band problem. Therefore the transition between type-I and type-II superconductivities is unchanged by the multi-band character of the system. In other words, the zero point of the interface energy in the two-band system still only depends on a single κ. This result puts into question the possibility of so-called *type-1.5* superconductivity as proposed in Refs. [38, 39], at least close to the critical temperature. Refs. [38] and [39] also used GL theory to describe a two-band superconductor, but did not include a coupling term. Instead the assumption was made that both uncoupled bands have the same critical temperature, which lead an intermediate state, or *type-1.5* superconductivity.

In the systems with competing superconductivity and anti-ferromagnetism, the transition between type-I and type-II superconductivity were found to be more complex. From the phase diagrams of the various Ln-FeAsO$_{1-x}$F$_x$ superconductors it was already evident that more than one interface scenario could occur. Building on an extension of GL theory which predicted the so-called reentrant behaviour which was experimentally observed[51], it was found that two distinct interfaces are possible in these systems. The first of these interfaces occurred between the two pure states, namely a pure superconducting state and a pure anti-ferromagnetic state. The second interface occurred between a pure anti-ferromagnetic state and a state of coexistence of the two phenomena. It was shown that the interface energy in this problem depends on four parameters: Γ and θ which together determine which interface is under consideration; η, the ratio of the length scales associated to the AFM- and the superconducting order parameter respectively; and κ.

For both these interfaces the border between type-I and type-II superconductivity in the presence of anti-ferromagnetism was investigated. In other words, at which critical values of the four parameters does the interface energy yield zero. Under the assumption that the phase transition occurring between a pure AFM state and a coexisting type-II superconducting- and AFM state at the upper critical field, H_{c2}, is of second-order, a theoretical expression for κ_c was found in terms of Γ and θ. The expression was shown to be independent of η.

The numerical analysis showed that the analytic approach is only valid in the limit where κ_c is large enough. It was found that the zero point of the interface energy does in general depend on η. This deviation was previously overlooked in Ref. [49] where only a specific limit of the coexistence problem was considered. However, the numerical results are in excellent agreement with those independently obtained in Ref. [49]. Due to this strong agreement, it is plausible to conclude that the discrepancy between the numerics and the analytic expression stems from the underlying assumption used in the analytic approach. In other words, the assumption that the phase transition occurring at H_{c2} is of second-order is invalid, which means that the transition is of first order. As the main trends in the theoretical and numerical results agree, and given that the deviations are relatively small, it is likely that this first order transition is weak.

A possible physical understanding is that one is dealing with order-order transitions at H_{c2} in these coexisting AFM and superconducting systems, as such transitions tend to be of first order. Thus, even if the two phases - anti-ferromagnetism and superconductivity - do not coexist in the homogeneous system, near H_{c2} the AFM order parameter becomes finite in the vortex cores.

One scenario to investigate would be to vary the relative energy penalty of magnetic and superconducting order parameters, in other words the quantity η, to find a regime where the analytic and numeric calculations agree. At this critical η, the transition at H_{c2} would be of second-order. In this way one would have obtained the tricritical point. In other words, the critical η corresponds to the point where the second-order transition becomes first order. This is a project for future investigations.

APPENDIX A
The conditions for simultaneous order

In section 8.1.2.1 it was shown that the conditions for a coexisting homogeneous state at zero field are

$$\Gamma < \theta < \Gamma^{-1}, \tag{A.1}$$

where

$$\Gamma = \frac{\gamma}{\sqrt{b_m b_s}} < 1 \ , \tag{A.2}$$

and

$$\theta^2 = \frac{a_m^2 b_s}{a_s^2 b_m} \ . \tag{A.3}$$

These conditions for simultaneous order can be cross-checked by comparing the energy density values, ϕ_i, of each state (1 for normal, 2 for pure superconducting, 3 for pure AFM and 4 for a coexisting state) as given in Eq. (8.8),

$$\begin{aligned}
\phi_1 &= 0, \\
\phi_2 &= -\frac{a_s^2}{2b_s}t^2, \\
\phi_3 &= -\frac{a_m^2}{2b_m}t^2, \\
\phi_4 &= -\frac{a_m^2 b_s + a_s^2 b_m - 2\gamma a_m a_s}{2\left(b_m b_s - \gamma^2\right)}t^2.
\end{aligned} \tag{A.4}$$

Under the two coexistence conditions, Eq. (A.1) and $\Gamma < 1$, one has that $\phi_4 < 0 = \phi_1$, by simple substitution. As ϕ_1 is not actually a stable solution for any values of Γ and θ, it is more important to compare the energy ϕ_4 of simultaneous order to $\phi_{2,3}$ under the conditions. From Eq. (A.4) and Eq. (A.1) one finds that

$$\begin{aligned}
\phi_4 - \phi_2 &= \phi_2 \frac{\left(\gamma - \frac{a_m b_s}{a_s}\right)^2}{\left(b_m b_s - \gamma^2\right)} < 0, \\
\phi_4 - \phi_3 &= \phi_3 \frac{\left(\gamma - \frac{a_s b_m}{a_m}\right)^2}{\left(b_m b_s - \gamma^2\right)} < 0,
\end{aligned} \tag{A.5}$$

which imply that ϕ_4 is indeed the stable solution once simultaneous order is allowed, i.e. once Eq. A.1.

Against this background, consider now the condition arising from Eq. (8.6) as mentioned previously. As $\mathbf{M}_s^2$ must be positive, by this equation it must hold that $|\psi|^2 < a_m t/\gamma$ in the coexisting regime. However, the value for $|\psi|^2$ in the coexisting state is already determined. From Eq. (8.5)

$$|\psi|^2 = \frac{a_s - \frac{\gamma}{b_m} a_m}{b_s \left(1 - \frac{\gamma^2}{b_s b_m}\right)} t \tag{A.6}$$

one therefore has the condition

$$\frac{a_s - \frac{\gamma}{b_m} a_m}{b_s \left(1 - \frac{\gamma^2}{b_s b_m}\right)} t < \frac{a_m t}{\gamma}. \tag{A.7}$$

Rearranging and substituting in favour of Γ and θ from Eqs. (A.2) and (A.3), this reads

$$\frac{\frac{\Gamma}{\theta} - \Gamma^2}{1 - \Gamma^2} < 1.$$

From this alone one cannot conclude that $\Gamma < 1$ in the coexisting state. For argument's sake assume this is known, then the above equation can be rewritten as

$$\frac{\Gamma}{\theta} - \Gamma^2 < 1 - \Gamma^2 \quad \Rightarrow \quad \Gamma < \theta.$$

This is exactly the condition found earlier in Eq. (A.1). The $\theta < 1/\Gamma$ condition can also be found along the same lines: instead of using the second equation of Eq. (8.4), use the first to obtain an expression for $|\psi|^2$ in terms of $\mathbf{M}_s^2$.

APPENDIX B
The summation technique

This appendix will explain why switching the pure AFM state from the left side to the right side influences $\widetilde{\kappa}_c$.

In order to calculate the interface energy numerically, the interface functional is discretized into equidistant increments. From the minimization process one therefore obtains three discretized functions. In other words, each function is only defined once per interval. As the interface energy is just a complicated summation of the area underneath each of these curves, where the actual function value is defined in the interval becomes important. This can easily be seen in Fig. B.1.

In Fig. B.1 the overall function may be simple, but as long as the function is strictly increasing or decreasing, the result will always hold. Indeed, all three functions obtained from the interface energy minimization are strictly increasing or decreasing.

By making the increment size smaller, the total sum will therefore strictly decrease or increase, depending from which side the functions are approached. This is exactly the behaviour that occurs in the numerical results of chapter 9. By switching the boundary conditions, the functions are essentially mirrored, leading to the change in direction of the interface energy value. In turn this shifts the value of $\widetilde{\kappa}_c$ from increasing to decreasing (or vice versa).

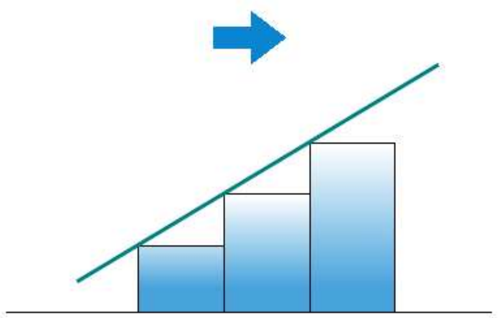

(a) The function values defined at the left side of the interval, leading to a smaller value for the area underneath the curve.

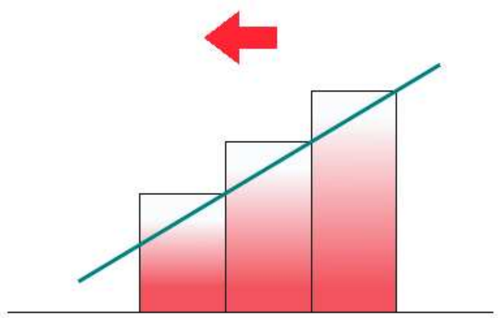

(b) The function values defined at the right side of the interval, leading to a larger value for the area underneath the curve.

Figure B.1: The results for the area underneath a strictly increasing discretized function.

BIBLIOGRAPHY

[1] A. A. Abrikosov, Sov. Phys. JETP **5**, 1174 (1957).

[2] http://www.supraconductivite.fr, accessed July 2011.

[3] V. L. Ginzburg and L. D. Landau, Zh. Eksp. Teor. Fiz. **20**, 1064 (1950).

[4] H. Suhl, B. T. Matthias, and L. R. Walker, Phys. Rev. Lett. **3** 552 (1959).

[5] V. A. Moskalenko, Fiz. Met. Metalloved. **8**, 503 (1959) [Phys. Met. Metallogr. **8**, 25 (1959)].

[6] H. Ding *et. al.*, Europhys. Lett. **83**, 47001 (2008).

[7] V. Moshchalkov, M. Menghini, T. Nishio, Q. H. Chen, A. V. Silhanek, V. H. Dao, L. F. Chibotaru, N. D. Zhigadlo, and J. Karpinski., Phys. Rev. Lett. **102,** 117001 (2009).

[8] A. A. Abrikosov, *Fundamentals of the Theory of Metals*, (North Holland, UK, 1988).

[9] M. Tinkham, *Introduction to superconductivity*, (Dover Publications, USA, 2004).

[10] J. Bardeen, L. N. Cooper, and J. R. Schrieffer, Phys. Rev. **106** 162-164 (1957).

[11] L. P. Gor'kov, Zh. Eksp. Teor. Fiz. **36** (1364) (1959).

[12] Daniel, V. Schroeder, *An Introduction to Thermal Physics*, (Addison-Wesley, USA, 2000).

[13] L. D. Landau and E. M. Lifshitz, *Statistical Physics*, (Pergamon Press, Inc., London, 1958).

[14] D. Saint-James, G. Sarma, and E. J. Thomas, *Type-II Superconductivity*, (Pergamon, New York, 1969).

[15] J. Kortus, I. I. Mazin, K. D. Belashchenko, V. P. Antropov, L. L. Boyer, Phys. Rev. Lett. **86**, 4656 (2001).

[16] I. N. Askerzade, A. Gencer, Solid State Communications **123**, 63 (2002).

[17] J. Nagamatsu, N. Nakagawa, T. Muranaka, Y. Zenitani, J. Akimitsu, Nature (London) **410**, 63 (2001).

[18] S. Bud'ko, G. Lapertot, C. Petrovic, C. E. Gunningham, N. Anderson, P. C. Canfield, Phys. Rev. Lett. **86**, 1877 (2001).

[19] Y. Kong, O. V. Dolgov, O. Jepsen, O. K. Andersen, Phys. Rev. B **64** 020501(R), (2001).

[20] M. Iavarone, G. Karapetrov, A. E. Koshelev, W. K. Kwok, G. W. Crabtree, D. G. Hinks, W. N. Kang, E.-M. Choi, H. J. Kim, H. J. Kim, and S. I. Lee, Phys. Rev. Lett. **89**, 187002 (2002).

[21] F. Giubileo, D. Roditchev, W. Sacks, R. Lamy, D. X. Thanh, J. Klein, S. Miraglia, D. Fruchart, J. Marcus, and P. Monod, Phys. Rev. Lett. **87**, 177008 (2001).

[22] M. R. Eskildsen, M. Kugler, S. Tanaka, J. Jun, S. M. Kazakov, J. Karpinski, and Ø. Fischer, Phys. Rev. Lett. **89**, 187003 (2002).

[23] P. Szabo, P. Samuely, J. Kacmarcik, T. Klein, J. Marcus, D. Fruchart, S. Miraglia, C. Marcenat, and A. G. M. Jansen, Phys. Rev. Lett. **87**, 137005 (2001).

[24] H. Schmidt, J. F. Zasadzinski, K. E. Gray, and D. G. Hinks, Phys. Rev. Lett. **88**, 127002 (2002).

[25] Y. Wang, T. Plackowski, and A. Junod, Physica C **355**, 179 (2001).

[26] F. Bouquet, R. A. Fisher, N. E. Phillips, D. G. Hinks, and J. D. Jorgensen, Phys. Rev. Lett. **87**, 47001 (2001).

[27] H. D. Yang, J.-Y. Lin, H. H. Li, F. H. Hsu, C. J. Liu, S.-C. Li, R.-C. Yu, and C.-Q. Jin, Phys. Rev. Lett. **87**, 167003 (2001).

[28] P. C. Canfield, S. L. Bud'ko, and D. K. Finnemore, Physica C **385**, 1 (2003).

[29] X. X. Xi, Rep. Prog. Phys. **71**, 116501 (2008).

[30] Neil W. Ashcroft and N. David Mermin, *Solid State Physics*, (Saunders College, Philadelphia, 1976) *pg. 734*.

[31] L. Y. L. Shen, N. M. Senozan, and N. E. Phillips, Phys. Rev. Lett. **14**, 1025 (1965).

[32] G. Binnig, A. Baratoff, H. E. Hoenig, and J. G. Bednorz Phys. Rev. Lett. **45**, 1352 (1980).

[33] M. Heinecke and K. Winzer Z. Phys. B **98**, 147 (1995).

[34] S. V. Shulga, S.-L. Drechsler, G. Fuchs, K.-H. Muller, K. Winzer, M. Heinecke and K. Krug. Phys. Rev. Lett. **80**, 1730 (1998).

[35] T. Yokoya, T. Kiss, A. Chainani, S. Shin, M. Nohara, H. Takagi, Science **294**, 2518 (2001).

[36] I. N. Askerzade, Physics Uspekhi **49**, 1003 (2006).

[37] M. E. Zhitomirsky and V.-H. Dao, Phys. Rev. B **69**, 054508 (2004).

[38] E. Babaev, M. Speight, Phys. Rev. B **72**, 180502(R) (2005).

[39] J.-P. Wang, Physics Letters A **374,** 58 (2009).

[40] E. H. Brandt and M. P. Das, *Journal of Superconductivity and Novel Magnetism*, Vol. 24, Numbers 1-2 (57-67), (Springer, New York, 2010).

[41] P.-G. de Gennes, *Superconductivity of Metals and Alloys*, (Benjamin, Inc., New York, N.Y., 1966).

[42] J. Geyer, R. M. Fernandes, V. G. Kogan and J. Schmalian, Phys. Rev. B **82** 104521 (2010).

[43] V. G. Kogan and J. Schmalian, Phys. Rev. B **83** 054515 (2011).

[44] H. Luetkens *et. al.*, Nature Materials **8**, 305-309 (2009)

[45] J. Zhao, Q. Huang, Clarina de la Cruz, Shiliang Li, J. W. Lynn, Y. Chen, M. A. Green, G. F. Chen, G. Li, Z. Li, J. L. Luo, N. L. Wang, and Pengcheng Dai, Nature Materials **7**, 953-959 (2008).

[46] C. R. Rotundu, D. T. Keane, B. Freelon, S. D. Wilson, A. Kim, P. N. Valdivia, E. Bourret-Courchesne, and R. J. Birgeneau, Phys. Rev. B **80**, 144517 (2009).

[47] A. J. Drew *et. al.*, Nature Materials **8**, 310 - 314 (2009).

[48] S. Nandi, M. G. Kim, A. Kreyssig, R. M. Fernandes, D. K. Pratt, A. Thaler, N. Ni, S. L. Bud'ko, P. C. Canfield, J. Schmalian, R. J. McQueeney, A. I. Goldman, Phys. Rev. Lett. **104**, 057006 (2010).

[49] M. Juneau, R. MacKenzie, and M.-A. Vachon, Annals of Physics **298**, 421-434 (2002).

[50] R. M. Fernandes, J. Schmalian, Phys. Rev. B **82**, 014521 (2010).

[51] R. M. Fernandes, D. K. Pratt, W. Tian, J. L. Zarestky, A. Kreyssig, S. Nandi, M.G. Kim, A. Thaler, N. Ni, P. C. Canfield, R. J. McQueeney, J. Schmalian, and A. I. Goldman, Phys. Rev. B **81**, 140501(R) (2010).